Nature of Bose Gases Near Feshbach Resonance

The Interplay Between Few-Body and Many-Body Physics

by

Mohammad S. Mashayekhi

B.Sc., Sharif University of Technology, 2006
M.Sc., The University of British Columbia, 2009

A THESIS SUBMITTED IN PARTIAL FULFILLMENT OF
THE REQUIREMENTS FOR THE DEGREE OF

DOCTOR OF PHILOSOPHY

in

The Faculty of Graduate and Postdoctoral Studies

(Physics)

THE UNIVERSITY OF BRITISH COLUMBIA

(Vancouver)

February 2014

Abstract

In this thesis, we investigated the physics of two- and three-dimensional ultra cold Bose gases in the strongly interacting regime at zero temperature. This regime can be experimentally accessed using a Feshbach resonance. We applied a self-consistent diagrammatic approach to determine the chemical potential of three-dimensional Bose gases for a wide range of interaction values. We showed that such strongly interacting Bose gases become unstable towards the formation of molecules at a finite positive scattering length. In fact, the interaction between atoms becomes effectively attractive and the system looses its metastability before reaching the unitary limit. We also found that such systems are nearly fermionized close to the instability point. Near this critical point, the chemical potential reaches a maximum and the contribution to the system energy due to three-body forces is estimated to be only a few percent. We also studied the same system using a self-consistent renormalization group method. This approach confirms the existence of an instability point towards the formation of molecules as well as fermionization. We showed that the instability and accompanying maximum are precursors of the sign change of the effective two-body interaction strength from repulsive to attractive near resonance. In addition, we examined the physics of two-dimensional Bose gases near resonance using a similar self-consistent diagrammatic approach as the one introduced for three-dimensional Bose gases. We demonstrated that a competition between three-body attractive interactions and two-body repulsive forces results in the chemical potential of two-dimensional Bose gases to exhibit a maximum at a critical scattering length beyond which these quantum gases possess a negative compressibility. For larger scattering lengths, the increasingly prominent role played by three-body attractive interactions leads to an onset instability at a second critical value. The three-body effects studied for these systems are universal, fully characterized by the effective two-dimensional scattering length and are, in comparison to the three-dimensional case, independent of three-body ultraviolet physics.

Preface

- A version of first part of chapter 1 is published in Annual Review of Cold Atoms and Molecules [1]. I wrote parts of the manuscript.
- A version of chapter 2 has been published in Phys. Rev. A [2]. I conducted part of analytical and numerical calculations in this research.
- A version of chapter 3 has been published in Annals of Physics [3]. I have conducted part of calculations and produced all plots.
- A version of chapter 4 has been published in Phys. Rev. Lett. [4]. I have conducted most of the analytical and numerical calculations of this research.

Table of Contents

List of Tables

List of Figures

Acknowledgements

I would like to acknowledge the advice and guidance of Dr. Fei Zhou, my supervisor. I also thank the members of my graduate committee, Dr. Mona Berciu, Dr. Gordon Semenoff and Dr. Jeff Young for their guidance and suggestions. Special thanks go to my friend Dr. Jean-Sebestien Bernier, without whose knowledge and assistance this study would not have been successful.

Finally, I would express my gratitude to my parents and my sisters, whose support and constant encouragement helped me through the hard times of this program. My deepest appreciation is expressed to them for their love, understanding, and inspiration. Without their blessings and encouragement, I would not have been able to finish this work.

I also would like to thank my colleagues Dr. Jun-Liang Song, Dmitry Borzov and Dr. Shizhong Zhang for their collaboration on this work.

Dedication

To my family.

Chapter 1

Introduction

Ultra cold gases are an excellent test bed to explore the fundamentals of many-body quantum physics. Since the first realization of a Bose-Einstein condensate of ultra cold atoms in 1995 [5, 6], a large number of experiments have been done to understand the complex behavior of these systems. This is achieved by reducing the of these gases to nano Kelvins in order to suppress thermal fluctuations and reveal the quantum nature of these systems. Ultra cold gases are quite unique as experimentalists have impressive control over the system Hamiltonian parameters. For example, the ability to tune the strength of the atom-atom interaction has facilitated the exploration of strongly interacting gases. Understanding such systems is of great importance as strong interactions can generate complex states that cannot be trivially inferred from the weakly interacting regime. Moreover, in this regime the crucial role played by many-body physics requires the development of novel theoretical frameworks. Consequently, exploring this regime is extremely exciting.

While all physical properties of weakly interacting Bose gases were understood theoretically in the 1950's [7–12], the physics of strongly correlated Bose gases is still poorly understood. Such gases, where complex many-body effects are important, can be produced using magnetic Feshbach resonances [13]. Applying this technique, experimentalists are able to vary the strength of the interaction between atoms and to access a strongly interacting regime close to a Feshbach resonance. Although the realization of stable strongly correlated Bose gases is limited by the large inelastic loss of atoms due to the formation of molecules, these Bose gases can be held for about a few miliseconds [14] before losing stability. The physics of these strongly correlated atomic gases remains to be fully understood. This is the main objective of this thesis. In the next sections, we first briefly review the basic theory of Feshbach resonances and the theory of dilute gases before presenting our results pertaining to the unusual physics of two- and three-dimensional strongly interacting Bose gases. Note that this is a rapidly developing subject with new data and theoretical attempts made after we finished the first version of this thesis toward the end of summer 2013. As a result, there are

some recent works that are not included in our review of previous studies.

1.1 Feshbach Resonances

Feshbach resonances are considered as an essential tool to control the interaction strength between the atoms of a quantum gas. To explain this phenomenon, we consider two molecular potentials V_{open} and V_{closed} which are named as open channel and closed channel respectively. As depicted in Fig. 1.1, at large inter-atomic distance, V_{open} asymptotically tends to two free atoms in the gas. This channel is called the open channel since the energy is very close to zero in collision between these two atoms. In contrast, the closed channel can have few molecular bound states which are close to the threshold of the open channel.

In magnetic Feshbach resonances, the energy difference between these two channels could be controlled by applying a magnetic field if the magnetic moments of channels are different. When the energy of one of the bound states of the closed channel is approaching the scattering state in open channel, even a weak coupling between the atoms can cause the mixing between two channels. On the other hand, scattering atoms spend a finite time as a bound state and as a result, the effective interaction between the scattering atoms could be very strong. Resonance happens when the energy of one of the bound states is equal to the scattering atoms energy. The effective interaction between atoms is described by a simple equation introduced in Ref. [15] for s-wave scattering length a as a function of magnetic field B:

$$a(B) = a_{bg}\Big(1 - \frac{\Delta}{B - B_0}\Big) \tag{1.1}$$

where a_{bg} is the scattering length defined for open channel and is known as the off-resonant value. B_0 is the magnetic field where the resonance happens and Δ is the resonance width. On the positive side of the resonance, where the energy of bound states of the closed channel is a little lower that the energy of the atoms in open channel, the scattering state known as "upper branch" is a metastable state and atoms will form bound state in sufficiently long time. The energy of these bound states is shown in Fig. 1.1. The bound state energy is zero at the resonance. Away from resonance, the bound state energy varies linearly with the magnetic field with slope $\delta\mu$. But near resonance, the strong mixing between two channels bends the molecular state and the binding energy is given by:

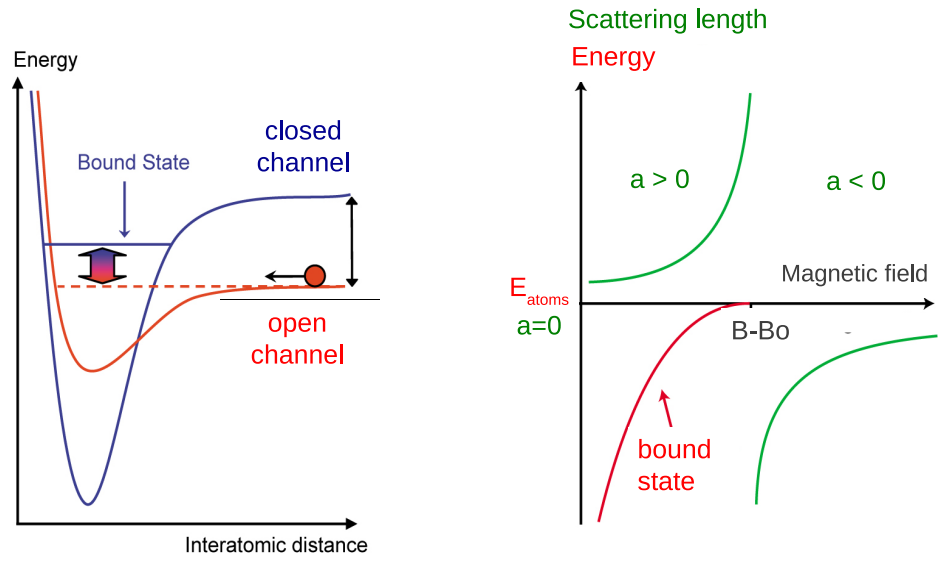

Figure 1.1: Schematic picture of magnetic Feshbach resonance. When the energy of the bound state of the closed channel approaches the energy of scattering atoms in open channels, the effective interaction between the atoms would be very high due to strong mixing of two channels. The positive side of the resonance labeled by $a > 0$ is known as upper branch and it is metastable. More discussions could be found in Ref. [16].

$$E_b = \frac{-\hbar^2}{ma^2} \tag{1.2}$$

which is proportional to $(B-B_0)^2$. The importance of near resonance regime is the existence of universal properties. Here, the state can be described only in terms of the scattering length independent of details of the interaction.

In this thesis, we are interested in physics of two- and three-dimensional ultra cold gases initially prepared in the metastable upper branch near Feshbach resonance. In the theoretical models presented in this thesis, the interaction between atoms is solely contact and therefore corresponds to the limiting case of a broad Feshbach resonance where the atomic (open) channel dominates the physics.

1.2 Three-Dimensional Bose Gases

The experimental ability to vary the Hamiltonian parameters of ultra cold atomic gases provides novel opportunities to create strongly interacting systems exhibiting phenomena previously associated only with condensed matter. In particular, the control over the magnitude and sign of the effective atom-atom interaction is achieved using Feshbach resonances [13]. In recent years, taking advantage of this tuning knob, a few experiments have been carried out to understand the properties of Bose gases near resonance [14, 17–19]. As attractive Bose gases are unstable at low temperatures, the primary focus of these experiments was to explore the properties of a repulsive molecule-free Bose gas, commonly referred as "upper branch physics". The results of these experiments suggest that when a resonance is approached from the side of small positive scattering lengths, Bose atoms in the upper branch form a metastable condensate as they appear to equilibrate on a short timescale compared to the one set by which atoms are lost.

Meanwhile, on the theoretical front, even though the properties of quantum degenerate gases far from resonance are well described by existing dilute gas theories [7–12, 20], near resonance, very little is known. Very few theoretical works have tried to address the physics of Bose gases at large positive scattering lengths. In fact, early numerical Monte Carlo simulations mainly explored the physics of repulsive bosonic systems [21, 22]. More recently, numerical energy minimization studies, conducted in a truncated Hilbert space of experimental relevance, consistently pointed out the near fermionization of Bose gases close to resonance [23–25]. By fermionization, we mean that

the physical properties of the Bose gases, such as the momentum distribution and the spatial density resemble that of a Fermi gas. However, whether the minimum of the restricted energy landscape still remains metastable once the full Hilbert space is considered remains to be addressed.

The complexity of this topic to a large extent appears to be two-fold:

1) the role of few-body physics (two-body, three-body states etc) in many-body systems. In other words, to what extent does the underlying few-body physics influence the many-body correlations and which channel dictates the many-body properties near resonance?

2) the effect of many-body background (condensate) on the few-body structures. How are the few-body structures or multiple scatterings affected by the presence of many other identical particles?

These two issues can be treated successfully and separately in the usual dilute limit. For instance, in the leading order, one can neglect the effect of finite-density background (condensed) atoms on multiple scatterings or underlying few-body structures; the energy density can therefore be calculated perturbatively by assuming the few-body scatterings are given by their properties in the vacuum and applying the low density expansion. The effects of few-body structures on many-body physics can be explored perturbatively. One can also further study the leading effect of quantum gases on two- and three-body bound states because the many-body states in the dilute limit are well-known. However, near resonance, these two issues are generically entangled and ideally have to be addressed self-consistently, which usually becomes very challenging.

In light of these theoretical challenges, and motivated by the recent experimental realizations of upper branch metastable condensates, we developed a novel non-perturbative self-consistent approach discussed in chapters 2 and 3 to explore the physics of long-lived condensates beyond the dilute limit. Our work highlights that a quantum gas at a positive scattering length near resonance is not always equivalent to a gas of effectively repulsive atoms. This idea will be further developed in this thesis.

1.2.1 Current Experimental Status

Despite the clear need for a solid experimental understanding of a strongly correlated bosonic fluid, fulfilling this task, in a cold atom context, has proven extremely challenging. In contrast to Fermi gases [26, 27], for Bose gases, difficulties arise as increasing the scattering length to very large positive values is accompanied by a catastrophic loss of atoms [28]. Nevertheless, using techniques requiring the gas to be probed for only a short time

compared to the time needed for the system to become unstable , a few experimental groups succeeded in exploring Bose gases beyond the dilute limit [14, 17–19]. We distinguish below two different regimes: the dilute limit, and the strongly interacting regime.

Physically speaking the dilute limit is characterized by the inequality $na^3 \ll 1$ where a is the s-wave scattering length and n the atomic density. In this regime, the ground state energy density is

$$\frac{E}{V} = \frac{4\pi\hbar^2 a n^2}{m}\left(\frac{1}{2} + \frac{64}{15\sqrt{\pi}}\sqrt{n\ a^3} + \dots\right) \tag{1.3}$$

where V is the volume of the system and m is the mass of the bosonic atoms. The first term in Eq. (1.3) is the mean-field energy density while the second term, the Lee-Huang-Yang (LHY) correction [8], describes the effect of quantum fluctuations.

To the best of our knowledge, Ref. [17] is the first experimental work which considered beyond-mean-field effects. The main focus of this experiment was to probe the excitation spectrum of a gas of ^{85}Rb atoms using a spectroscopic technique. For $a < 300a_0$, where a_0 is the Bohr radius, their findings agreed well with mean-field predictions. However, for larger scattering lengths, their results deviated significantly from its mean-field value. These measurements agreed somewhat qualitatively with the predicted Beliaev corrections [9]. This experiment was followed by the study of a Feshbach resonance in a gas of ^{7}Li [18]. This study mapped the Feshbach resonance in a very large range of interaction strengths, and identified a region where mean-field predictions were inapplicable. In turn, this experiment was followed by a third one which carried out a quantitative measurement of the thermodynamical equation of state of a strongly interacting Bose gas of ^{7}Li [14]. Using density profile measurements, and assuming that all measurements were done in the zero-temperature regime, this study found, for scattering lengths between $700a_0$ and $2150a_0$, the equation of state to be well described by LHY theory. Moreover, Ref. [14] probed physics beyond the dilute limit, these results will be further discussed in the next section. Finally, the most recent experiment used a fast-probing technique to investigate local many-body equilibrium in a trapped gas of ^{85}Rb atoms [19]. Using radio-frequency spectroscopy, they measured the two-body contact, C_2, an extensive thermodynamical variable related to the derivative of the total energy of the system as a function of the scattering length and the ultra-violet properties of the momentum distribution function. These universal contact parameter has been first introduced for fermionic systems in Ref. [29] and later on authors of Refs. [30, 31] utilized it to establish an exact expression

for the energy density. In this experiment, the contact measurements were found to be larger than the mean-field predictions but not as large as the values predicted when LHY corrections were included. In addition, in regions where beyond mean-field effects were expected, no measurable contribution coming from three-body physics was found.

The strategy commonly used to access the strongly interacting limit consists in preparing an equilibrated weakly interacting gas and to later ramp up the interaction strength to the desired value. Consequently, as the scattering length is increased, the dilute limit condition, $na^3 \ll 1$, stops being fulfilled. Probing such a strongly interacting system is fairly complicated as, near resonance, the timescales of recombination processes become comparable to the equilibration time. Recombination process is a scattering event in which three atoms interact and form a diatomic molecule and a free atom. In this process, the binding energy is released into the kinetic energy of the outgoing two-body bound state and the third atom which leads to immediate trap loss. Hence, ramping up the scattering length cannot be done adiabatically, and non-equilibrium effects must be taken into considerations. The study presented in Ref. [14] considered these effects in order to extract universal thermodynamical properties near unitarity (near Feshbach resonance where the physics is universal and it only depends on the scattering length). Under the assumption of universality, near resonance, the equation of state should be given by $\mu \propto \frac{\hbar^2}{m} n^{2/3}$ as the only relevant length scale should be the inter-atomic spacing $n^{-1/3}$ where μ is the chemical potential. This expression is identical, up to a multiplicative factor, to the equation of state for a Fermi gas and can be written as $\mu = \xi \epsilon_F$ where ϵ_F is the Fermi energy at the same density. At large scattering length, due to the gas metastability, the authors of this work deduced a lower bound for the value of ξ by extrapolating their data at unitarity. They found $\xi > 0.44(8)$ meaning that the system is nearly fermionized.

1.2.2 Current Theoretical Understanding

In the last six decades, various theoretical frameworks were developed to study three-dimensional Bose gases in the dilute limit. In this regime, $na^3 \ll 1$, the average distance between the atoms is much larger than the scattering length (corresponding, in this limit, to the interaction strength between bosons). The mean-field description for these systems was devised by Bogoliubov in 1947 [7] and the energy density is given by the first term of Eq. (1.3). Later on, Lee, Huang and Yang [8] found the first correction to the mean-field expression. In fact, the first corrections to the chemical potential,

condensate fraction, and energy density are all proportional to $\sqrt{na^3}$, the perturbation parameter in the dilute limit. It is worth noting that Beliaev, using field theoretical methods, rederived LHY-type corrections and further analyzed the excitation spectrum [9]. In addition, Wu [10], Sawada [11, 12] and later Braaten et al. [20] succeeded in calculating the next order corrections to the mean-field result.

Unfortunately, these corrections are only valid for a dilute gas, as beyond this limit, na^3 is not a small parameter. The perturbation method presented in the previous section is then inapplicable as all terms of the expansion are diverging. Therefore, one needs to define a whole new framework to study the behavior of Bose gases near resonance where the scattering length is extremely large.

In general, one can classify the scattering processes between atoms in terms of (a) the order of perturbation in a given parameter (for example $\sqrt{na^3}$) or (b) the number of virtual atoms involved in these processes. In (a), one takes into account all processes of the same perturbative order and consequently the number of virtual particles involved is not fixed. On the other hand, using the classification explained in (b), one takes into account all processes involving a fixed number of virtual particles and sums over all orders in the perturbative parameter of classification (a). Using this second classification method, one can find the contribution of irreducible M-body processes to the thermodynamical properties of a system beyond the dilute regime. For example, in this case, the total energy density of the system is written as

$$\frac{E}{V} = \sum_{M=2}^{\infty} \frac{n_0^M}{M!} g_M(n_0, \mu) \tag{1.4}$$

where n_0 is condensate density and g_M is the irreducible M-body interaction potential. Consequently, classification (b) is not a perturbative approach and we claim that the sum over the irreducible M-body processes is converging rapidly (See Sec. 2.2 for more details). To verify this statement, we compare the effect of the first and second terms of Eq. (1.4) on the self-consistent value of the chemical potential. This approach is motivated by the observation that, in the first order in perturbative parameter $\sqrt{na^3}$, the dominating part of the LHY correction comes from irreducible two-body interaction, involving only two virtual particles, and that the combined effect of the other processes, involving more than two virtual atoms, is less than one percent. In addition, in the recent study in Ref. [32], using ϵ-expansion near four dimensions, it was found that near resonance the physics of these ultra cold gases is mainly dictated by two-body forces and the contribution

of the scattering processes with more than two virtual particles involved in the interaction is negligible when ϵ goes to zero. This study will be explained in more detail in chapter 2.

Then, using the analytical expression of $g_2(n_0, \mu)$ in conjunction with the number equation (which sets the number of particles in the system), one can find a self-consistent equation for the chemical potential.

We present here the main features and predictions emerging from the self-consistent framework at zero temperature explained above, and compare these results with other existing theories. Within this self-consistent approach, we found, as a first salient result, that the system is nearly fermionized as the maximum of the chemical potential is almost 93% [1] of the Fermi energy (see chapter 2). This effect has also been identified in other theoretical studies, although the ratios of fermionization were different. In Ref. [23], using the lowest order constrained variational method with a modified Jastrow wave function, they found in the dense limit that the chemical potential is equal to $2.92\epsilon_F$, exceeding complete fermionization. By comparison, using a truncated Hilbert space variational method, Ref. [24] found that the chemical potential saturates at a value of $0.8\epsilon_F$, while in Ref. [33], using a renormalization group approach, the fermionization ratio near resonance was found to be $0.66\epsilon_F$. Finally, more recently, a sophisticated variational method found the Bose gas to be fermionized at 83% [25].

A clear advantage of the self-consistent approach discussed in chapters 2 and 3 is that it agrees in the dilute limit with LHY results. In fact, 99.96% of LHY corrections to the chemical potential are reproduced by only taking into account all the irreducible two-body processes (i.e. scattering processes involving only two virtual atoms). In Fig. 3.1(a), one sees that the dashed line representing the chemical potential obtained from the mean-field and LHY correction overlaps with the self-consistent results for small $an^{1/3}$. Note that in the atom-molecule field theory calculations presented in Refs. [25, 33], the sign of the correction of order $\sqrt{na^3}$ is opposite to the LHY effect. However, in Ref. [25], the LHY effect is reproduced correctly in their numerical simulation.

For negative bare interactions, there are two channels on the side of the resonance where the scattering length goes to positive infinity, namely the molecule channel and the atom channel, known as the *upper branch*. While the molecule channel is lower in energy, one can prepare the Bose gas in the upper branch at very small positive scattering length. Such an upper

[1] The value of $\xi = 0.93$ found in self-consistent diagrammatic approach for three-dimensional Bose gases is for a range of three-body parameters relevant for cold atoms.

branch state can remain stable during a long time before collapsing to the molecule channel. Using the self-consistent method one can show that, when the scattering length is increased, the system will become unstable towards the formation of molecules at the maximum of the chemical potential before reaching the resonance point. Unfortunately, this approach does not offer a complete picture of how molecules and atoms interact. Technically, this instability appears in these calculations as the solution for the chemical potential becomes complex. The imaginary part of the chemical potential is interpreted as the hybridization of the molecule and atom channels. In our study, this instability was first pointed out to be correlated with the occurrence of a maximum in the chemical potential.

These highly non-trivial results were also obtained using a renormalization group approach by looking at the running of the two-body coupling constant at different energies (see chapter 3). This study shows that when the resonance is approached from small positive scattering length in the upper branch, at a given scattering length, the effective interaction between the atoms becomes attractive and the atomic and molecular channels hybridize. We found the effective two-body interaction as a function of the scattering length to be given by

$$g_2 = \frac{4\pi\hbar^2}{m} \frac{1}{1/a - \sqrt{2m\mu/\hbar^2}}. \tag{1.5}$$

One sees from the above expression that, when a is sufficiently large, the second term in the denominator dominates, and g_2 becomes negative. This result is strikingly different from the picture commonly accepted by the cold atom community where it is usually thought that, for negative bare interactions, where scattering length is positive, the atoms repel each other.

A key concept we are going to focus on is the effective interaction between condensed atoms near resonance. The common belief is that although the underlying short range resonance interaction has to be attractive, at low energy scales the two-body interaction is effectively repulsive when the scattering length a is positive. The argument runs as the following. The phase shift due to a short range attractive potential is given as $\delta = -\arctan ka$ which yields $\delta = -ka$ when k is small. The phase shift approaches $-\pi/2$ when ka is much bigger than unity but much smaller compared to a/R^*, $R^*(\ll a)$ is the range of the attractive interaction. The low energy phase shift $\delta = -ka$ turns out also to be the phase shift of any repulsive interaction with the same positive scattering length. And so the atoms interact effectively repulsively if one is interested in the scatterings at small k. However, the phase shifts of a short range attractive potential and a repulsive

interaction can become significantly different whenever ka is bigger than unity; for instance, for a hard-core potential with radius $R = a$, $\delta = -ka$ for all momenta, differing from the value of $-\pi/2$ for attractive potentials when $ka \gg 1$. Near resonance, a approaches infinity and the issue of the effective interaction between condensed atoms becomes very subtle. Indeed, near resonance we show that condensed atoms no longer interact with an effective repulsive interaction even when the scattering lengths are positive, a somewhat surprising conclusion to many.

In fact, in chapters 2 and 3 we showed that the behavior of the system is set by the effective two-body interaction which becomes negative for sufficiently large positive scattering length. The emergence of this instability is a many-body effect which modifies the two-body physics. The effect of the background (condensed) atoms on two-body bound state energy is to shift the bound state channel by an amount proportional to the chemical potential for a range of scattering lengths we are interested in. In vacuum, the energy of the bound state touches zero at resonance. However, adding the effect of the background, one sees that the energy of the bound state now touches zero at a finite and positive scattering length far before resonance. At this point, the system becomes unstable and hybridization between the molecule and atom channels occurs.

Finally, in chapter 2, the effects of the three-body interactions on the chemical potential are also considered. These effects are obtained by taking into account the second term, g_3, in the energy expansion (Eq. (1.4)) [2]. For three-dimensional gases, including this three-body potential does not change qualitatively the form of the solution. In fact, it only shifts the position of the instability point. The effects of the three-body interaction were calculated to be around a few percent near the instability point. compared with the other studies cited earlier, the study presented in chapter 2 is the only work that investigated the effect of Efimov physics beyond the dilute limit.

By Efimov physics, we mean the three-body physics of three-dimensional Bose gases studied by Efimov. He showed that there are three-body bound states on the both sides of the resonance. He predicted that near resonance, there would be an infinite sequence of weakly three-body bound states with a universal scaling behavior. Each successive Efimov state is weaker in binding energy by a universal factor of 515 [34].

The self-consistent approach produces various interesting predictions. To

[2] In chapters 2 and 3, three-body recombination effects have been excluded in order to explore the thermodynamics of a quasi-static upper branch condensate on a relatively short timescale.

summarize, using this method, one finds that an instability sets in at a positive critical scattering length beyond which the near-resonance Bose atomic gas becomes strongly coupled to molecules, and loses its metastability. Near this point of instability, the chemical potential reaches a maximum whose value is interpreted as the fermionization ratio. In addition, where near-resonance physics sets in, the effect of the three-body forces were estimated in three dimensions to vary the value of the chemical potential by only a few percent. These three-body forces were considered for a range of parameters relevant for cold atoms.

Two of these predictions are consistent with current experimental findings. In Ref. [14], the lower bound of the chemical potential was deduced to be $0.44(8)\epsilon_F$. This result is in agreement with the self-consistent approach which predicts a fermionization ratio of 93% near the instability point (see chapter 2). Additionally, in a recent attempt to understand Bose-Einstein condensates close to resonance, Ref. [19] used radio-frequency spectroscopy to probe the effects of Efimov physics. In the accessible region beyond the dilute limit, three-body effects were found to play no significant role. This observation is consistent with the theoretical prediction obtained in chapter 2. In this study, three-body effects were estimated to be negligible compared to two-body contributions in the dilute limit as well as at the point where near-resonance physics fully sets in.

1.3 Two-Dimensional Bose Gases

Two-dimensional quantum many-body systems have been an interesting topic for both condensed matter and nuclear physicists for many years. After realization of confined quantum Bose gases to two-dimensional geometries [35–38], the cold atom community also got attracted to this subject. However, to this day, most of these experimental studies have investigated these cold gases near the Berezinskii-Kosterlitz-Thouless phase transition where quasi-condensates are destroyed by thermal fluctuations [39–41]. Nevertheless, the fundamental properties of two-dimensional Bose gases near absolute zero, where quantum fluctuations prevail thermal effects, have not been completely explored yet. To be more specific, there have been a very limited number of studies conducted on properties of 2D Bose gases near the Feshbach resonance, both on theoretical and experimental aspects.

Two-dimensional Bose gases have two important advantages in comparison with 3D Bose gases near resonance. The first advantage is the fact that the ratio between elastic and inelastic collision cross sections could be in-

creased by a significant amount when atoms are confined to two-dimensional geometries and as a result, the atom loss could be reduced [42]. The second advantage is the universal nature of trimers (three-body bound states) and few-body physics in these gases as two-body binding energy is the only relevant energy scale of the spectrum. This universality implies that physics of trimers in 2D is independent of short distance property of three-body scatterings [43–46], in contrast to the physics of Efimov states in 3D where the absolute energy scale is set by the ultraviolet physics of three-body interactions [34].

Most of the previous studies on two-dimensional Bose gases are carried out in the regime where the range of the repulsive interactions or the core size of the hard-core bosons, a_0, were much smaller than the average distance between the particles [47–49]. Accordingly, the results of these works are only applicable when $\left|\frac{1}{\ln(na_0^2)}\right|$ (n is the density of bosons) is much smaller than unity. This regime is known as the dilute limit of the two-dimensional Bose gases. In our work presented in chapter 4, we focused on the physics beyond the dilute limit for a 2D Bose gas prepared on the upper branch and interacting via strong contact interaction. This setup could be obtained experimentally by using Feshbach resonance and optical confinement (trap geometry) [50–52]. To study 2D Bose gases near resonance, we introduced a 2D effective scattering length a_{2D} that is defined as the position of the node in the wave function for two scattering particles and it is also identified as the size of two-body bound state. In principle, this parameter could be tuned to be larger than inter-atomic spaces and even be infinite.

We applied the same self-consistent approach introduced in Sec. 1.2 to examine the contribution of two- and three-body interactions to physics of 2D Bose gases beyond the dilute limit. Our studies show that there is a competition between three-body attractive interactions and two-body repulsive interactions that determines the behavior of a Bose gas near resonance. We also found that the energetics of these gases in large scattering lengths are universal as they are fully characterized by the effective 2D scattering length.

Finally, we looked into the behavior of the chemical potential for a wide range of interaction strengths. We found that the chemical potential first increases with a_{2D} but very quickly reaches a maximum at $\frac{1}{ln(na_{2D}^2)} = -0.135$ beyond which the Bose gas develops a negative compressibility, where the gas is unstable in size and finally shrinks to a droplet phase. Increasing a_{2D} further brings about an onset instability at $\frac{1}{ln(na_{2D}^2)} = -0.175$. We identified both critical values to be a direct consequence of the significant role played by three-body attractive interactions.

One might wonder how good is our truncation of diagrams by only keeping two- and three-body interactions in our calculations. In Ref. [53], using variational quantum Monte Carlo method, the physics of two-dimensional Bose gases beyond dilute limit is investigated. In this study, the inverse compressibility of the system is calculated for a wide range of $\left|\frac{1}{\ln(na_0^2)}\right|$ and it is shown that the compressibility becomes negative beyond $\frac{1}{ln(na_{2D}^2)} \simeq -0.31$. The inverse compressibility becoming negative is interpreted as the appearance of an instability in the system. This result is consistent with our observation of the maximum point in the chemical potential beyond which the compressibility is negative. The ratio of the contribution to the chemical potential due to three-body interactions to the one due to two-body interactions is negligible for very small scattering lengths, deep in dilute limit, when the physics is mainly dictated by two-body interactions. This ratio grows fast when the gas approaches the resonance, identifying the increasingly prominent role played by three-body attractive interactions. Within our approach, we can estimate the contributions from three-body interactions to the two-body ones to be around 27% near the maximum of chemical potential and 73% in the vicinity of the onset instability.

Chapter 2

Nature of Three-Dimensional Bose Gases: Self-Consistent Approach

2.1 Introduction

Recently, impressive experimental attempts have been made to explore the properties of Bose gases near the Feshbach resonance [14, 17–19]. In these experiments, it has been suggested that when approaching the resonance from the side of small positive scattering lengths in the upper branch, Bose atoms appear to be thermalized within a reasonably short time, well before the recombination processes set in, and so to form a quasi-static condensate. Furthermore, the life-time due to the recombination processes is much longer than the many-body time scale set by the degeneracy temperature. This property of Bose gases near resonance and the recent measurement of the chemical potentials for a long-lived condensate by Navon *et al.* [14] motivate us to make further theoretical investigations on the fundamental properties of Bose gases at large scattering lengths.

The theory of dilute Bose gases has a long history, starting with the Bogoliubov theory of weakly interacting Bose gases [7]. A properly regularized theory of dilute gases of bosons with contact interactions was first put forward by Lee, Huang, and Yang [8] and later by Beliaev [9, 54], who developed a field-theoretical approach. Higher-order corrections were further examined in later years [10, 12, 20]. Since these results were obtained by applying an expansion in terms of the small parameter $\sqrt{na^3}$ (here n is the density and a is the scattering length), it is not surprising that, formally speaking, each of the terms appearing in the dilute-gas theory diverges when the scattering lengths are extrapolated to infinity. As far as we know, resummation of these contributions, even in an approximate way, has been lacking [3]. This aspect, to a large extent, is the main reason why a quali-

[3] Resummation is possible for two scattering atoms in a box of size L. The interaction

tative understanding of Bose gases near resonance has been missing for so long.

There have been a few theoretical efforts to understand the Bose gases at large positive scattering lengths. The numerical efforts have been focused on the energy minimum in truncated Hilbert spaces, which have been argued to be relevant to Bose gases studied in experiments [23–25]. These efforts are consistent in pointing out that the Bose gases are nearly fermionized near resonance. However, there are two important unanswered questions in the previous studies. One is whether the energy minimum found in a restricted subspace is indeed metastable in the whole Hilbert space. The other equally important issue is what is the role of three-body Efimov physics in the Bose gases near resonance.

Below we outline a non-perturbative approach to study the long-lived condensates near resonance. We have applied this approach to explore the nature of Bose gases near resonance and to address the above issues. One concept emerging from this study is that a quantum gas (either fermionic or bosonic) at a positive scattering length does not always appear to be equivalent to a gas of effectively repulsive atoms; this idea, which we believe has been overlooked in many recent studies, plays a critical role in our analysis of Bose gases near resonance.

Our main conclusions are fourfold: (a) energetically, the Bose gases close to unitarity are nearly *fermionized*, i.e., the chemical potentials of the Bose gases approach the Fermi energy of a Fermi gas with equal mass and density; (b) an onset instability sets in at a positive critical scattering length, beyond which the Bose gases appear to lose the metastability as a consequence of the sign change of effective interactions at large scattering lengths; (c) because of a strong coupling with molecules near resonance, the chemical potential reaches a maximum in the vicinity of the instability point; (d) at the point of instability, we estimate, via summation of loop diagrams, the effect of three-body forces to be around a few percent.

Feature (a) is consistent with previous numerical calculations [23–25]; both (b) and (c) are surprising features, not anticipated in the previous numerical calculations or in the standard dilute-gas theory [8, 54]. Our attempt here is mainly intended to reach an in-depth understanding of the energetics, metastability of Bose gases beyond the usual dilute limit as well as the contributions of three-body effects. The approach also reproduces quantitative features of the dilute-gas theory. In Sec. 2.2 and Appendices

energy should scale like $\frac{4\pi a}{mL^3}(1 + A\frac{a}{L} + ...)$ when a is much less than L (A is a constant) but generically saturate at a value of the order of $1/2mL^2$ when a becomes infinite.

A-C, we outline our main calculations and arguments. In Sec. 2.3, we present the conclusion of our studies.

2.2 Chemical Potential, Metastability and Efimov Effects

The Hamiltonian we apply to study this problem is

$$\begin{aligned} H &= \sum_{\mathbf{k}}(\epsilon_{\mathbf{k}}-\mu)b^{\dagger}_{\mathbf{k}}b_{\mathbf{k}} + 2U_0 n_0 \sum_{\mathbf{k}} b^{\dagger}_{\mathbf{k}}b_{\mathbf{k}} \\ &+ \frac{1}{2}U_0 n_0 \sum_{\mathbf{k}} b^{\dagger}_{\mathbf{k}}b^{\dagger}_{-\mathbf{k}} + \frac{1}{2}U_0 n_0 \sum_{\mathbf{k}} b_{\mathbf{k}}b_{-\mathbf{k}} \\ &+ \frac{U_0}{\sqrt{\Omega}}\sqrt{n_0}\sum_{\mathbf{k}',\mathbf{q}} b^{\dagger}_{\mathbf{q}}b_{\mathbf{k}'+\frac{\mathbf{q}}{2}}b_{-\mathbf{k}'+\frac{\mathbf{q}}{2}} + \text{H.c.} \\ &+ \frac{U_0}{2\Omega}\sum_{\mathbf{k},\mathbf{k}',\mathbf{q}} b^{\dagger}_{\mathbf{k}+\frac{\mathbf{q}}{2}}b^{\dagger}_{-\mathbf{k}+\frac{\mathbf{q}}{2}}b_{\mathbf{k}'+\frac{\mathbf{q}}{2}}b_{-\mathbf{k}'+\frac{\mathbf{q}}{2}} + \text{H.c.} \end{aligned} \tag{2.1}$$

Here $\epsilon_{\mathbf{k}} = |\mathbf{k}|^2/2m$, and the sum is over nonzero momentum states. U_0 is the strength of the contact interaction related to the scattering length a via $U_0^{-1} = m(4\pi a)^{-1} - \Omega^{-1}\sum_{\mathbf{k}}(2\epsilon_{\mathbf{k}})^{-1}$, and Ω is the volume. n_0 is the number density of the condensed atoms and μ is the chemical potential, both of which are functions of a and are to be determined self-consistently. Above Hamiltonian is generated by explicitly putting the momenta of some of the creation and annihilation operators equal to zero. For some of the terms, there are more than one way to set the momenta equal to zero. These choices cause different numerical prefactors in front of the terms in the Hamiltonian. For example, the second term in the Hamiltonian is produced by setting the momentum of one of the creation and one of the annihilation operators equal to zero. This term represents the interaction between one condensed atom and one non-condensed atom as incoming particles and one condensed atom and one non-condensed atom as outgoing particles. There are four different ways to produce this term and therefore the numerical prefactor in front of this term is 2 instead of 1/2.

The chemical potential μ can be expressed in terms of $E(n_0,\mu)$, the energy density for the Hamiltonian in Eq. (2.1), with n_0 fixed [9, 55];

$$\mu = \frac{\partial E(n_0,\mu)}{\partial n_0}, \qquad E(n_0,\mu) = \sum_{M=2}^{\infty} g_M(n_0,\mu)\frac{n_0^M}{M!}, \tag{2.2}$$

where $g_M (M = 2, 3, ...)$ are the irreducible M-body potentials that we will focus on below (See Fig. 2.1). The density of condensed atoms n_0 is further constrained by the total number density n as

$$n = n_0 - \frac{\partial E(n_0, \mu)}{\partial \mu}, \tag{2.3}$$

In the dilute limit, the Hartree-Fock energy density is given by Eq. (2.2), with $g_2 = 4\pi a/m$ and the rest of the potentials $g_M, M = 3, 4...$ set to zero. The one-loop contributions to g_M for $M = 3, 4, ...$ in Figs. 2.2(c) and 2.2(d) all scale like $g_2\sqrt{na^3}$, and their sum yields the well-known Lee-Huang-Yang (LHY) correction to the energy density [8]. When evaluated in the usual dilute-gas expansion, g_2 as well as one-loop contributions formally diverge as a becomes infinite. Below we regroup these contributions into effective potentials $g_{2,3...}$ at a finite density n_0 via resummation of a set of diagrams in the perturbation theory. The approximation produces a convergent result for μ.

Before proceeding further, we make the following general remark. In the standard diagrammatic approach [9, 55], the chemical potentials can have contributions from diagrams with L internal lines, S interaction vertices, and X incoming or outgoing zero momentum lines, and $X = 2S - L$. For the normal self-energy (Σ_{11}[4]) and the anomalous counterpart (Σ_{02}) introduced by Beliaev, by classifying the diagrams Hugenholtz and Pines had shown that, in general, the following identity holds [55] in the limit of zero energy and momentum: $\mu = \Sigma_{11} - \Sigma_{02}$. Normal self-energy describes processes in which the number of particles out of the condensate is conserved (one incoming and one outgoing non-condensed particle) and anomalous self-energy describes the absorption of two non-condensed particles to condensate. Similarly, mu describes the processes from condensate to condensate. Hugenholtz-Pines theorem proves that for a general scattering process with different types of internal vertices, zero-energy normal and anomalous self-energies and chemical potential differ by the numerical factors and this numerical factor comes from the number of different ways to connect the external lines of the diagram. For normal self-energy there are two ways to connect the external lines to body of the diagram and for anomalous self-energy and the chemical potential there is only one way to connect these lines. As a result, at low energies $\Sigma_{11} \simeq \mu$. Following a very similar calculation, we further find that

$$\Sigma_{11}(n_0, \mu) = \mu + n_0 \frac{\partial \mu}{\partial n_0}, \tag{2.4}$$

[4]To simplify the notation, in chapters 3, 4 and Appendices we denote Σ_{11} by Σ.

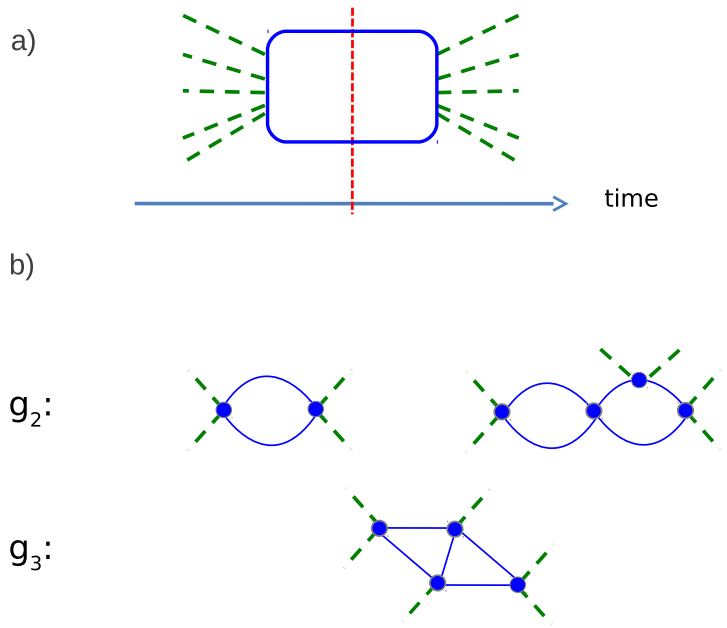

Figure 2.1: (a) Classification of M-body scattering processes: A diagram give contribution to M-body potential if at most M virtual lines of the diagram are cut at time t (dashed red line). All scattering processes are time-ordered from left to right. (b) Sample of diagrams give contribution to two- and three-body potentials.

where $\mu = \partial E(n_0, \mu)/\partial n_0$. The equality in Eq. (2.4) is effectively of a hydrodynamic origin. Following Eq. (2.4), the speed of Bogoliubov phonons [7] v_s can be directly related to an *effective compressibility* $\partial n_0/\partial \mu$ via $mv_s^2 = \Sigma_{11} - \mu = n_0 \frac{\partial \mu}{\partial n_0}$, where the first equality is due to the Hugenholtz-Pines theorem on the phonon spectrum [5]. Note that hydrodynamic considerations had also been employed previously by Haldane to construct the Luttinger-liquid formulation for one-dimensional (1D) Bose fluids [56]. When na^3 is small, Eq. (2.4) leads to the well-known result, $\Sigma_{11} = 2\mu$ (see Appendix D).

The self-consistent approach outlined below is mainly suggested by an observation that a subclass of one-loop diagrams [shown in Fig. 2.2(c)] yields almost all contributions in the LHY correction (see below and Appendices A and B). Resummation of these and their N-loop counterparts can be conveniently carried out by introducing the *renormalized* or effective potentials $g_{2,3}$ as shown in Figs. 2.2(a) and 2.2(b), where all internal lines represent, instead of the noninteracting Green's function $G_0^{-1}(\epsilon, \mathbf{k}) = \epsilon - \epsilon_{\mathbf{k}} + \mu + i\delta$, the interacting Hartree-Fock Green's function, $G^{-1}(\epsilon, \mathbf{k}) = \epsilon - \epsilon_{\mathbf{k}} - \Sigma_{11} + \mu + i\delta$. This approximation captures the main contributions to the chemical potential in the dilute limit because the renormalization of two-body interactions is mainly due to virtual states with energies higher than μ where the Hartree-Fock treatment turns out to be a good approximation (see Appendix D). The self-consistent equation for μ can be derived by estimating $g_{2,3,\ldots}(n_0, \mu)$ diagrammatically (see examples in Fig. 2.2). When neglecting $g_{3,4,\ldots}$ potentials in Eq. (2.2), one obtains

$$\begin{aligned}
\mu &= n_0 g_2(n_0, \mu) + \frac{n_0^2}{4} g_2^2(n_0, \mu) \int \frac{d^3\mathbf{k}}{(2\pi)^3} \frac{\partial \Sigma_{11}/\partial n_0}{(\epsilon_{\mathbf{k}} + \Sigma_{11} - \mu)^2}, \\
n &= n_0 + \frac{n_0^2}{4} g_2^2(n_0, \mu) \int \frac{d^3\mathbf{k}}{(2\pi)^3} \frac{1 - \partial \Sigma_{11}/\partial \mu}{(\epsilon_{\mathbf{k}} + \Sigma_{11} - \mu)^2}, \\
\frac{1}{g_2} &= \frac{m}{4\pi a} + \frac{1}{2} \int \frac{d\mathbf{k}}{(2\pi)^3} \left(\frac{1}{\epsilon_k + \Sigma_{11} - \mu} - \frac{1}{\epsilon_k} \right).
\end{aligned} \tag{2.5}$$

Eqs. (2.4) and (2.5) can be solved self-consistently.

We first benchmark our results with the LHY correction or Beliaev's results for μ by solving the equations in the limit of small na^3. We find $\mu = \frac{4\pi}{m} n_0 a (1 + 3\sqrt{2\pi}\sqrt{n_0 a^3} + \ldots)$, and the number equation yields an es-

[5] If we attribute the energy density to the zero-point energy of Bogoliubov phonons, for an arbitrary scattering length, one can, using Eqs. (2.3) and (2.4), express the condensation density as $n_0 = n - 1/3\pi^2 (\partial \mu/\partial \ln n_0)^{3/2} m^{3/2}$. The long-wavelength dynamics thus sets an upper bound on the value of $\partial \mu/\partial \ln n_0$. The upper bound can be estimated to be $2^{1/3}\epsilon_F$, where $\epsilon_F = (6\pi^2)^{2/3} n^{2/3}/2m$ is the Fermi energy defined for a gas of density n.

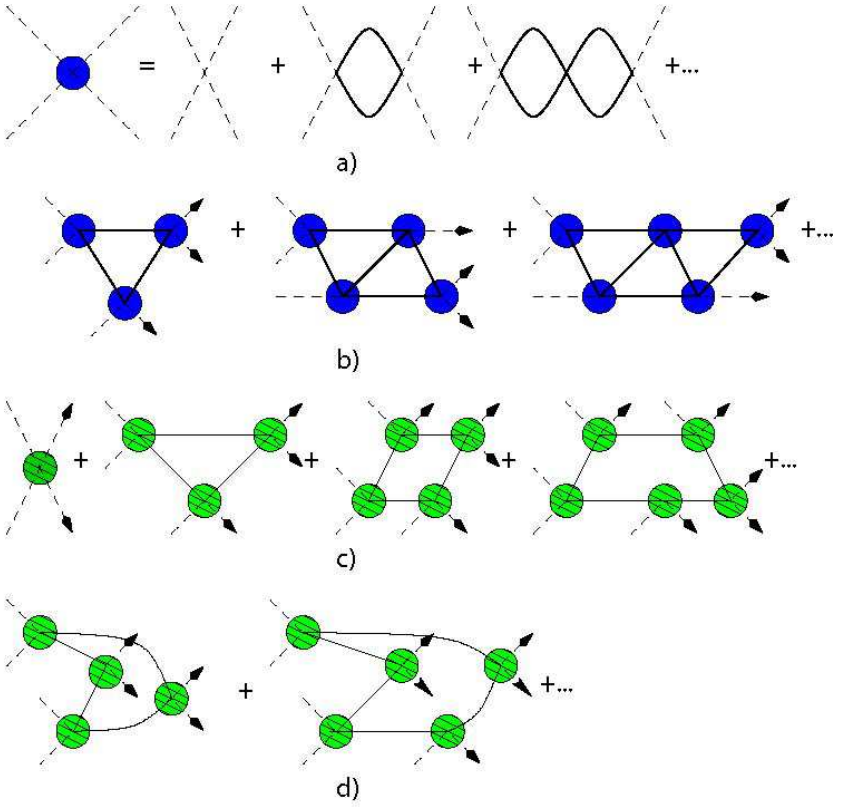

Figure 2.2: Diagrams showing contributions to the total energy $E(n_0, \mu)$. The dashed lines are for $k = 0$ condensed atoms, thick solid internal lines in (a) and (b) are for interacting Green's functions $G^{-1}(\epsilon, \mathbf{k}) = \epsilon - \epsilon_{\mathbf{k}} - \Sigma_{11} + \mu + i\delta$, and thin solid lines in (c) and (d) are for noninteracting Green's function $G_0^{-1}(\epsilon, \mathbf{k}) = \epsilon - \epsilon_{\mathbf{k}} + \mu + i\delta$. (a) The blue circle is for $g_2(n_0, \mu)$; vertices here represent the bare interaction U_0 in Eq. (2.1). (b) $(N = 1, 2, ...)$-loop diagrams that lead to the integral equation for $G_3(-3\eta, p)$ in Eq. (2.6). Note that the usual tree-level diagram violates the momentum conservation and does not exist; the one-loop diagram has already been included in $g_2(n_0, \mu)$ and therefore needs to be subtracted when calculating $g_3(n_0, \mu)$. Arrowed dashed lines here as well as in (c) and (d) stand for outgoing condensed atoms, and the remaining dashed lines stand for incoming ones. (c) and (d) The tree level and examples of one-loop diagrams that yield the usual Lee-Huang-Yang corrections in the limit of small na^3. The self-consistent approach contains contributions from (c)-type diagrams but not (d)-type ones (see further discussion in the text). Patterned green circles also represent the sum of diagrams in (a), but with thin internal lines, or the noninteracting Green's function G_0 lines. All vertices are time ordered from left to right.

timate $n_0/n = (1 - \frac{\sqrt{2\pi}}{2}\sqrt{na^3} + ...)$. The second terms in the parentheses are of the same nature as the LHY correction. Comparing to Beliaev's perturbative result for chemical potential, $\mu = \frac{4\pi}{m} n_0 a(1 + \frac{40}{3\sqrt{\pi}}\sqrt{n_0 a^3} + ...)$ [9], and for the condensation fraction $n_0/n = 1 - \frac{8}{3\sqrt{\pi}}\sqrt{na^3} + ...$, one finds that the self-consistent solution reproduces $99.96\%(= 9\pi\sqrt{2}/40)$ of the Beliaev's correction for the chemical potential, and $83.30\%(= 3\pi\sqrt{2}/16)$ of the depletion fraction in the dilute limit. Technically, one can further examine $g_2(n_0, \mu)$ by expanding it in terms of a and Σ_{11} and then compare with the usual diagrams in the dilute gas theory [9]. One indeed finds that $g_2(n_0, \mu)$ in Eq. (2.5) effectively includes *all* one-loop diagrams with $X = 3, 4, 5, ...$ incoming or outgoing zero-momentum lines that involve a *single pair* of virtually excited atoms [between any two consecutive scattering vertices; Fig. 2.2(c)]. The one-loop diagrams with $X = 4, 5, ...$ incoming or outgoing zero-momentum lines that involve multiple pairs of virtual atoms [Fig. 2.2(d)] have been left out, but they only count for less than 0.04% of Beliaev's result [6].

Following the same line of thought, one can also verify that $g_2(n_0, \mu)$ further contains $(N = 2, 3, 4, ..)$-loop contributions that only involve *one pair* of virtual atoms; each two adjacent loops only share one interaction vertex and are reducible. $g_3(n_0, \mu)$ included below, on the other hand, includes $(N = 2, 3, 4, ..)$-loop contributions with $S = 4, 5...$ interaction vertices that only involve three virtual atoms; two adjacent loops share one internal line instead of a single vertex [see Fig. 2.2(b)] and are irreducible, *i.e.*, cannot be expressed as a simple product of individual loops. Effectively, we take into account all the virtual processes involving either two or three dressed excited atoms in the calculation of the chemical potential μ by including the effective $g_{2,3}$ (defined in Fig. 2.2) in Eq. (2.2). The processes involving four or more excited atoms only appear in $g_{4,5...}$ and are not included here; at the one-loop level following the above calculations, the corresponding contributions from the processes involving multiple pairs of virtual atoms are indeed negligible.

A solution to Eq. (2.5) is shown in Fig. 2.3. An interesting feature of Eq. (2.5) is that it no longer has a real solution once $n^{1/3}a$ exceeds the critical value of 0.18, implying an onset instability; this is not anticipated in the dilute-gas theory [8]. So as a approaches infinity, condensed atoms with a chemical potential μ typically see each other as attractive rather

[6] Two diagrams in Fig. 2.2(d) correspond to the lowest-order contribution to the irreducible renormalized g_4.

than repulsive, resulting in molecules [7]. Thus, beyond the critical point the upper branch atomic gases become strongly coupled to the molecules with a strength proportional to the imaginary part of μ. Consequently, we anticipate that μ decreases quickly beyond the critical scattering length due to the formation of molecules, leading to a maximum in μ in the vicinity of the critical point [8].

A renormalization group approach based on atom-molecule fields was also applied in a previous study to understand Bose gases near resonance[9] [33]. Our results differ from theirs in two aspects. First, in our approach, an onset instability sets in near resonance even when the scattering length is positive, a key feature that is absent in that previous study. Second, when extrapolated to the limit of small na^3, the results in Ref. [33] imply a correction of the order of $\sqrt{na^3}$ to the usual Hartree-Fock chemical potential but with a negative sign, opposite to the sign of LHY corrections. In a recent study [25], a self-consistent mean-field equation was employed, leading to a similar conclusion as the approach in Ref. [33]; the approach does not yield the correct sign of the LHY corrections. And so the onset instability pointed out in our study, which is surprising from the point of view of dilute-gas theory, is also absent there.

The chemical potential near the critical point can be estimated using Eq. (2.5) and is close to $0.93\epsilon_F$, where $\epsilon_F = (6\pi^2)^{2/3}n^{2/3}/2m$ is the Fermi energy defined for a gas of density n. This is consistent with the picture of nearly fermionized Bose gases suggested by the previous calculations and experiments [14, 23–25, 33].

We now turn to the effect of $g_3(n_0, \mu)$ on the chemical potential by including it in Eq. (2.2). We estimate g_3 by summing up all N-loop diagrams with $X = 3$ incoming or outgoing zero momentum lines, which are repre-

[7] One should thus expect an instability in a near-resonance Fermi gas as well. The pairing dynamics previously emphasized in D. Pekker, M. Babadi, R. Sensarma, N. Zinner, L. Pollet, M. W. Zwierlein, and E. Demler, Phys. Rev. Lett. **106**, 050402 (2011) is consistent with this conclusion. Molecule dynamics in a Bose-Einstein condensate was also studied in L. Yin, Phys. Rev. A **77**, 043630(2008). Although LHY corrections and three-body forces were not taken into account in that random phase approximation, the molecule formation discussed there appears to be consistent with our conclusion on the loss of metastability.

[8] Interestingly, a maximum in the Bragg line shift at a finite wave vector was found when the LHY correction is 0.22 in Ref. [17]. The maximum in μ in this paper occurs when the LHY correction is 0.45.

[9] For field-theory-based approaches to the lower-branch unitary gases, see Y. Nishida and D. T. Son, Phys. Rev. Lett. **97**, 050403 (2006), P. Nikolic and S. Sachdev, Phys. Rev. A **75**, 033608 (2007) and M. Y. Veillette, D. E. Sheehy, and L. Radzihovsky, Phys. Rev. A **75**, 043614 (2007).

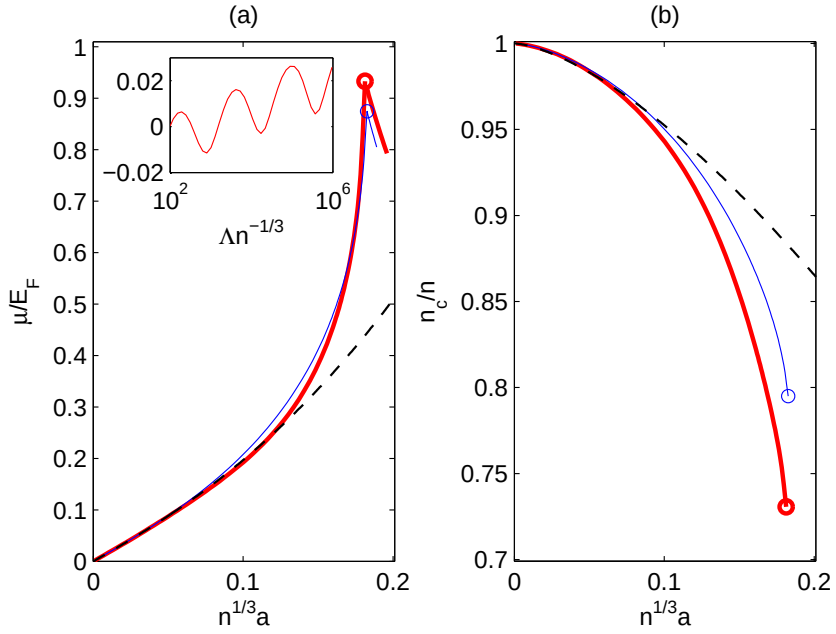

Figure 2.3: (a) Chemical potential μ in units of the Fermi energy ϵ_F and (b) condensation fraction as a function of $n^{1/3}a$. Beyond a critical value of 0.18 (shown as circles), the solutions become complex, and only the real part of μ is plotted; the imaginary part of μ scales like $\epsilon_F(a/a_{cr}-1)^{1/2}$ near a_{cr}. (However, the sharp transition would be smeared out if the small imaginary part of G_3 is included.) Dashed lines are the result of the Lee-Huang-Yang theory, thin solid blue lines are the solution without three-body effects (i.e. $g_3 = 0$). Thick solid red lines are the solution with g_3 included; the momentum cutoff is $\Lambda = 100n^{1/3}$. The inset is the relative weight of three-body effects in the chemical potential as a function of $\Lambda n^{-1/3}$ at the critical point.

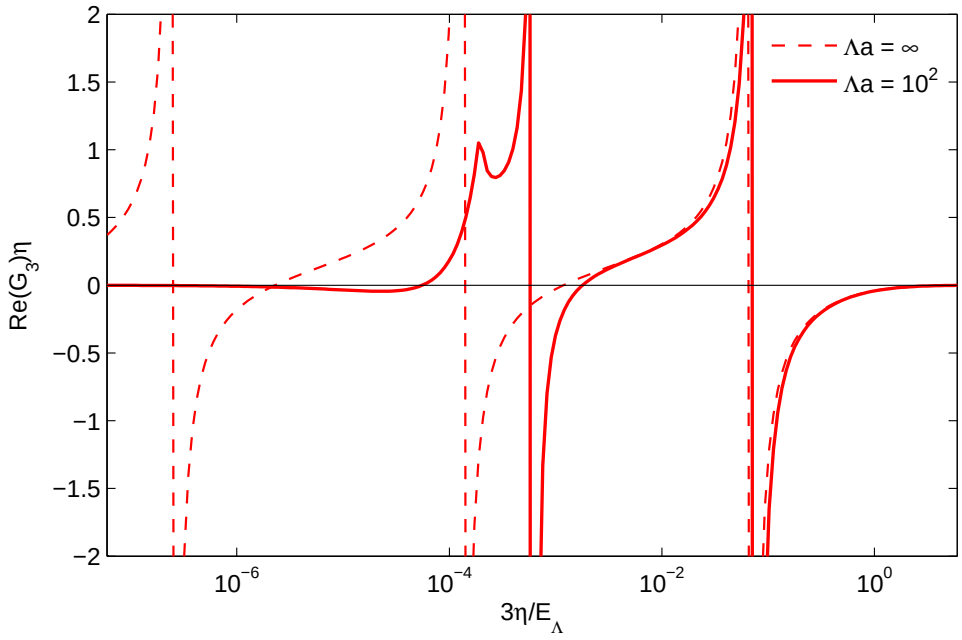

Figure 2.4: $\mathrm{Re}G_3(-3\eta,0)\eta$ as a function of $\eta = \Sigma_{11}(n_0) - \mu$. $E_\Lambda = \Lambda^2/2m$ and Λ is the momentum cut-off. The imaginary part of G_3 (not shown) is zero once $3\eta > 1/(ma^2)$.

sented in Fig. 2.2(b). All diagrams have three incoming or outgoing zero momentum lines but with $N = 2, 3, ..$ loops. The effect of three-body forces due to Efimov states [34] was previously studied in the dilute limit [20]. The deviation of the energy density from the usual universal structures (i.e., only depends on na^3) was obtained by studying the Efimov forces in the zero-density limit. The contribution obtained there scales like a^4, apart from a log-periodic modulation [57], and again formally diverges as other terms when approaching a resonance.

It is necessary to regularize the usual a^4 behavior at resonance in the three-body forces by further taking into account the interacting Green's function when calculating the N-Loop six-point correlators. Including the self-energy in the calculation, we remove the a^4 dependence that usually appears in the Bedaque-Hammer-Van Kolck theory for the three-body interactions [57]; when setting μ, Σ_{11} to zero, the equation collapses into the corresponding equation for three Bose atoms in vacuum, which was previously employed to obtain the β function for the renormalization flow in an atom-dimer field-theory model. The sum of loop diagrams in Fig. 2.2(b), $G_3(-3\eta, p)$, satisfies a simple integral equation (m set to be unity; see Appendix C):

$$\begin{aligned} G_3(-3\eta, p) &= \frac{2}{\pi}\int dq K(-3\eta; p, q) \\ &\times \frac{q^2}{\sqrt{\frac{3q^2}{4} + 3\eta} - \frac{1}{a}}[G_3(-3\eta, q) - \frac{1}{q^2 + 3\eta}], \\ K(-3\eta; p, q) &= \frac{1}{pq}\ln\frac{p^2 + q^2 + pq + 3\eta}{p^2 + q^2 - pq + 3\eta}, \end{aligned} \tag{2.6}$$

where we have introduced $\eta = \Sigma_{11}(n_0) - \mu$. $G_3(-3\eta, 0)$ is plotted numerically in Fig. 2.4. Three-body potential $g_3(n_0, \mu)$ is related to $G_3(-3\eta, 0)$ via $g_3(n_0, \mu) = 6g_2^2 \mathrm{Re}\tilde{G}_3(-3\eta, 0)$ where $\tilde{G}_3$ is obtained by further subtracting from G_3 the one-loop diagram in Fig. 2.2(b) because its contribution has already been included in $g_2(n_0, \mu)$. The structure of $G_3(-3\eta, 0)$ is particularly simple at $a = +\infty$, as shown in Fig. 2.4: It has a desired log-periodic behavior reflecting the underlying Efimov states [34]. When 3η is close to an Efimov eigenvalue $B_n = B_0 \exp(-2\pi n/s_0)$ [$n = 1, 2, 3....$,$\exp(2\pi/s_0) = 515$] that corresponds to a divergence point in Fig. 2.4, the three-body forces are the most significant. When 3η is in the close vicinity of zeros in Fig. 2.4, the three-body forces are the negligible and Bose gases near resonance are dictated by the g_2 potential.

When including the real part of $g_3(n_0, \mu)$ in the calculation of $E(n_0, \mu)$, we further get an estimate of three-body contributions to the energy density and chemical potential μ. The contribution is non-universal and depends on the momentum cutoff in the problem. For typical cold Bose gases, it is reasonable to assume the momentum cutoff Λ in the integral equation Eq. (2.6) to be $100n^{1/3}$ or even larger. Quantitative effects on the chemical potential are presented in Fig. 2.3.

Note that $G_3(-3\eta, 0)$ also has an imaginary part even at small scattering lengths; this corresponds to the well-known contribution of three-body recombination. The onset instability discussed here will be further rounded off if the imaginary part of G_3 is included. However, for the range of parameters we studied, both the real and imaginary parts of G_3 appear to be numerically small (see also Fig. 2.3); the energetics and instabilities near a_{cr} are found to be mainly determined by the renormalized two-body interaction $g_2(n_0, \mu)$.

2.3 Summary

In conclusion, we have investigated the energetics of Bose gases near resonance beyond the Lee-Huang-Yang dilute limit via a simple resummation scheme. We have also pointed out an onset instability and estimated three-body Efimov effects that had been left out in recent theoretical studies of Bose gases near resonance [23–25, 33]. In addition, we showed that the Bose gases are nearly fermionized before an onset instability sets in near resonance. The non-perturbative method presented above becomes exact in the dilute limit if one only keeps the virtual processes involving two atoms. In this limit, this approach reproduces 99.96% of the LHY result for the chemical potential. Near resonance, it was established that the three-body Efimov effect only contributes a few percent to the overall chemical potential. Unless the contributions coming from M-body interactions are a non-monotonic function of M, we believe the contributions from four-, five-, etc. body interaction processes should be even smaller and hence negligible.

The recent study presented in Ref. [32] supports the above argument. In this study, the authors combined ϵ-expansion method near four dimensions with the self-consistent approach introduced in this chapter to investigate the physics of Bose gases in higher dimensions. Using this technique, they could estimate the full expression of the total energy density of the system including all the M-body potentials. They found that near resonance, only contribution from the one-loop diagrams are important and higher order

loops contributions are suppressed by higher powers of ϵ. Moreover, they showed that the two-body interaction potential has the main contribution to the chemical potential of a Bose gas found by solving self-consistent equations, indicating the dominant role of two-body scattering events in higher dimensions. This study implies that the contribution of M-body potentials with $M > 2$ becomes less and less important when one goes to higher dimensions. On the other hand, in our study on two-dimensional Bose gases presented in chapter 4 we have shown that three-body interaction plays an important role in the physics of these gases beyond the dilute limit. But, as mentioned in this chapter in three dimensions the contribution of these scattering events is approximated to be around a few percent near the instability point. So, we predict that the non-trivial results we found in this chapter would remain qualitatively unchanged by adding the contribution of M-body interaction potentials with $M > 3$.

Chapter 3

Nature of Three-Dimensional Bose Gases: Renormalization Group Approach

3.1 Introduction

In this chapter, we make an attempt to understand the fundamental properties of Bose gases near Feshbach resonance via examining the intriguing interplay between the few- and many-body physics in Bose gases at large positive scattering lengths. For this purpose, we introduce a simple self-consistent renormalization-group-equation approach to address both sides of the coin. Many-body properties of a quantum gas are shown to influence the renormalization flow of few-body running coupling constants resulting in the change of the sign of the effective two-body interaction constants. That in return completely dictates the many-body physics near resonance and leads to peculiar features in the chemical potentials. We limit ourselves to the resonances with a very short effective range.

The approach outlined in this chapter is an alternative to the more elaborated diagrammatic resummation mentioned in chapter 2. The two approaches yield almost identical results. In Sec. 3.2, we first carry out a simple scaling argument, as a caricature of resonating Bose gases, illustrating the relevance of fermionization in Bose gases near resonance, and discuss the limitation of the coarse grain procedure. We also remark on a close relation between the effective two-body interactions and Lee-Huang-Yang corrections in Ref. [8]. In Secs. 3.3 and 3.4, we discuss the energetics of dimers and trimers in condensates and explore the implications on the many-body physics. Especially, we point out that in addition to the fermionization phenomenon, an instability sets in at a positive critical scattering length as a signature of formation of dimers in condensates. We also show this aspect is a consequence of the sign-change of the renormalized two-body interactions between the condensed atoms; the effect of the condensate on the two-body

interaction constant is investigated via taking into account the self-energy of dimers and via imposing an infrared boundary condition for the renormalization flow. In Sec. 3.5, we summarize the results of diagrammatic resummation presented in chapter 2. In Sec. 3.6, we conclude our studies.

3.2 A Caricature

3.2.1 Relevance of Fermionization: A Scaling Argument

The energetics of Bose gases near resonance can be qualitatively understood via a coarse grain procedure which is more or less equivalent to the real space renormalization transformation. The simplest implementation of this is to first divide a quantum gas into N blocks each of which is of the size of $\xi \times \xi \times \xi$ where $\xi = 1/\sqrt{2m\mu}$ is the coherence length and μ is the chemical potential. Because the chemical potential is a non-additive thermodynamic quantity, it is natural to define it as the change of energy when adding an additional atom to a particular block and the effect of other blocks is to set an appropriate boundary condition. Therefore, the chemical potential can be considered as the interaction energy between the added atom and existing atoms in the block. If we further assume the interaction energy is dictated by a pairwise one, then

$$\mu = \epsilon_2(\xi, a; n) n\xi^3 \tag{3.1}$$

where $\epsilon_2(L = \xi, a; n)$ is the characteristic interaction energy between two atoms in the block and $n\xi^3$ is the number of atoms in the block with n being the number density. This is a standard coarse grain procedure which relates a microscopic quantity $\epsilon_2(\xi, a; n)$ and a thermodynamic quantity, the chemical potential μ. The estimate of $\epsilon_2(\xi, a; n)$ itself is a full many-body problem that is usually very difficult to carry out. In the dilute limit, however, one can show that when two atoms interact in a box of size ξ, the probability of being scattered by the third particle is negligible because the mean free path l is proportional to $1/n4\pi a^2$ (a is the scattering length) much longer than ξ. In fact,

$$\frac{\xi}{l} \sim \frac{a}{\xi} \sim \sqrt{na^3} \tag{3.2}$$

which is small in the low density dilute limit. So at least in this limit, we can approximate $\epsilon_2(L = \xi, a; n)$ as the energy of two interacting atoms

$\epsilon_2(L=\xi, a; n=0)$ in an empty box of the size of the block. If we assume this is also qualitatively correct even in the unitary limit, then we have a very simple self-consistent equation; the only knowledge we need to solve this equation is how two atoms interact in a box of size ξ at arbitrary scattering length a. $\epsilon_2(\xi, a; 0)$ for a contact resonance interaction can be worked out, either by assuming two atoms are in a harmonic trap of harmonic length ξ or in a block of size ξ. The asymptotic behaviors are universal up to numerical prefactors. For two atoms in a block of size L,

$$\epsilon_2(L, a; 0) = \begin{cases} \frac{4\pi a}{mL^3}(1 + C_1\frac{a}{L} + ...) & \text{when } a \ll L; \\ \frac{C_2}{2mL^2} & \text{when } a \gg L. \end{cases} \tag{3.3}$$

$C_{1,2}$ are two positive prefactors depending on the details of the block and are of little importance for our qualitative discussions here. It is important to notice that at resonance, $\epsilon_2(L=\xi, a=\infty; 0)$ is finite and scales like the kinetic energy of an atom moving in an empty box of size ξ.

Substituting the results in Eq. (3.3) into Eq. (3.1), one obtains the estimate of chemical potential. In the dilute limit,

$$\mu = \frac{4\pi a n}{m}(1 + C_1\sqrt{8\pi n a^3} + ...); \tag{3.4}$$

the correction to the first Hartree-Fock term is the leading finite size correction to the interaction energy and belongs to the well-known Lee-Huang-Yang effect. When a approaches infinity on the other hand, this simple procedure leads to the prediction of fermionization. That is

$$\mu = \frac{1}{2m\xi^2} = \frac{C_2 n\xi}{2m}, \qquad \text{or} \qquad \mu \sim \frac{n^{2/3}}{2m}, \tag{3.5}$$

which scales as the Fermi energy of a Fermionic quantum gas with the same density and mass. Although crude, the coarse grain shown here points to a phenomenon that was previously seen in a few numerical calculations. Given that it is very simple, we consider it quite a success. The relevance of fermionization to Bose gases near resonance was observed in a few theoretical studies [23–25, 33].

This aspect of Bose gases near resonance is also an essential feature of Tonks-Girardeau gases or hard-core bosons in one dimension [58, 59]. The one-dimensional Bose fluids were later further studied using the Luttinger liquid formulation [56].

3.2.2 Running Two-Body Interaction Constants

But how good is the starting point that near resonance we can approximate $\epsilon_2(L, a; n)$ as the two-particle interaction in an empty box completely neglecting the effect of many other identical particles? To address this, we estimate $\epsilon_2(L, a; n)$, the interaction of two atoms in a box of size L via employing a more sophisticated approach, the real space renormalization transformation (RSRT) which further takes into account the many-body effect on $\epsilon_2(L, a; n)$. This approach indicates that fermionization cannot be the whole story.

Consider, instead of $\epsilon_2(L, a; 0)$ discussed above,

$$g_2(L, a; n) = \epsilon_2(L, a; n)L^3 \tag{3.6}$$

which is the effective strength of the short range two-body interaction. Again we divide the length scales in RSRT into two regimes that are separated by ξ: the short distance regime in which two- and few-body physics dominates and the long wavelength regime where the many-body collective effect dominates. ξ defines the interface where the microscopic few-body parameter g_2 at shorter distance needs to match the macroscopic coarse grain condition.

So at scales smaller than ξ, we can employ the RSRT of the two-body running coupling constant $g_2(L, a; 0)$ in vacuum to monitor the effective interaction. This approximation could be done because the finite density has very little effect in this regime i.e. $g_2(L, a; n) = g_2(L, a; 0) + O(L/\xi)$. At larger distances, because g_2 defined here is subject to a thermodynamic constraint of the chemical potential at $L \sim \xi$, the effect of the condensate on g_2 or ϵ_2 is to impose a boundary condition on the flow of $g_2(L, a; n)$ via the coarse-grain condition in Eq. (3.1). And in this approach, the collective physics at scales larger than ξ influences the flow solely through a simple boundary condition.

Practically, since L defines the size of micro-blocks in the renormalization procedure, it therefore defines the momentum cut-off via $\Lambda = L^{-1}$. The transformation from L to L' is equivalent to rescaling the momentum from Λ to $\Lambda' = L'^{-1}$. To obtain the running coupling constant, one can use the standard momentum-shell renormalization procedure to track the transformation from the original g_2 to the new g_2' when the Hilbert space or the momentum cut-off is rescaled from Λ' to $\Lambda = \Lambda' - \delta\Lambda$ (see Fig. 3.1).

The reduced two-body Hamiltonian we use for this illustration is

$$
\begin{aligned}
H_{2-body} &= H_< + H_> + H_{><} \\
H_< &= \sum_{\mathbf{k}} \epsilon_{\mathbf{k}} b^\dagger_{\mathbf{k}} b_{\mathbf{k}} + \frac{g_2}{2\Omega} \sum_{\mathbf{k},\mathbf{k}'} (b^\dagger_{\mathbf{k}} b^\dagger_{-\mathbf{k}} b_{\mathbf{k}'} b_{-\mathbf{k}'} + h.c.) \\
H_> &= \sum_{\mathbf{p}} \epsilon_{\mathbf{p}} b^\dagger_{\mathbf{p}} b_{\mathbf{p}} + \frac{g_2}{2\Omega} \sum_{\mathbf{p},\mathbf{p}'} (b^\dagger_{\mathbf{p}} b^\dagger_{-\mathbf{p}} b_{\mathbf{p}'} b_{-\mathbf{p}'} + h.c.) \\
H_{><} &= \frac{g_2}{2\Omega} \sum_{\mathbf{k},\mathbf{p}} b^\dagger_{\mathbf{k}} b^\dagger_{-\mathbf{k}} b_{\mathbf{p}} b_{-\mathbf{p}} + h.c.. \qquad (3.7)
\end{aligned}
$$

Here $b^\dagger_{\mathbf{k}}(b_{\mathbf{k}})$ is the creation (annihilation) operator for a Bose atom with momentum $\mathbf{k}$ and Ω is the volume. The sum in $H_<$ is over momenta $|\mathbf{k}|, |\mathbf{k}'|$ smaller than Λ and the sum in $H_>$ is over the states within the shell in Fig. 3.1, i.e. $|\mathbf{p}|, |\mathbf{p}'| \in [\Lambda, \Lambda']$. $H_{><}$ describes the off-shell scattering from low momentum states with $|\mathbf{k}| < \Lambda$ into the high energy states with momenta $\mathbf{p}$ within the shell and vice versa. This interaction can induce an effective scattering between low momentum states $(\mathbf{k}, -\mathbf{k})$ and $(\mathbf{k}', -\mathbf{k}')$, $|\mathbf{k}|, |\mathbf{k}'| \leq \Lambda$, via virtual states $(\mathbf{p}, -\mathbf{p})$ within the shell.

When rescaling, the states within the shell thus lead to an additional contribution to the two-body interaction in $H_<$. One can obtain the beta-function for the renormalization equation diagrammatically. This calculation is very similar to the T-matrix calculation except one should restrict to the virtual states within the shell between Λ' and $\Lambda = \Lambda' - \delta\Lambda$. The diagram in Fig. 3.1 represents such an additional contribution to the effective two-body interaction,

$$
\begin{aligned}
-i\delta g_2(\Lambda') &= i^4 g^2(\Lambda') \int' \frac{d\mathbf{p}}{(2\pi)^3} \int \frac{d\epsilon}{2\pi} G^0(\epsilon, \mathbf{p}) G^0(-\epsilon, -\mathbf{p}), \\
G^0(\epsilon, \mathbf{p}) &= \frac{1}{\epsilon - \frac{\mathbf{p}^2}{2m} + i\delta^+}. \qquad (3.8)
\end{aligned}
$$

Here the momentum integral $\int'$ is over the states within the shell shown in Fig. 3.1, i.e. $\Lambda' > |\mathbf{p}| > \Lambda$.

After carrying out the energy and momentum integrals, one can easily find the transformation for the two-body interaction constant

$$
g_2(\Lambda' - \delta\Lambda) = g_2(\Lambda') - \frac{m}{2\pi^2} g_2^2(\Lambda') \delta\Lambda + O(\delta\Lambda^2). \qquad (3.9)
$$

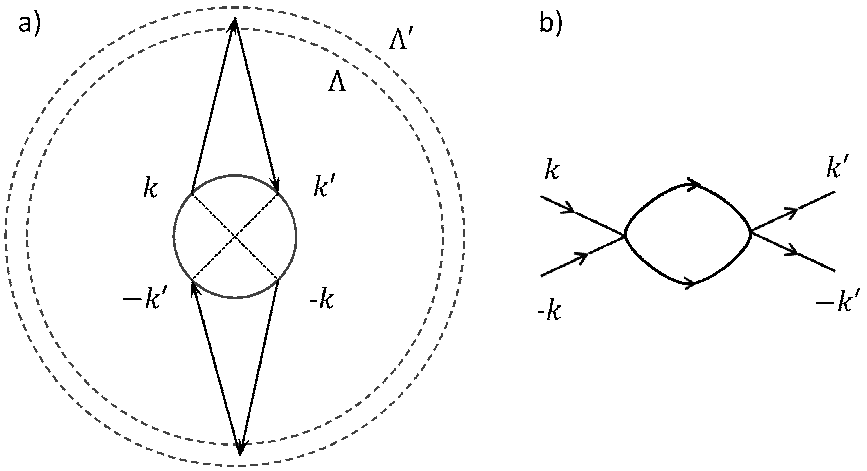

Figure 3.1: a) Schematic of the renormalization of the low energy on-shell scattering amplitude. An initial state $(\mathbf{k}, -\mathbf{k})$ on the inner sphere is first scattered into off-shell high energy states $(\mathbf{p}, -\mathbf{p})$ represented by the shell region between two outer momentum spherical surfaces (dashed) before finally being scattered back into $(\mathbf{k}', -\mathbf{k}')$ on the inner sphere. Here the outer dashed spherical surface is defined by Λ' and the inner dashed one by Λ; $\Lambda \leq |\mathbf{p}| \leq \Lambda'$. b) The one-loop diagram that leads to the renormalization equation below. The internal lines are for states within the shell region described in a). Each vertex stands for the two-body interaction $g_2(\Lambda')$.

The transformation of g_2 under the real space rescaling can be obtained by converting Λ to L^{-1}. For a quantum gas with a finite density, we therefore have ($\tilde{g}_2 = g_2/L$)

$$\frac{\partial \tilde{g}_2(L)}{\partial \ln L^{-1}} = \frac{m}{2\pi^2}\tilde{g}_2^2(L) + \tilde{g}_2(L),$$
$$\tilde{g}_2(L = R^*) = \frac{U_0}{R^*}, \quad \tilde{g}_2(L = \xi) = \frac{\mu}{n\xi}. \tag{3.10}$$

The boundary condition at $L = \xi$ is exactly the condition in Eq. (3.1), i.e. at scale ξ the microscopic running coupling constant has to match the thermodynamic constraint suggested by μ, assuming the main contribution to μ is from the two-body interaction $g_2(L, a; n)$. At a very short distance R^*, the boundary condition is set by U_0, the strength of the *bare* two-body short range attractive interaction with range R^*. For the resonance phenomena we are interested in, R^* is always much smaller than a.

By contrast, in a vacuum the coupling constant g_2 should flow to the value of $4\pi a/m$, the standard form of the two-body effective interaction, or

$$\frac{\partial \tilde{g}_2(L)}{\partial \ln L^{-1}} = \frac{m}{2\pi^2}\tilde{g}_2^2(L) + \tilde{g}_2(L),$$
$$\tilde{g}_2(L = R^*) = \frac{U_0}{R^*}, \quad \tilde{g}_2(L \to \infty, a; n = 0) = \frac{4\pi a}{mL}. \tag{3.11}$$

For a bare attractive two-body interaction with strength $U_0(< 0)$ and range R^*, the boundary condition at $L = \infty$ in Eq. (3.11) establishes a well-known relation between U_0 and the scattering lengths a. $g_2 = L\tilde{g}_2(L)$ as the solution to Eq. (3.11) can be expressed in terms of a,

$$g_2(L, a; n = 0) = \frac{4\pi a}{m}\frac{1}{1 - \frac{2a}{\pi L}}. \tag{3.12}$$

Obviously, g_2 appears to be repulsive only in the limit of long wavelength when $L \gg a$. At short distances $R^* < L \ll a$,

$$g_2(L, a; n = 0) \to -\frac{2\pi^2 L}{m} \tag{3.13}$$

is negative and independent of R^* or a. Eq. (3.13) indicates a universal form of the two-body running coupling constant that induces resonance scatterings. This crossover from repulsive to attractive interactions happens at $L^* \sim a$.

One can further show that for a repulsive interaction that leads to the same zero energy scattering length a, g_2 also flows toward the value of $4\pi a/m$ when L is much longer than the range of interaction. For instance for a hard-core potential with $a = R^*$ where R^* is the radius of the hard-core, one obtains the same expression as Eq. (3.12) except that the range of L is $2a/\pi < L < \infty$; and not surprisingly, g_2 in this case is repulsive for arbitrary length scales.

So only in the long wavelength limit, the attractive interaction with positive scattering lengths yields the same physics as the repulsive ones even though at short distances they are distinctly different. At the zero energy, the effective interaction is $4\pi a/m$, repulsive as long as a is positive disregarding whether the bare interactions are repulsive or attractive. For a long time, this has been a common belief in the field of cold atom physics.

As we will see below, this no longer holds near resonance when the many-body renormalization effects due to condensed atoms are further taken into account. The reason for this is that the low energy window where we can approximate the resonance interaction as a repulsive one (which is of order $1/ma^2$) gets so narrow that the effect of condensates on the two-body coupling becomes particularly pronounced near resonance.

The renormalization-equation approach had been previously applied to analyze the effective field theories for few-body scattering phenomena [60]. They were also successfully employed to identify the coupling constants and quantum phases in the field theory models for the lower branch unitary gases [61–63]. It was later employed to explore the physics of geometric resonances and confinement induced scattering phenomena [64]. Our application to Bose gases is perhaps another excellent example to demonstrate that the simple and generic approach of renormalization can lead to some surprising breakthroughs.

Eq. (3.10) is a RSRT equation which satisfies Eq. (3.1) and yields an estimate of $\epsilon_2(\xi, a; n)$ or g_2. The boundary condition leads to a self-consistent equation for μ. When expressing in terms of a using the solution to Eq. (3.11), one finds

$$\mu = n\frac{4\pi a}{m}\frac{1}{1 - \frac{2}{\pi}\sqrt{2m\mu}a}. \tag{3.14}$$

Again in the limit where a is much less than ξ, the equation yields the Hartree-Fock energy plus the correction of Lee-Huang-Yang character;

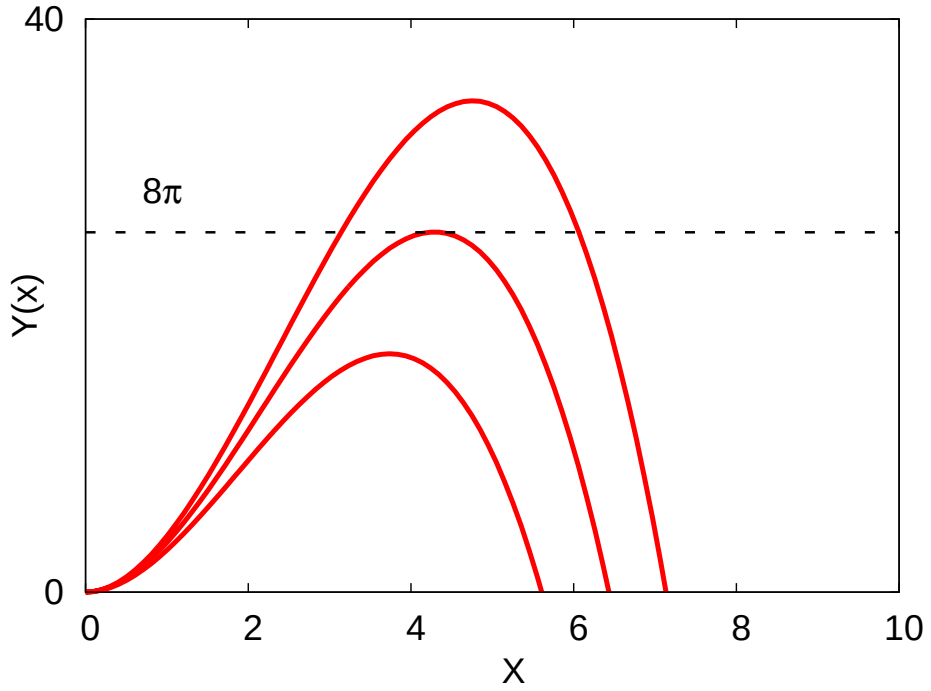

Figure 3.2: The solution to the self-consistent boundary condition, Eq. (3.14). The solution is obtained by solving $Y(x) = x^2/(n^{1/3}a) - (2/\pi)x^3 = 8\pi$, where $x^2 = 2m\mu/n^{2/3}$. From the top to bottom are $Y(x)$ for $a < a_{cr}$, $a = a_{cr}$ and $a > a_{cr}$. At a_{cr}, the equation has only one solution and above a_{cr} there are no real solutions.

$$\mu = \frac{4\pi a n}{m}(1 + \frac{4\sqrt{2}}{\sqrt{\pi}}\sqrt{na^3} + ...). \tag{3.15}$$

Another solution of μ scales as $1/a^2$ consistent with the binding energy of lower branch molecules and we do not consider here. In the unitary limit however, the equation not only indicates fermionization but also suggests a critical point beyond which there are no real solutions to the equation. This is most obvious when a is infinity and g_2 becomes *negative*. This property of Eq. (3.14) is illustrated in Fig. 3.2. One can show that at the critical point,

$$n^{1/3}a_{cr} = \frac{1}{6}\pi^{1/3}, \quad \mu_{cr} = 2\pi^{4/3}\frac{n^{2/3}}{m}; \tag{3.16}$$

two real solutions merge into a single one. Beyond this point, the equation yields a complex solution to the chemical potential.

The RSRT suggests an important feature that is absent in the simplest coarse grain approach (Eqs. (3.1) and (3.3)). It turns out that near resonance, there is a substantial modification of the underlying two-body physics, i.e. dimer energetics and therefore the interaction energy between condensed atoms ϵ_2; it can no longer be justified to approximate $\epsilon_2(\xi, a; n)$ as the interaction energy in an empty box or at zero density. In fact as shown below, the uplifted dimers (towards condensates) cause an instability of atomic condensates when approaching the resonance from the molecular side. The emergency of the imaginary part of the chemical potential beyond the critical point signifies a hybridization between atoms and molecules which is missing in the simplest coarse grain argument. In the next section, we further elaborate on this fascinating aspect of Bose gases near resonance.

3.3 Dimers and Trimers in a Condensate: The Spectrum Flow

How are the dimers or trimers formed in the presence of a condensate or of a quantum gas? In the context of quantum mixtures, there have been a few attempts to answer this question: how are the few-body structures affected by the presence of a Fermi surface [65–68]? Surprisingly, so far little effort has been made to understand the dimers and trimers in the presence of a condensate, partially because the background of a condensate is more dynamical compared to that of a Fermi sea. Since this plays a critical role

in the interplay between few- and many-body physics that interests us, here we make an effort to estimate the effect.

It is possible to solve the two-body and three-body S-matrices in the presence of the many-body effect due to the self-energy. Assuming the self-energy of quasi-particles is Σ, [10] one finds that for two incoming atoms with momentum $\mathbf{p}, -\mathbf{p}$ scattered into $\mathbf{p}', -\mathbf{p}'$ and with total frequency E,

$$G_2(E;\mathbf{p},\mathbf{p}') = U_0 + U_0 \int \frac{d^3\mathbf{q}}{(2\pi)^3} \frac{1}{E - 2\eta - 2\epsilon_{\mathbf{q}} + i\delta^+} G_2(E;\mathbf{q},\mathbf{p}') \quad (3.17)$$

where $\eta = \Sigma - \mu$. A diagrammatic representation is given in Fig. 3.3(a). In the dilute limit, $\eta = \mu = 4\pi an/m$; in general, Σ, μ and η are unknown and need to be determined self-consistently later on. For now, we simply assume that η is a given parameter (see Appendix D).

$G_2(E;\mathbf{p},\mathbf{p}') = G_2(E)$ as a result of the short range interaction and note that when $\eta = 0$ or in vacuum, $G_2^0(E=0) = 4\pi a/m$ (superscript 0 indicates the case of vacuum) and $G_2^0(E) = 4\pi a/m(1 - ia\sqrt{mE})$. One can then show that in the presence of the condensate,

$$G_2(E) = G_2^0(E - 2\eta); \quad (3.18)$$

the pole of $G_2(E)$ is shifted from the pole in vacuum by 2η. The pole defines the dimer binding energy and so

$$\epsilon_D = \epsilon_D^0 + 2\eta \quad (3.19)$$

where ϵ_D and ϵ_D^0 are the binding energy of dimers in the presence of a condensate and in vacuum, respectively. At a given positive scattering length, the dimer spectrum flows (in the energy space) towards the zero energy where the condensate lives as one increases the η.

One can also calculate the amplitude of three-body scatterings corresponding to the processes described in Fig. 3.3(b). We consider a general case where three incoming momenta are $\mathbf{k}_1 = \mathbf{p}/2 - \mathbf{q}$, $\mathbf{k}_2 = \mathbf{p}/2 + \mathbf{q}$ and $\mathbf{k}_3 = -\mathbf{p}$, and outgoing ones are $\mathbf{k}_1' = \mathbf{p}'/2 - \mathbf{q}'$, $\mathbf{k}_2' = \mathbf{p}'/2 + \mathbf{q}'$ and $\mathbf{k}_3' = -\mathbf{p}'$. The scattering amplitude between theses states are then given by $A_3(E;\mathbf{p},\mathbf{p}')$ where $\mathbf{q}$ and $\mathbf{q}'$ do not enter explicitly; it represents the sum of diagrams identical to Fig. 3.3(b).

It is more convenient to work with the reduced amplitude $G_3(E;\mathbf{p}) = A_3(E;\mathbf{p},0)$ where $\mathbf{p}'$ is already taken to be zero. $G_3(E;\mathbf{p})$ itself obeys a

[10] As explained in chapter 2, Σ stands for Σ_{11}

simple integral equation as can be seen by listing the terms in the summation explicitly. The diagrams in Fig. 3.3(b) yield (see Appendix E; the mass is set to be one, i.e. $m = 1$),

$$\begin{aligned}\frac{1}{4}G_3(E,p) &= -\frac{1}{2}K(E-3\eta;p,0) \\ &+ \frac{2}{\pi}\int dq \frac{K(E-3\eta;p,q)q^2}{\sqrt{\frac{3}{4}q^2+3\eta-E+i\delta^+}-\frac{1}{a}}\frac{-1}{q^2+3\eta-E} \\ &+ \left(\frac{2}{\pi}\right)^2\int dqdq'\left(\frac{K(E-3\eta;p,q)q^2}{\sqrt{\frac{3}{4}q^2+3\eta-E}-\frac{1}{a}}\frac{K(E-3\eta;q,q')q'^2}{\sqrt{\frac{3}{4}q'^2+3\eta-E}-\frac{1}{a}}\right. \\ &\times \left.\frac{-1}{q'^2+3\eta-E}\right)+\cdots \end{aligned} \tag{3.20}$$

where $K(E-3\eta;p,q)$ is the kernel defined as

$$K(E-3\eta;p,q) = \frac{1}{pq}\ln\frac{p^2+q^2+pq+3\eta-E}{p^2+q^2-pq+3\eta-E}, \tag{3.21}$$

The sum of the above infinite series leads to the following integral equation of G_3 as

$$G_3(E,p) = -2K(E-3\eta;p,0)+\frac{2}{\pi}\int dq\frac{K(E-3\eta;p,q)q^2}{\sqrt{\frac{3}{4}q^2+3\eta-E}-\frac{1}{a}}G_3(E,q). \tag{3.22}$$

When $\eta = 0$ as in vacuum, this equation is identical to an integral equation previously obtained in an atom-dimer model to study the renormalized three-body forces [57]. Comparing to $G_3(E,p)$ in vacuum when $\eta = 0$, again one finds that the energy of a trimer in a condensate ϵ_T is related to ϵ_T^0, its vacuum value via

$$\epsilon_T = \epsilon_T^0 + 3\eta. \tag{3.23}$$

What Eq. (3.23) shows is a simple fact of a condensate. If all the finite momentum atoms have a mean-field energy shift $\Sigma - \mu$ with respect to condensed atoms, the energy of few-body bound states (with finite k components) experiences the corresponding energy shifts. As a consequence,

when $\epsilon_T = 0$, we should expect that the three-body forces in a condensate should be divergent. This was observed numerically in our study presented in chapter 2; the three-body potential is divergent when $3\eta = -\epsilon_n$ where ϵ_n are the Efimov eigenvalues with $n = 1, 2, 3, ...$

What is the consequences of the spectrum flow or the energy shift due to the condensate? The main consequence is that in a condensate, a dimer crosses the zero energy, or the energy of condensed atoms at a positive critical scattering length a_D or $\epsilon_D = 0$ when

$$2\eta(a_D) = \frac{1}{ma_D^2}, \tag{3.24}$$

where η itself is a function of a_D. By contrast, in vacuum a dimer crosses the zero energy or the scattering threshold at resonance or $a = \infty$. If we simply apply the Hartree-Fock approximation $\Sigma = 2\mu = 8\pi an/m$, we find $\eta = \mu$ and

$$n^{1/3}a_D = (1/8\pi)^{1/3}. \tag{3.25}$$

Beyond this point, one has to take into account the hybridization between atoms and molecules. The dimer formation in condensates was previously studied in a random-phase approximation; those results are qualitatively consistent with the picture painted here [69]. Pairing instability and formation of molecules in the upper branch Fermi gas was emphasized in Ref. [70].

Since it is necessary to have molecules below condensates for the condensed atoms to have effective repulsive interactions, the penetration of dimers into the condensate implies a change of the sign of interactions, from repulsive to attractive ones that can lead to a potential instability. Below we further amplify this aspect.

3.4 Sign Change of g_2: A Consequence of Spectrum Flow

In a condensate, the low energy two-body interaction constant is renormalized not only by the virtual scattering states as in vacuum but also by the interactions with the condensed atoms. The latter effect is many-body in nature. Below we focus on the particular many-body effect related to the self-energy of virtual states and include this in the renormalization procedure. The self-energy of non-condensed atoms is due to scatterings by the condensate and depends on the interaction strength and density of atoms.

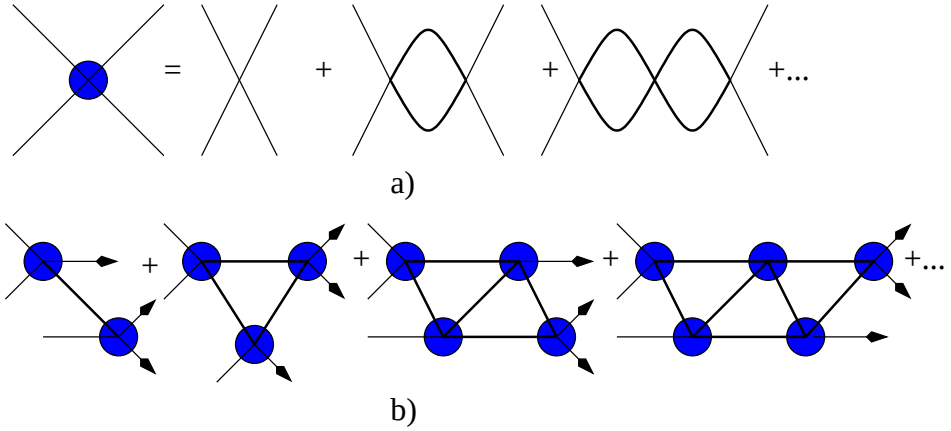

Figure 3.3: Diagrams for the calculations of dimer and trimer energy in a condensate. a) is for two-atom channels. Each solid internal line here is for a Green's function of non-condensed atoms with the self-energy effect taken into account, $G^{-1}(\epsilon, \mathbf{k}) = \epsilon - \epsilon_{\mathbf{k}} - \Sigma + \mu + i\delta^+$. b) is the loop diagrams for the three-atom channel.

We now apply a self-consistent renormalization group equation (RGE) to investigate this issue. To study the coupling constant, we start with the assumption that the self-energy and the chemical potential of non-condensed particles are already given as Σ and μ. The simplest Hartree-Fock Green's function for virtual atoms is of the form

$$G(\epsilon, \mathbf{p}) = \frac{1}{\epsilon - \frac{\mathbf{p}^2}{2m} - \Sigma + \mu + i\delta^+}. \tag{3.26}$$

We then calculate $g_2^0(\Sigma, \mu)$, the zero energy effective interaction between condensed particles for a given $\eta = \Sigma - \mu$ using a very similar procedure as that in Sec. 3.2 except G^0 in Eq. (3.8) now should be replaced with G defined here. This replacement effectively takes in the multiple scatterings by a condensate in two-body scattering processes shown explicitly in Fig. 3.3(c). The corresponding renormalization group equation (RGE) for the running couple constant $\tilde{g}_2 = g_2(\Lambda)\Lambda_h$ can be found to be,

$$\begin{aligned} \frac{\partial \tilde{g}_2(\Lambda_h)}{\partial \ln \Lambda_h} &= \frac{m}{2\pi^2}\tilde{g}_2^2(\Lambda_h) + \tilde{g}_2(\Lambda_h), \\ \Lambda_h &= \Lambda - \sqrt{2m\eta}\ \arctan\frac{\Lambda}{\sqrt{2m\eta}}, \end{aligned} \tag{3.27}$$

where Λ_h is the dynamical length relevant to the renormalization transformation and depends on the many-body parameter η. When $\eta = 0$ as in vacuum, g_2 flows to the desired value of $4\pi a/m$. With a finite η, we find that g_2 runs to the following value

$$g_2^0 = \lim_{\Lambda_h \to 0} \frac{\tilde{g}_2(\Lambda_h)}{\Lambda_h} = \frac{4\pi a}{m} \frac{1}{1 - \sqrt{2m\eta}a} \tag{3.28}$$

as Λ_h becomes zero and all the $k \neq 0$ virtual states are included in the renormalization transformation. The resultant g_2^0 is the effective interaction between condensed atoms after all non-condensed or virtual states are integrated out. Eq. (3.28) was proposed in chapter 2 as an effective interaction for condensed atoms. This is also fully consistent with the RSRT result presented in Sec. II.

At first sight, the structure of Eq. (3.28) appears to be very similar to the zero-density expression for the two-body running coupling constant $\tilde{g}_2(L)$ in Eq. (3.12). However, the physical implication is entirely surprising. First of all, g_2^0, the effective interaction between condensed atoms, now depends on $k_\eta = \sqrt{2m\eta}$; so it is now a function of $\Sigma - \mu$, or the density of the gas, reflecting a many-body effect. In the dilute limit,

$$g_2^0 = \frac{4\pi a}{m}(1 + \sqrt{8\pi n a^3} + ...); \tag{3.29}$$

the first term stands for the Hartree-Fock energy and the second one yields the Lee-Huang-Yang type correction to the energy density of Bose gases.

Most importantly, unlike in vacuum where the zero energy effective interaction constant $4\pi a/m$ is always positive as far as a, the scattering length, remains positive, in condensates $g_2^0(\Lambda = 0)$ is positive only in the dilute limit when $\sqrt{m\eta}a \sim \sqrt{na^3} \ll 1$. When approaching the resonance, for a given $\Sigma - \mu$, the effective interaction between condensed atoms becomes negative before a becomes infinity as indicated in Fig. 3.4. In other words, the presence of a condensate completely *alters* the flow of the coupling constant at the low energy limit; it changes the sign of the effective interaction constant near resonance.

The property of Bose gases near resonance is dictated by this change of the sign of interactions. In fact as a precursor of this, pure atomic condensates lose metastability as seen in chapter 2. Microscopically, the change of sign of g_2^0 is correlated with and driven by the molecules entering the condensate. In the approximation employed here, the sign change occurs exactly

when the molecules penetrate into the condensates at scattering length a_D (see Eq. (3.24)).

To further determine η or μ and Σ and understand the effect of the sign change of g_2^0 on the condensate, we should specify a boundary condition in the RGE. The following steps have to be carried out. Once g_2^0 is found as a function of Σ and μ, one can apply it to calculate $E(n_0, \mu)$, the energy density of the system with n_0 condensed atoms and non-condensed particles at chemical potential μ. Following the general thermodynamic relations, the chemical potential for the condensed particles μ_c should be

$$\mu_c = \frac{\partial E(n_0, \mu)}{\partial n_0}, \qquad E = \frac{1}{2} g_2^0 n_0^2. \tag{3.30}$$

For the ground state we further require that the condensed atoms are in equilibrium with the non-condensed reservoir at chemical potential μ:

$$\mu = \mu_c \tag{3.31}$$

as first suggested by Pines and Hugenholtz [55]. One can verify that Eqs. (3.28),(3.30) and (3.31) are identical to the corresponding self-consistent diagrammatic equations employed in chapter 2. More explicitly, one finds that for g_2^0,

$$g_2^0 n_0 + \frac{n_0^2}{2} \frac{\partial g_2^0}{\partial \eta} \frac{\partial \Sigma}{\partial n_0} = \mu_c \tag{3.32}$$

One can view Eq. (3.30) and (3.31) as a boundary condition for $\tilde{g}_2(\Lambda_h)$ in the RGE in Eq. (3.27) when $\Lambda_h = 0$ and if $\partial\Sigma/\partial n_0$ is given. To finally solve the equation self-consistently, one needs to supply Eq. (2.4) in previous chapter to further determine that $\partial\Sigma/\partial n_0 = 2\eta/n_0$ and the set of equations produced in this way are identical to the set in chapter 2 derived diagrammatically.

To illustrate the main features, we now make a few further simplifications without losing the generality. One is that we neglect the n_0-dependence in Σ so that $\mu_c = g_2^0 n_0$. Second is that we further approximate n_0 as n because they are of the same order in the regime of our interest. We then have a single parameter renormalization equation Eq. (3.27) with the following boundary condition

$$g_2^0 = \lim_{\Lambda_h \to 0} \frac{\tilde{g}_2(\Lambda_h)}{\Lambda_h} = \frac{\mu}{n}. \tag{3.33}$$

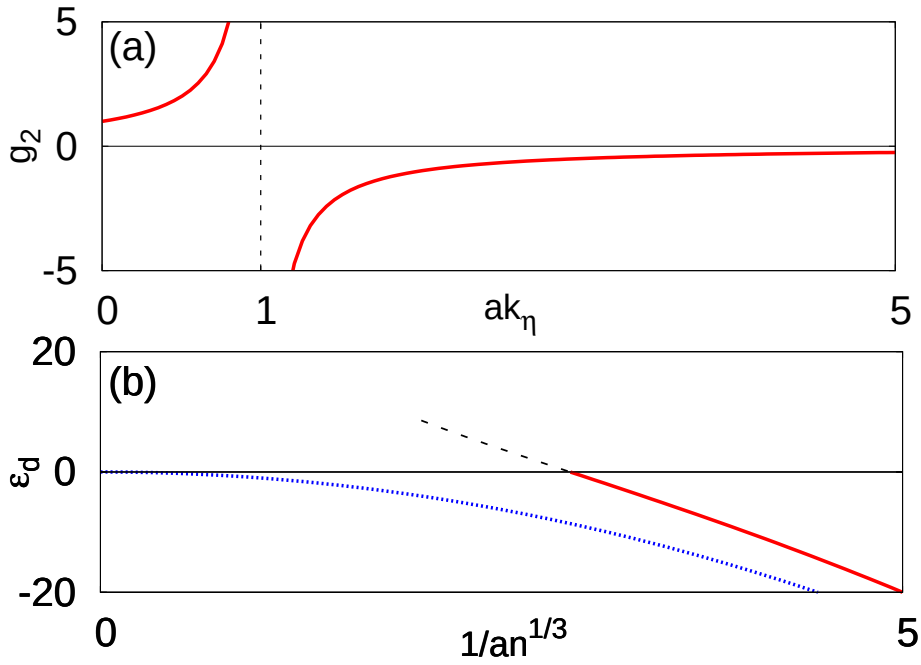

Figure 3.4: a) g_2 (in units of $4\pi a/m$) as a function of $k_\eta = \sqrt{2m\eta}$ at a given scattering length a; $\eta = \Sigma - \mu$ is a function of density and is equal to $4\pi na/m$ in the dilute limit. Note that when $ak_\eta = \sqrt{8\pi na^3} \ll 1$ or in the dilute limit, g_2 approaches its vacuum value of $4\pi a/m$ but deviates from it substantially once $k_\eta a$ is of order of unity. At resonance when $1/a = 0$, g_2 is negative for any arbitrary η implying attractive interactions between condensed atoms. b) Illustration of the dimer energy (in units of $n^{2/3}/2m$) in the presence of a condensate (the upper curve). The dashed line indicates dimers are no longer well defined because of the coupling to the continuum. As a reference we also show the dimer energy in vacuum (the lower curve). Note that in vacuum, the dimers reach zero energy right at resonance.

Last, although $\eta = \Sigma - \mu$ in general should be $\beta\mu$ with β being an unknown but smooth function of a, n_0 and μ, in the dilute limit $\beta = 1$ (see Appendix D). Eq. (2.4) in previous chapter implies that β varies between 1 in the dilute limit and 2/3 in the fermionized limit that interests us. So we can neglect its variation by simply setting $\beta = 1$ for this part of discussion. Eq. (3.27) and the boundary condition for the RGE in Eq. (3.33) now lead the following single parameter self-consistent equation for μ,

$$\frac{\mu}{n} = \frac{4\pi a}{m(1 - \sqrt{2m\mu}a)} \tag{3.34}$$

which, apart from a numerical prefactor in the denominator, is identical to Eq. (3.14) which was obtained empirically. The numerical solution of this is presented in Fig. 3.5.

Two essential features are shown in Fig. 3.5. First, the chemical potential reaches a maximum at a_{cr} as a precursor of the sign-change of two-body interaction g_2^0 near resonance. The value of the maximum is around $89\%\epsilon_F$, very close to the values obtained in a constrained variational approach [24] and in a diagrammatic resummation approach in chapter 2 (see Table 3.1 for details). Here $\epsilon_F = (6\pi^2)^{2/3}n^{2/3}/2m$ is the Fermi energy for a gas with the number density n.

Above the critical scattering length, the chemical potential develops an imaginary part.

$$Im\mu = \frac{8}{(3\pi)^{2/3}}\epsilon_F(\frac{a}{a_{cr}} - 1)^{1/2} \tag{3.35}$$

when the scattering length a is increased slightly beyond the critical point $a_{cr} = 0.18n^{-1/3}$.

The drop in the chemical potential beyond the critical scattering length a_{cr} implies a negative compressibility and hence an energetic instability. This occurs at the same time as the chemical potential becomes complex and an onset dynamic instability sets in. Therefore, a quantum gas completely loses its metastability beyond this critical point. The maximum in the chemical potential and the correlated emergent dynamic instability remain to be probed within the current experimental time scales.

A different renormalization group approach based on an atom-molecule model was also applied in a previous study to understand Bose gases near resonance [33]. Our results differ from theirs in two aspects. First, in our approach, an onset instability sets in near resonance even when the scattering length is positive, a feature that is absent in that previous study. Second,

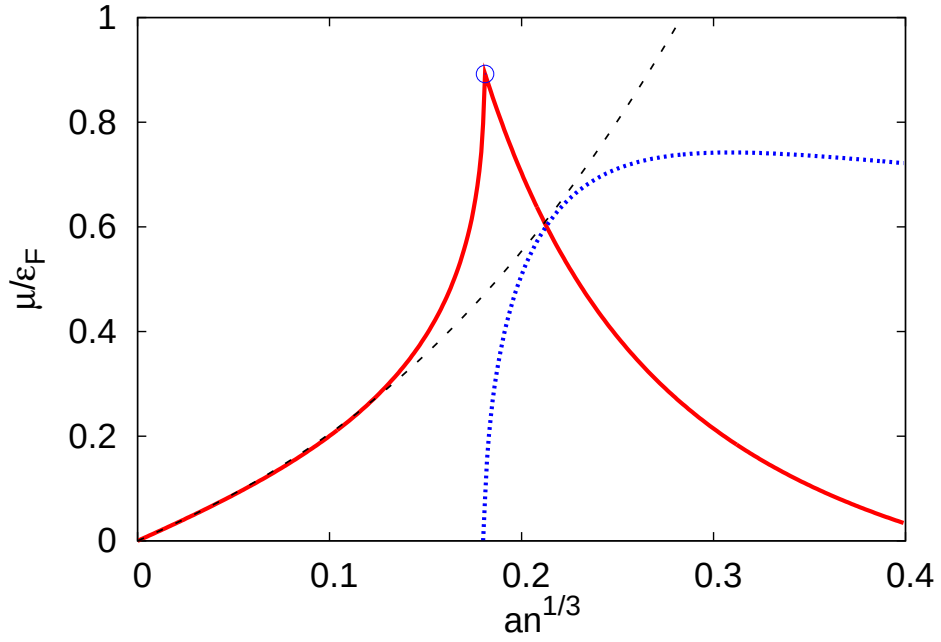

Figure 3.5: The numerical solution to the self-consistent equation Eq. (3.34). The chemical potential (the real part) reaches the maximum (blue circle) when $n^{1/3}a = 0.18$; beyond this point the chemical potential develops an imaginary part (dotted line). The dashed line is the chemical potential in the Lee-Huang-Yang theory. The smooth contributions from the three-body potential g_3 (not shown here) were studied in the previous diagrammatic calculations explained in chapter 2 and turn out to be around a few percent of the effect shown here.

when extrapolated to the limit of small na^3, the results in Ref. [33] imply a correction of the order of $\sqrt{na^3}$ to the usual Hartree-Fock chemical potential but with a negative sign, opposite to the sign of LHY corrections and/or our results. The results of the self-consistent approach in Ref. [25] are similar to the ones in Ref. [33] but differ from ours. In table 3.1, we make further comparisons by listing the main features in different approaches.

	Fermionized*	LHY effect	Efimov physics	Max. in μ, instability
Cowell *et al.*, 2002[23]	Yes $(2.92\epsilon_F)^\dagger$	No	No	No
Song *et al.*, 2009[24]	Yes $(0.80\epsilon_F)$	No	No	No
Lee *et al.*, 2010[33]	Yes $(0.66\epsilon_F)$	No††	No	No
Diederix *et al.*, 2011[25]	Yes $(0.83\epsilon_F)$	No††	No	No
Borzov *et al.*, 2012[2]	Yes $(0.93\epsilon_F)$	Yes	Yes	Yes†††

Table 3.1: Comparison of different theory approaches.
* The lower bound of μ was measured to be around $0.44\epsilon_F$ in the ENS experiment [14].
† The value in the bracket indicates the estimated chemical potential; same below. The estimated chemical potential $2.92\epsilon_F$ exceeds the result for a completely fermionized gas.
†† In the field theory approaches there, the signs of the correction of the order of $\sqrt{na^3}$ are opposite to the LHY effect. However, the LHY effect was reproduced in the numerical program in Ref. [25].
††† This is seen both in the diagrammatic resummation and the RG approach outlined here. Note that $0.93\epsilon_F$ is for a range of three-body parameters relevant to cold atoms.

3.5 Diagrammatic Resummation: A Self-Consistent Approach

From a phenomenological point of view, it is quite appealing to generalize the self-consistent coarse grain relation in Eq. (3.1) by further taking into account the three-body effective interaction g_3;

$$\mu = ng_2(\xi, a; n) + \frac{n^2}{2} g_3(\xi, a; n) \tag{3.36}$$

where $g_{2,3}(L, a; n)$ are the renormalized two- and three-body interaction constants respectively at length scale L and $\xi^{-1} = \sqrt{2m\mu}$. If one can calculate these renormalized quantities, then one is able to obtain μ which includes the effect of g_3. We have proceeded further from here using the renormalization group equations similar to what was discussed in Secs. 3.2 and 3.3; they yield qualitatively the same results as the diagrammatic approach presented in chapter 2. However, when benchmarking against the dilute gas theory, the diagrammatics turn out to be numerically superior; the diagrammatic resummation used in previous chapter reproduces 99.96% of Lee-Huang-Yang corrections in the dilute limit. Here, we review the framework of the diagrammatic calculations and briefly comment on the results.

In the diagrammatic approach, we first define the chemical potential of non-condensed particles as μ and the number density of condensed atoms as n_0. The energy density can be calculated as $E(n_0, \mu)$ (see below). Then one should have the following set of self-consistent equations for a gas with total number density n,

$$\begin{aligned} \mu_c &= \frac{\partial E(n_0, \mu)}{\partial n_0} \\ n &= n_0 - \frac{\partial E(n_0, \mu)}{\partial \mu} \\ \mu &= \mu_c \end{aligned} \tag{3.37}$$

where μ_c is the chemical potential for the condensed atoms and has to be equal to the chemical potential μ in equilibrium. We further introduce the self-energy Σ of non-condensed atoms or virtual particles to facilitate the calculation of $E(n_0, \mu)$ that now explicitly depends on $\Sigma(n_0, \mu)$. Thus, Eq. (3.37) has to be further supplemented by

$$\Sigma(n_0, \mu) = \mu_c(n_0, \mu) + \frac{\partial \mu_c}{\partial \ln n_0} \tag{3.38}$$

which can be proven in the same fashion as the Pines-Hugenholtz theorem [55]. Eq. (3.37) and (3.38) have been applied to obtain the chemical potential in 3D Bose gases near resonance in chapter 2.

Calculations of $E(n_0, \mu)$ for a given $\Sigma(= \eta + \mu)$ can be carried out diagrammatically. If we restrict ourselves to the virtual processes involving only two or three excited atoms and truncate the Hilbert space accordingly, then diagrammatically we only need to collect the diagrams which contribute to the effective two- and three-body interaction constants $g_{2,3}$. As far as the chemical potential is concerned, this truncation turns out to be highly precise in the dilute limit (refer to Sec. 2.3). The result is listed below. The mass m is set to be one:

$$\begin{aligned} E(n_0,\mu) &= \frac{1}{2}n_0^2 g_2(2\eta) + \frac{1}{3!}n_0^3 g_3(3\eta) \\ g_2(2\eta) &= 4\pi a \frac{1}{1-\frac{2}{\pi}\sqrt{2\eta}a} \\ g_3(3\eta) &= 6g_2^2(3\eta) Re \frac{2}{\pi}\int dq \frac{K(-2\eta;0,q)q^2}{\sqrt{\frac{3}{4}q^2+3\eta}-\frac{1}{a}} G_3^{'}(-3\eta,q) \end{aligned} \tag{3.39}$$

where $G_3^{'}(-3\eta, p)$ is a solution of the following integral equation

$$G_3^{'}(-3\eta,p) = \frac{2}{\pi}\int dq \frac{K(-3\eta;p,q)q^2}{\sqrt{\frac{3}{4}q^2+3\eta}-\frac{1}{a}}[\frac{-1}{q^2+2\eta} + G_3^{'}(-3\eta,q)]. \tag{3.40}$$

$-\frac{1}{2}K(-3\eta;p,q)$ is again the one-particle Green's function projected to the S-wave channel; it is defined as

$$K(-3\eta;p,q) = \frac{1}{pq}\ln\frac{p^2+q^2+3\eta+pq}{p^2+q^2+3\eta-pq}. \tag{3.41}$$

The numerical solution to these self-consistent equations was shown in chapter 2 and they are qualitatively the same as the solution to the self-consistent RGE for g_2 and we are not going to repeat here [11]. Here we want to make a few further comments on the resummation technique.

First, g_2 defined this way is an effective two-body interaction renormalized by the condensate and includes a subset of N-body interactions

[11] There are two ways of estimating G_3 which slightly differ from each other; the difference is due to singular behavior of the Green's function at $k = 0$ in the Hatree-Fock approximation as commented on in Appendix C. Here we evaluate G_3 by first setting all external lines to be the condensed atoms.

defined in the vacuum. At the one-loop level, it yields the most dominating contribution; the residue effects are from the irreducible $N = 4, 6, ...$-body interactions which contains less than one thousandth of the total contribution.

Second, the three-body contribution in our self-consistent approach appears to be around a few percent and numerically insignificant. Since when compared to g_2, the contribution from g_3 in the dilute limit as well as near resonance is small, it is reasonable to conjecture that further inclusion $g_{4,5,...}$ would not change our result presented here in a substantial way (refer to Sec. 2.3). The truncation of the energy density expression at g_3 should be accurate enough for all the practical purposes of studying Bose gases near resonance. We hope these statements can be tested in precision measurements of chemical potentials as well as in future quantum Monte Carlo simulations.

Third, the energy density expression in Eq. (3.39) becomes exact in the limit where only the processes involving two or three virtual atoms are allowed. Effectively, this is equivalent to truncating the Hilbert space and including the correlations up to the trimer channel.

3.6 Summary

The RGE approach is instrumental to our understanding of the emergent phenomena in quantum few- and many-body systems. The application to Bose gases near resonance perhaps is another example of what a simple RGE transformation can lead to. We have applied this approach to understand the nature of Bose gases near resonance and found that energetically, the Bose gases close to unitarity are nearly *fermionized* before an onset instability sets in, *i.e.* the chemical potentials of the Bose gases approach that of the Fermi energy of a Fermi gas with equal mass and density. Beyond the instability point, the chemical potential has an imaginary part indicating strong hybridization with molecules.

The model we have employed to study the Bose gases near resonance is a short range *attractive* potential which has a range much shorter than the inter-atomic distance of the gases or effectively a contact potential. This is a very good approximation of real physical interactions between cold atoms. If the potential is a short range but repulsive , then Bose gases are always in the dilute limit because the scattering lengths are bounded by the range of interactions, disregarding the strength of potential. For bosons interacting with a repulsive potential but with a range comparable to the inter-particle

distance, we should anticipate the physics in this limit to be very similar to what happens in liquid ^4He [54, 71–75]. The excitation spectrum should develop roton minima that imply strong short range crystal correlations. When the range of interactions is further increased, eventually there should be a quantum transition to a crystal where all bosons are depleted from the condensate. The physics of repulsive bosons and liquid ^4He belong to a different universality class which fundamentally differs from what we described in this thesis, i.e. the properties of nearly fermionized Bose gases near resonances with a contact interaction.

Chapter 4

Nature of Two-Dimensional Bose Gases

4.1 Introduction

Two-dimensional quantum many-body systems have been, for many years, a subject of fascination for condensed matter and nuclear physicists alike. More recently, this topic also caught the attention of the cold atom community with the realization of quantum Bose gases confined to two-dimensional geometries [35–38]. These experimental studies have so far explored these systems at temperatures close to the Berezinskii-Kosterlitz-Thouless phase transition [39–41]. They highlighted the loss of long-range order due to the proliferation of vortices above the transition temperature, and the existence of two-dimensional quasi-condensates with algebraic long-range order and long wavelength thermal fluctuations below the transition. However, the fundamental properties of two-dimensional Bose gases near absolute zero, where quantum effects are dominant, have yet to be addressed. In particular, on both theoretical and experimental sides, very little work has been carried out to study two-dimensional Bose gases near resonance. The main purpose of this chapter is to provide new light on the properties of two-dimensional Bose gases in this limit.

Compared to three-dimensional Bose gases near resonance, which received more attention in recent years [14, 17–19], two-dimensional gases possess important advantages. First, the ratio between elastic and inelastic collision cross sections can be significantly enhanced when atoms are confined to two-dimensional traps [42]. Second, in two dimensions, trimers and few-body structures are all universal as the absolute energy scale of the spectrum is uniquely set by the two-body binding energy and is independent of the short distance property of three-body interactions [43–46]. This is distinctly different from the physics of Efimov states in three dimensions as, in this case, the absolute energy scale is set by the ultraviolet physics of three-boson scatterings [34].

These advantages are related to the dramatic suppression of the low energy effective interactions and phase shifts by coherent interference in two-dimensional Bose gases. In fact, for an arbitrary repulsive interaction, the low energy two-body scattering phase shifts are logarithmically small indicating an asymptotically free limit. This aspect of scattering theory plays a critical role in the physics of two-dimensional dilute Bose gases. Most previous works on two-dimensional Bose gases considered systems where the range of the repulsive interactions or the core size of the hard-core bosons, a_0, were much smaller than the inter-particle distances [47–49]. Consequently, the results of these studies are only applicable when $\frac{1}{\ln(na_0^2)}$ (n is the density of bosons) is much smaller than unity, a limit corresponding to dilute gases in two dimensions. Here, we focus on the physics beyond the dilute limit to study two-dimensional Bose gases prepared on the upper branch and interacting via a resonating contact interaction. Such a setup can be achieved experimentally through a combination of Feshbach resonance and optical confinement [50–52]. Theoretically, to study two-dimensional near-resonance Bose gases, we introduce a two-dimensional effective scattering length a_{2D}. This new tuning parameter is formally defined as the position of the node in the wave function for two scattering particles and is also identified as the size of the two-body bound state. In general, a_{2D} can be tuned to values larger than the averaged inter-atomic distance and can even be infinite.

Our study of two-dimensional Bose gases at large scattering lengths unveils that near resonance the properties of these gases are primarily dictated by the competition between three-body attractive interactions and two-body repulsive forces. We also show that the energetics of two-dimensional Bose gases near resonance are universal as they only depend on the parameter na_{2D}^2. Finally, we investigate the behavior of the chemical potential for a wide range of scattering lengths. We find that the chemical potential first increases with a_{2D} but very quickly reaches a maximum at $\frac{1}{ln(na_{2D}^2)} = -0.135$ beyond which the Bose gas develops a negative compressibility. Increasing a_{2D} further brings about an onset instability at $\frac{1}{ln(na_{2D}^2)} = -0.175$. We identify both critical values to result from the important role played by three-body attractive interactions. In Ref. [53], using variational quantum Monte Carlo method, the physics of two-dimensional Bose gases beyond dilute limit was investigated. In this study, the inverse compressibility of the system is calculated for large range of two-dimensional scattering lengths and it is shown that the compressibility becomes negative beyond $\frac{1}{ln(na_{2D}^2)} \simeq -0.31$, for large gas parameters. The vanishing of inverse of compressibility is in-

terpreted as the onset of instability against cluster formation. This result is consistent with our observation of the maximum point in the chemical potential beyond which the compressibility is negative and the instability of the system at the second critical point. Within our approach, we can estimate the contributions from three-body interactions to the two-body ones to be around 0.27 near the maximum of chemical potential and 0.73 in the vicinity of the onset instability.

4.2 Self-Consistent Approach for Two-Dimensional Bose Gases

To carry out this study of two-dimensional Bose gases, we employ a method we previously developed to understand the physics of three-dimensional Bose gases near resonance [2, 3] explained in chapter 2. In this approach, the chemical potential of non-condensed particles, μ, and the density of condensed atoms, n_0, are first introduced as given parameters. The Hamiltonian describing such a condensate interacting with non-condensed atoms through a short-range interaction is the same the three-dimensional Hamiltonian in Eq.(2.1) except that three-dimensional volume, Ω, is now replaced by two-dimensional area, S. Later, we will evaluate n_0 and μ self-consistently as a function of the two-dimensional scattering length, a_{2D}, and of the total density n.

Once the full system energy density $E(n_0, \mu)$ is known, one can calculate μ_c, the chemical potential for the condensed atoms, and $n - n_0$, the density of non-condensed atoms using the thremodynamical relations introduced in chapter 2. In addition, in the ground state, one requires μ_c, the chemical potential for the condensed atoms, to be equal to the chemical potential μ. This equilibrium condition, first emphasized in Ref. [55], yields a self-consistent equation. The evaluation of $E(n_0, \mu)$ for a given μ and n_0 is usually carried out diagrammatically [9, 55]. To capture the role of three-body interactions and to compare it with two-body contributions, we restrict ourselves to the virtual processes involving only two or three excited atoms. Truncating the Hilbert space accordingly, we can then sum up all connected diagrams contributing to the energy density. Within this truncation scheme, only the irreducible two- and three-body effective interaction potentials $g_{2,3}$ appear in the final expression for $E(n_0, \mu)$. In order to implement the self-consistency condition and simplify the computation of $E(n_0, \mu)$, we introduce for the non-condensed or virtual atoms an additional parameter $\eta = \Sigma - \mu$ where $\Sigma(n_0, \mu)$ is the self-energy. Physically, η

can be understood as an energy shift due to the interaction between condensed and non-condensed atoms. Using the same series of diagrams as in our study of three-dimensional Bose gases near-resonance, but carrying out the calculations in two spatial dimensions, we obtain for the energy density

$$\begin{aligned} E(n_0,\mu) &= \frac{1}{2}n_0^2 g_2(2\eta) + \frac{1}{3!}n_0^3 \mathrm{Re}\ (g_3(3\eta)) \\ \text{with } g_2(2\eta) &= \frac{\hbar^2}{m}\frac{4\pi}{\ln\frac{B_2}{2\eta}}, g_3(3\eta) = 6g_2^2(2\eta)g_3^*(3\eta) \\ \text{where } g_3^*(3\eta) &= \frac{\hbar^2}{m}\int \frac{4qdq}{2\eta+q^2}\frac{G_3^{'}(-3\eta,q)}{\ln\frac{B_2}{3q^2/4+3\eta}}. \end{aligned} \tag{4.1}$$

$g_{2,3}$ stand for, respectively, the *renormalized* two- and three-body interactions in a condensate. We will discuss this point in more details below. $G_3^{'}(-3\eta,p)$ represents the three-atom off-shell scattering amplitude (corresponding to the sum of all N-loop contributions with $N=1,2,3,...$). $G_3^{'}$ is the solution to the following integral equation (see Appendix F for more details), where $\hbar$ and m were intentionally set to unity to improve readability,

$$\begin{aligned} G_3^{'}(-3\eta,p) &= \int \frac{4qdq}{\ln\frac{B_2}{3q^2/4+3\eta}}\frac{1}{\sqrt{(3\eta+p^2+q^2)^2-(pq)^2}} \\ &\times \Big(\frac{-1}{2\eta+q^2} - G_3^{'}(-3\eta,q)\Big). \end{aligned} \tag{4.2}$$

Note that in Eqs. (4.1) and (4.2), $B_2 = \Lambda\exp\left(\frac{4\pi\hbar^2}{U_0 m}\right)$ where Λ is an energy cutoff related to the effective interaction range, R^*, via $\Lambda = \frac{\hbar^2}{mR^{*2}}$. As $B_2 = \frac{\hbar^2}{ma_{2D}^2}$, $g_{2,3}$ are uniquely determined by the parameter $\frac{n\hbar^2}{mB_2}$ or na_{2D}^2.

For repulsive interactions (or positive U_0), B_2 is larger than Λ and so a_{2D} is bounded from above by the interaction range R^*. When U_0 is infinite (hard-core potential), a_{2D} is equal to the core size a_0. For attractive interactions (or negative U_0), the case we focus on here, B_2 is precisely the dimer binding energy, and a_{2D} is the size of the bound state and can well exceed R^*. As a consequence, na_{2D}^2, the fundamental tuning parameter for $E(n_0,\mu)$, can take values larger than unity. The gas can hence be tuned away from the dilute limit[12].

[12]For a quasi two-dimensional cold gas near Feshbach resonance, a_{2D} is a function of l_0, the confinement radius along the perpendicular direction, and of the free space scattering length a_{3D}. For shallow 2D bound states, $a_{2D} = \sqrt{\frac{\pi}{0.915}}l_0\exp\left(-\sqrt{\frac{\pi}{2}}\frac{l_0}{a_{3D}}\right)$ [50–52].

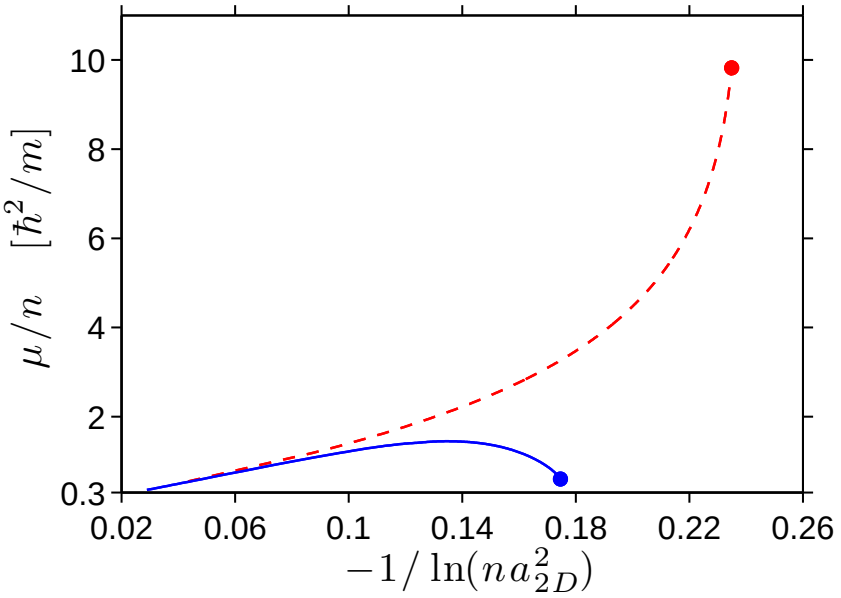

Figure 4.1: The chemical potential, in units of $\frac{\hbar^2 n}{m}$, as a function of na_{2D}^2. The dashed (red) line is the solution of the self-consistent equation when only two-body interactions are included. The full (blue) line is the solution when both two- and three-body interactions are included. This figure highlights that the behavior of the chemical potential is drastically altered by three-body physics.

Three-dimensional self-consistent equations were used in chapter 2 to obtain the chemical potential of 3D Bose gases near resonance. These self-consistent equations provided highly precise estimates for the chemical potential in the dilute limit. Near resonance, this approach predicted a maximum in the chemical potential and an accompanied onset instability. These features were fully consistent with the conclusions drawn from a renormalization group equation approach in chapter 3. This first study concluded that in three dimensions the dominating contribution to the chemical potential came from irreducible two-body interactions; for cold atoms, the three-body contribution was negligible. For two-dimensional Bose gases, the story is very different: three-body interactions play here a much more important role as can be seen on Fig. 4.1.

To analyze the contribution coming from the three-body effect, we first solve self-consistent equations excluding the contribution of g_3, and obtain the chemical potential solely due to two-body interactions (see Fig. 4.1 dashed red line). Here, g_2 is defined as the effective two-body interaction renormalized by scattering events off condensed atoms and includes a subset of N-body interactions defined in the vacuum[13]. Neglecting g_3 interactions, the self-consistent equations take the simple form

$$\tilde{\mu} \;=\; \frac{4\pi}{\ln\frac{1}{2\alpha\tilde{\mu}}}+\frac{8\pi^2}{\tilde{\mu}\ln^3\frac{1}{2\alpha\tilde{\mu}}},\;\frac{1}{\tilde{n}_0}=1+\frac{2\pi}{\tilde{\mu}}\frac{1}{\ln^2\frac{1}{2\alpha\tilde{\mu}}} \tag{4.3}$$

where $\tilde{\mu}=\frac{m\mu}{\hbar^2 n_0}$, $\tilde{n}_0=\frac{n_0}{n}$ and $\alpha=n_0 a_{2D}^2$[14]. The solution of Eq. (4.3) in the limit of small α is

$$\mu=\frac{n}{m}\frac{4\pi\hbar^2}{\ln\frac{1}{\alpha}}\left(1-\frac{1}{\ln\frac{1}{\alpha}}[\ln|\ln\alpha|-\ln 4\pi+C]+...\right) \tag{4.4}$$

where $C=\ln\frac{1}{2}$ within this self-consistent approach. This solution, valid in the dilute limit, agrees well with previous studies [47, 48, 76]. Another solution with μ approaching $\frac{\hbar^2}{ma_{2D}^2}$ exists in this limit but is unstable. As α or na_{2D}^2 is increased, the dilute gas solution approaches this higher energy unstable solution, and at the critical value $na_{2D}^2=1.42\times10^{-2}$ the two

[13] In the dilute limit, g_2 reproduces the most dominating contribution; the residue effects are from the irreducible $N=4,6,...$-body interactions, and are parametrically smaller than the contributions from g_2, i.e. smaller by a factor of $\frac{1}{ln(na_{2D}^2)}$. See also similar discussions on 3D cases in chapter 2.

[14] In obtaining this equation, we take into account Eq. (2.4) and set $\partial\eta/\partial\mu=1$, $\partial\eta/\partial n_0=g_2$ and $\eta=\mu$ to simplify the structure.

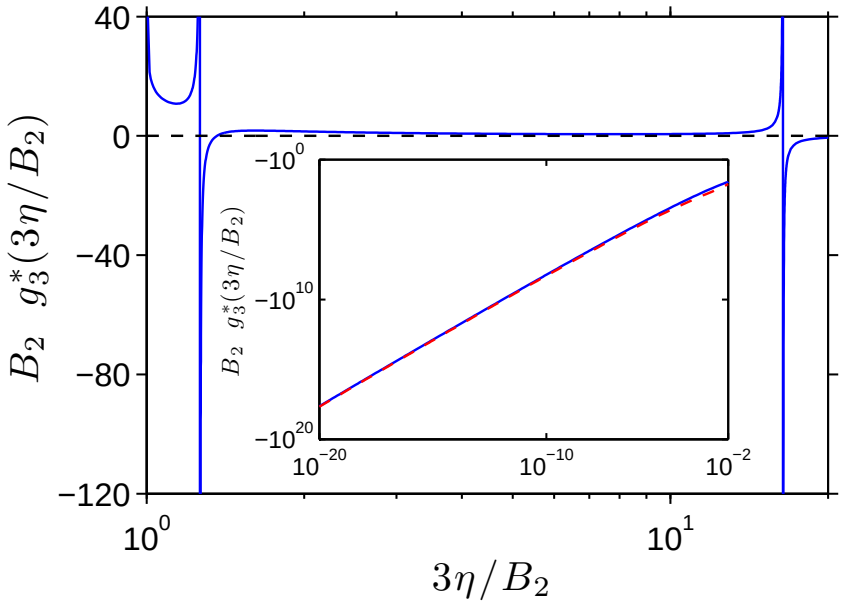

Figure 4.2: Three-body interaction g_3^* (defined in Eq. (4.1)) as a function of the energy shift $\eta = \Sigma - \mu$; η is determined self-consistently together with μ. Inset: full and two-loop behavior of g_3^* for small η values (respectively, full (blue) and dashed (red) lines). For $\frac{3\eta}{B_2} < 1$, the numerical integration over the momentum was done from 0 to $50\frac{\sqrt{B_2 m}}{\hbar}$.

solutions coalesce into one. Beyond this point, no real solution to Eq. (4.3) exists revealing the presence of an instability. The basic structure sketched here, when three-body contributions are neglected, is qualitatively the same as that of 3D Bose gases: μ is maximum when an onset instability sets in, and for larger na_{2D}^2 develops an imaginary part implying the formation of molecules.

4.3 Competing Three- and Two-Body Interactions

We now turn our attention to the contribution of $g_3(3\eta)$. $g_3(3\eta)$ is obtained by first numerically solving Eq. (4.2) for $G_3'(-3\eta, p)$ and then by carrying

out the integral involving $G_3'(-3\eta, q)$ in Eq. (4.1) (see Appendix G for more details). The result of this procedure is shown in Fig. 4.2 where we plot $g_3^*(3\eta)$. We chose to plot $g_3^*(3\eta)$ and not $g_3(3\eta)$ as the former is not cluttered by trivial effects due to $g_2^2(2\eta)$. We identify two kinds of resonant scattering processes defining the basic structure of $g_3(3\eta)$. The first one is a three-body resonance between three condensed atoms with zero energy and a dimer plus a non-condensed atom with total energy $3\eta - B_2$. Here 3η is the mean-field energy shift due to the exchange interaction between the non-condensed atom-dimer structure and the condensate. This leads to the first peak (from left to right) at $3\eta = B_2$. The second process is a three-body resonance between three condensed atoms and a trimer with either binding energy $B_3^{(1)}$ or $B_3^{(2)}$ (or total energies $3\eta - B_3^{(1)}$ or $3\eta - B_3^{(2)}$). This process produces the second and third peaks at $3\eta = B_3^{(1,2)}$. We find numerically that $B_3^{(1)} = 1.296 B_2$ and $B_3^{(2)} = 16.643 B_2$. These energies are fully consistent with the results of two previous few-body studies [43, 45]. Unlike in three dimensions where a logarithmically large number of Efimov states exist, in two dimensions there are only two trimer states. Remarkably, their energies are uniquely determined by B_2 without involving an additional three-body parameter, a fascinating feature emphasized in Refs. [43, 45].

The effect of three-body scatterings on the quantum gas is mainly determined by the property of g_3 when η is relatively small. We checked numerically that in the limit of very small η, g_3 can be well fitted by an attractive interaction of the scaling form $\frac{\hbar^4}{2m^2\eta}\frac{1}{\ln^2\frac{B_2}{2\eta}\ln^2\frac{B_2}{3\eta}}$, capturing the dominant two-loop contribution[15] (see Fig. 4.2). Including the contribution due to three-body physics in the evaluation of the chemical potential results in two main effects. First, due to the attractive tail of g_3 in the small η limit, as shown in Fig. 4.3, the instability is shifted away from $na_{2D}^2 = 1.42 \times 10^{-2}$ and occurs at a much smaller value of $na_{2D}^2 = 3.26 \times 10^{-3}$. At this new instability point, the chemical potential is dramatically reduced, from $9.82\frac{\hbar^2 n}{m}$ to $0.601\frac{\hbar^2 n}{m}$ when g_3 is included. In other words, the three-body effective interaction further destabilizes the quantum gas. The second and equally important effect is that the inclusion of three-body interactions results in the appearance of a maximum in the chemical potential at $na_{2D}^2 = 0.604 \times 10^{-3}$ before the onset instability occurs. The maximum value of the chemical

[15] A diagrammatic calculation similar to the one presented in chapter 2 suggests that the leading N-loop contributions to g_3 for small values of η/B_2 are $g_3^{(\text{N-loop})} = C_N\frac{\hbar^4}{2m^2\eta}\frac{1}{\ln^2\frac{B_2}{2\eta}\ln^N\frac{B_2}{3\eta}}$ with $N = 2, 3, 4...$; the prefactor C_N can be computed numerically. For the most dominating two-loop contribution, $C_2 = -6.3 \times 10^3$.

potential is $\mu_{max} = 1.45\frac{\hbar^2 n}{m}$ and the condensation fraction at the maximum is 91%.

Between the maximum and instability points, the quantum gas exhibits a negative compressibility and can potentially collapse into a high density phase. Although the fate of the Bose gases with negative compressibilities and the details of the corresponding dynamics are beyond the scope of our investigation, we speculate that in this regime a quantum gas eventually evolves into the droplet matter discussed in Ref. [45]. In three dimensions, the instability originated from a shift of the dimers due to scatterings off condensates and was a precursor of the sign change of the effective two-body interaction g_2 [3]. For two-dimensional Bose gases, the situation is completely different. Here, the instability is a consequence of the competition between the repulsive two-body interaction (positive g_2) and the attractive three-body interaction (negative g_3) in the low energy limit. For a two-dimensional Fermi gas, the Pauli blocking effect was recently demonstrated to lead to an instability at a finite scattering length [52].

We also plot in Fig. 4.3 the relative weight of the three-body to two-body contributions to the chemical potential. As anticipated, the three-body contribution is negligible in the dilute limit when $na_{2D}^2 \ll 1$ but quickly becomes important as na_{2D}^2 is increased. The prominent role played by three-body scattering leads to a maximum in the chemical potential before the instability point. At this maximum, the ratio between the three-body and two-body contributions reaches 0.27. The shift of the instability is also caused by the attractive three-body interactions.

4.4 Summary

In conclusion, we demonstrated that the properties of 2D Bose gases at large scattering lengths or near resonance are dictated by three-body effects. We showed that the contributions of trimer states are universal as they only depend on the effective two-body scattering length a_{2D} and not on the short distance properties of three-body interactions; an aspect unique to two-dimensional Bose gases. Our results also suggest the existence of strong correlations in the three-atom channel near resonance. This feature remains to be probed experimentally.

The important point is that, in this study, we only investigated the effects of two- and three-body potentials and since three-body physics plays an important role in two dimensions, we expect the contributions from n-body potentials ($n > 3$) to be also important. However, since the similar physics

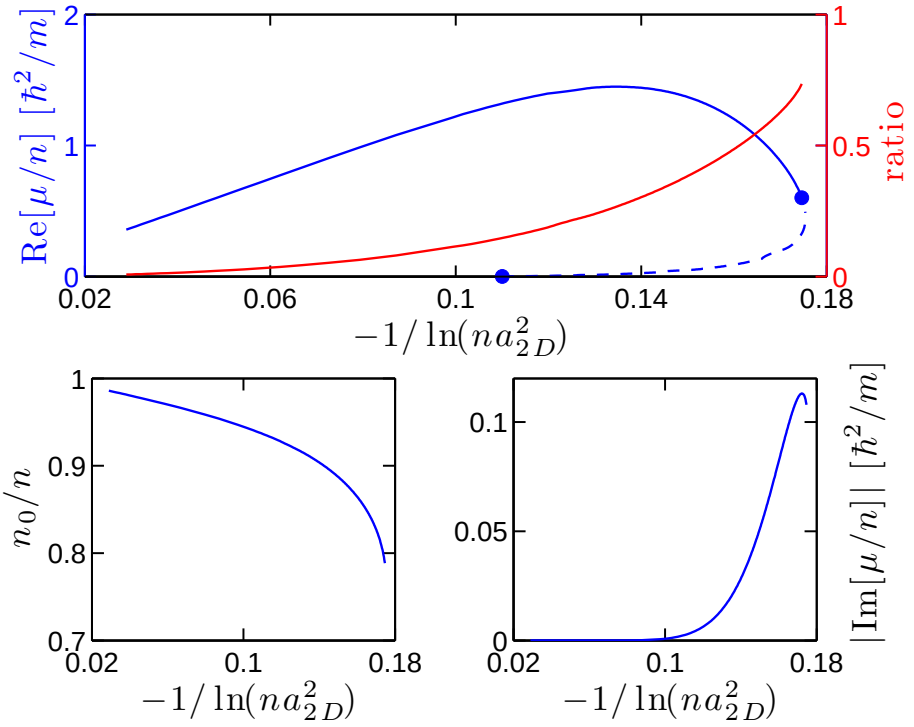

Figure 4.3: Top panel: ratio between the contributions of three-body and two-body interactions as a function of na_{2D}^2 (full red line), chemical potential two-dimensional 2D Bose gases (full blue line). An additional metastable solution (dashed blue line) also exists when g_3 is included. The maximum value of μ is $1.45\frac{\hbar^2 n}{m}$ and occurs at $na_{2D}^2 = 0.604 \times 10^{-3}$. Bottom left panel: condensation fraction n_0/n as a function of na_{2D}^2. Bottom right panel: imaginary part of the chemical potential when taking into account the contribution of all three-body recombination processes. Note that $|\text{Im } \mu| \ll \text{Re } \mu$ for all considered na_{2D}^2, indicating the quasi-static nature of the Bose gases. Hence, three-body recombination plays very little role in our energetic analysis and can be safely neglected for the range of parameters considered.

have been predicted using variational quantum Monte Carlo method in Ref. [53], we expect that considering the contributions from n-body ($n > 3$) scattring processes does not change the physics qualitatively.

Chapter 5

Conclusion

In conclusion, we have studied the physics of two- and three-dimensional ultra cold Bose gases near Feshbach resonance using a self-consistent framework. Within this framework, once the full energy density of the system as a function of chemical potential of non-condensed atoms and condensate density is known, one can calculate the chemical potential of condensed atoms and density of non-condensed particles. The self-consistent equation is formed by satisfying the equilibrium condition in the ground state in which the chemical potential of condensed atoms is equal to to the chemical potential of non-condensed atoms.

In chapter 2, we estimated the full energy density of a three-dimensional Bose gas using a diagrammatic method. In this method, we classified scattering processes in terms of the number of virtual particles involved in the process. We pointed out an onset instability toward formation of molecules beyond the dilute limit and fermionization of the Bose gas near resonance. This instability originates from a shift of the dimers due to scatterings off condensates and is a precursor of the sign change of the effective two-body interaction. This sign change is a strikingly different result from the picture commonly accepted by the cold atom community where it is usually thought that, for negative bare interactions where the scattering length is positive, the atoms repel each other. In addition, we found that the effect of three-body scattering processes is only a few percent to the chemical potential close to instability point. In chapter 3, these highly non-trivial results were obtained using a renormalization group approach by looking at the running of the two-body coupling constant at different energies.

In chapter 4, we investigated the properties of two-dimensional ultra cold gases at large scattering lengths emphasizing the role played by three-body scattering processes. Within this diagrammatic approach, we showed that the physics of these gases near resonance is primarily dictated by the competition between three-body attractive interactions and two-body repulsive forces. This competition results in the chemical potential of Bose gases to exhibit a maximum at a critical scattering length beyond which these quantum gases have a negative compressibility. Furthermore, we showed

that for larger scattering lengths, the increasingly prominent role played by three-body forces leads to an onset instability at a second critical point. We also showed that the contributions of trimer states are universal as they only depend on the effective two-body scattering length and not on the short distance properties of three-body interactions; an aspect unique to two-dimensional Bose gases.

In the future, it would be interesting to answer this obvious question on how it is possible to experimentally detect the peculiar behavior of the chemical potential in these two- and three-dimensional Bose gases, i.e. whether there exists a spectrometry that one can apply to accurately map out the value of the chemical potential near resonance. Another question is whether the behavior of Fermi gases close to Feshbach resonances [70, 77] can also be understood within this novel formalism. In addition, one can investigate the physics of n-body scattering processes for $n > 3$ both in two and three dimensions. In three dimensions, the question is whether these higher-body interactions are negligible compared to two-body potential. However, in two dimensions, although we already know that these contributions should be important and comparable to two-body potential contribution, one can examine whether the physics is changing qualitatively or quantitatively. The other interesting future direction could be studying the physics of two- and three-dimensional Bose gases beyond instability point where our self-consistent framework is not able to explore this regime.

Bibliography

[1] M. S. Mashayekhi, J. -S. Bernier, and F. Zhou, *Annual Review of Cold Atoms and molecules*, Vol. **1**, Chap. **4**, (World Scientific, Hackensack, NJ, 2013).

[2] D. Borzov, M. S. Mashayekhi, S. Zhang, J.-L. Song and F. Zhou , Phys. Rev. A **85**, 023620 (2012).

[3] F. Zhou and M. S. Mashayekhi, Ann. Phys. **328**, 83 (2013).

[4] M. S. Mashayekhi, J. -S. Bernier, D. Borzov, J. -L. Song, and F. Zhou, Phys. Rev. Lett. **110**, 145301 (2013).

[5] M. H. Anderson, J. R. Ensher, M. R. Matthews, C. E. Wieman, and E. A. Cornell, Science **269** (5221), 198-201 (1995).

[6] K. B. Davis, M. -O. Mewes, M. R. Andrews, N. J. van Druten, D. S. Durfee, D. M. Kurn and W. Ketterle, Phys. Rev. Lett. **75**, 3969 (1995).

[7] N. N. Bogoliubov, J. Phys. USSR **11**, 23 (1947).

[8] T. D. Lee, and C. N. Yang, Phys. Rev. **105**, 1119 (1957); T. D. Lee, K. Huang, and C. N. Yang, Phys. Rev. **106**, 1135 (1957).

[9] S. T. Beliaev, Sov. Phys. JETP. **7**, 289 (1958); Sov. Phys. JETP. **7**, 299 (1958).

[10] T. T. Wu, Phys. Rev. **115**, 1390 (1959).

[11] K. A. Brueckner and K. Sawada, Phys. Rev. **106**, 1117 (1957).

[12] K. Sawada, Phys. Rev. **116**, 1344 (1959).

[13] For the early observation of Feshbach resonance in ^{23}Na gases, see S. Inouye, M. R. Andrews, J. Stenger, H.-J. Miesner, D. M. Stamper-Kurn and W. Ketterle , Nature **392**, 151 (1998).

[14] N. Navon, S. Piatecki, K. J. Günter, B. Rem, T. C. Nguyen, F. Chevy, W. Krauth, and C. Salomon, Phys. Rev. Lett. **107**, 135301 (2011).

[15] A. J. Moerdijk, B. J. Verhaar, and A. Axelsson, Phys. Rev. A **51**, 4852 (1995).

[16] For an excellent review on Feshbach resonances in cold gases, see Cheng Chin, Rudolf Grimm, Paul Julienne and Eite Tiesinga, Rev. Mod. Phys. **82**, 1225 (2010).

[17] S. B. Papp, J. M. Pino, R. J. Wild, S. Ronen, C. E. Wieman, D. S. Jin, and E. A. Cornell, Phys. Rev. Lett. **101**, 135301 (2008).

[18] S. E. Pollack, D. Dries, M. Junker, Y. P. Chen, T. A. Corcovilos, and R. G. Hulet, Phys. Rev. Lett. **102**, 090402 (2009).

[19] R. J. Wild, P. Makotyn, J. M. Pino, E. A. Cornell and D. S. Jin, Phys. Rev. Lett. **108**, 145305 (2012).

[20] E. Braaten, H.-W. Hammer and T. Mehen, Phys. Rev. Lett. **88**, 040401 (2002).

[21] S. Giorgini, J. Boronat and J. Casulleras, Phys. Rev. A **60**, 5129 (1999).

[22] D. Blume and C. H. Greene, Phys. Rev. A **63**, 063601 (2001).

[23] S. Cowell, H. Heiselberg, I. E. Mazets, J. Morales, V. R. Pandharipande, and C. J. Pethick, Phys. Rev. Lett. **88**, 210403 (2002).

[24] J.-L. Song, and F. Zhou, Phys. Rev. Lett. **103**, 025302 (2009).

[25] J. M. Diederix, T. C. F. van Heijst, H. T. C. Stoof, Phys. Rev. A **84**, 033618 (2011).

[26] S. Nascimbene, N. Navon, K. Jiang, F. Chevy and C. Salomon, Nature **463**, 1057 (2010).

[27] N. Navon, S. Nascimbne, F. Chevy and C. Salomon, Science **328**, 729 (2010).

[28] P. O. Fedichev, M. W. Reynolds and G. V. Shlyapnikov, Phys. Rev. Lett. **77**, 2921 (1996).

[29] S. Tan, Ann. Phys. **323**, 2952 (2008); Ann. Phys. **323**, 2971 (2008).

[30] F. Werner and Y. Castin, ArXiv: **1001.0774**; Y. Castin and F. Werner, Phys. Rev. A **83**, 063614 (2011).

[31] E. Braaten, D. Kang and L. Platter, Phys. Rev. Lett. **106**, 153005 (2011).

[32] S. -J. Jiang, W. -M. Liu, G. W. Semenoff and F. Zhou, ArXiv: **1307.4263**.

[33] Y. L. Lee and Y. W. Lee, Phys. Rev. A **81**, 063613 (2010).

[34] V. Efimov, Phys. Lett. B. **33**, 563 (1970); Sov. J. Nucl. Phys. **12**, 589 (1971).

[35] Z. Hadzibabic, P. Krüger, M. Cheneau, B. Battelier and J. Dalibard, Nature **441**, 1118 (2006).

[36] V. Schweikhard, S. Tung and E. A. Cornell, Phys. Rev. Lett. **99**, 030401 (2007).

[37] P. Cladé, C. Ryu, A. Ramanathan, K. Helmerson and W. D. Phillips, Phys. Rev. Lett. **102**, 170401 (2009).

[38] C.-L. Hung, X. Zhang, N. Gemelke and C. Chin, Nature **470**, 236 (2011).

[39] V. L. Berezinskii, Sov. Phys. JETP. **34**, 610 (1972).

[40] J. M. Kosterlitz and D. J. Thouless, J. Phys. C **6**, 1181 (1973).

[41] N. D. Mermin, H. Wagner, Phys. Rev. Lett. **17**, 1133 (1966).

[42] Z. Li and R. V. Krems, Phys. Rev. A **79**, 050701 (2009).

[43] L.W. Bruch and J. A. Tjon, Phys. Rev. A **19**, 425 (1979).

[44] E. Nielsen, D. V. Fedorov, and A. S. Jensen, Few-Body Syst. **27**, 15 (1999).

[45] H. W. Hammer and D. T. Son, Phys. Rev. Lett. **93**, 250408 (2004).

[46] D. Blume, Phys. Rev. B **72**, 094510 (2005).

[47] M. Schick, Phys. Rev. A **3**, 1067 (1971).

[48] V. N. Popov, Theor. Math. Phys. **11**, 565 (1972).

[49] D. S. Fisher and P. C. Hohenberg, Phys. Rev. B **37**, 4936 (1988).

[50] D.S. Petrov and G.V. Shlyapnikov, Phys. Rev. A **64**, 012706 (2001).

[51] I. Bloch, M. Dalibard and W. Zwerger, Rev. Mod. Phys. **80**, 855 (2008).

[52] V. Pietilä, D. Pekker, Y. Nishida and E. Demler, Phys. Rev. A **85**, 023621 (2012).

[53] S. Pilati, J. Boronat, J. Casulleras, and S. Giorgini, Phys. Rev. A **71**, 023605 (2005).

[54] P. Nozieres and D. Pines, *The Theory of Quantum Liquids, Vol 2, Superfluid Bose Liquids*, (Addison-Wesley, Redwood City, CA, 1990).

[55] N. M. Hugenholtz and D. Pines, Phys. Rev. **116**, 489 (1959).

[56] F. D. M. Haldane, Phys. Rev. Lett. **47**, 1840 (1981).

[57] P. F. Bedaque, H.-W. Hammer and U. van Kolck, Phys. Rev. Lett. **82**, 463 (1999); Nucl. Phys. A **646**, 444 (1999).

[58] M. Girardeau, J. Math. Phys. **1**, 516 (1960).

[59] E. H. Lieb and W. Liniger, Phys. Rev. **130**, 1605 (1963).

[60] D. Kaplan, M. J. Savage and M. B. Wise, Nucl. Phys. B **534**, 329 (1998).

[61] Y. Nishida and D. T. Son, Phys. Rev. Lett. **97**, 050403 (2006).

[62] M.Y. Veillette, D. E. Sheehy and L. Radzihovsky, Phys. Rev. A **75**, 043614 (2007).

[63] P. Nikolic and S. Sachdev, Phys. Rev. A **75**, 033608 (2007).

[64] X. Cui, Y. Wang, and F. Zhou, Phys. Rev. Lett. **104**, 153201 (2010).

[65] D. J. MacNeill, F. Zhou, Phys. Rev. Lett. **106**, 145301 (2011).

[66] J. L. Song, and F. Zhou, Phys. Rev. A **84**, 013601 (2011).

[67] C. J. M. Mathy, M. M. Parish, and D. A. Huse, Phys. Rev. Lett. **106**, 166404 (2011).

[68] Nicolai G. Nygaard and N. T. Zinner, ArXiv: **1110.5854.**

[69] Lan Yin, Phys. Rev. A **77**, 043630 (2008).

[70] D. Pekker, M. Babadi, R. Sensarma, N. Zinner, L. Pollet, M. W. Zwierlein and E. Demler, Phys. Rev. Lett. **106**, 050402 (2011).

[71] *Superfluids*, F. London (John Wiley and Sons, New York 1954).

[72] L. Landau, Jour. Phys. U.S.S.R **5**, 71 (1941).

[73] R. P. Feynman, Phys. Rev. **94**, 262 (1954).

[74] O. Penrose and L. Onsager, Phys. Rev. **104**, 576 (1956).

[75] For ^4He liquid in nanopores, see a recent study in A. Del Maestro, M. Boninsegni and I. Affleck , Phys. Rev. Lett. **106**, 105303 (2011).

[76] S. Beane, Phys. Rev. A **82**, 063610 (2010).

[77] G.-B. Jo, Y.-R. , J.-H. Choi, C. A. Christensen, T. H. Kim, J. H. Thywissen, D. E. Pritchard and W. Ketterle, Science **325** (5947), 1521-1524 (2009).

Appendix A

Solving Self-Consistent Eq. (2.5) in the Dilute Limit

We apply Eq. (2.5) to calculate the leading-order correction beyond the mean-field theory. We notice that the equations for g_2 and μ are arranged in such a way that the next-order correction can be obtained by applying the results from the lowest-order approximation to the right-hand side. In the lowest-order approximation, we find $\Sigma = 8\pi n_0 a$ and $\mu = 4\pi n_0 a$; this leads to a correction to g_2 as

$$\begin{aligned} g_2 &= 4\pi a + \frac{(4\pi a)^2}{2}\int \frac{d^3k}{(2\pi)^3}\left(\frac{1}{\epsilon_k} - \frac{1}{\epsilon_k + \mu}\right) \\ &= 4\pi a\left(1 + \sqrt{8\pi n_0 a^3}\right). \end{aligned} \tag{A.1}$$

Similarly, from the relation $\frac{\partial\Sigma}{\partial n_0} = 8\pi a$ and $\frac{\partial\Sigma}{\partial\mu} = 0$, we can get the correction for the chemical potential μ as,

$$\begin{aligned} \mu &= 4\pi a n_0 + \frac{(4\pi a)^3 n_0^2}{2}\int \frac{d^3k}{(2\pi)^3}\frac{1}{(\epsilon_k + \mu)^2} \\ &= 4\pi a n_0\left(1 + 3\sqrt{2\pi n_0 a^3}\right) \end{aligned} \tag{A.2}$$

and the depletion fraction

$$\frac{n_p}{n} = \frac{n_0}{4} g_2^2 \int \frac{d^3k}{(2\pi)^3}\frac{1}{(\epsilon_k + \mu)^2} = \sqrt{\frac{\pi}{2} n_0 a^3}. \tag{A.3}$$

For a comparison we list the results from the dilute-gas theory,

$$\mu_{Beliaev} = 4\pi n_0 a\left[1 + \frac{40}{3}\sqrt{\frac{1}{\pi} n_0 a^3}\right], \tag{A.4}$$

$$\left(\frac{n_p}{n}\right)_{Beliaev} = \frac{8}{3}\sqrt{\frac{1}{\pi} n_0 a^3}. \tag{A.5}$$

Our self-consistent approach produces $\frac{9\sqrt{2}\pi}{40}(= 99.96\%)$ of Beliaev's result for the chemical potential, and $\frac{3\sqrt{2}\pi}{16}(= 83\%)$ for the depletion fraction.

Appendix B

A Comparison Between the Self-Consistent Approach and the Dilute Gas Theory in Three Dimensions

In the following, we show explicitly that our self-consistent equation corresponds to a subgroup of diagrams [in Fig. 2.2(c)] in the usual dilute gas theory. The two-body T-matrix used in the dilute-gas theory [represented by the green circles in Figs. 2.2(c) and 2.2(d)] are obtained using the non-interacting Green's function $G^{-1}(\epsilon, k) = \epsilon - \epsilon_k + \mu + i0^+$; in the dilute limit, we can expand the T-matrix as

$$t(\omega, Q) = 4\pi a \left[1 + 4\pi a \int \frac{d^3k}{(2\pi)^3} \left(\frac{1}{\omega - \frac{Q^2}{4} - k^2 + 2\mu + i0^+} + \frac{1}{k^2} \right) + \cdots \right], \tag{B.1}$$

where ω and Q are the total energy and momentum of the incoming atoms. The contribution from the first two diagrams in Fig. 2.2(c) are

$$\begin{aligned} E_{(c1)} &\simeq \frac{t(0,0)n_0^2}{2} \simeq 2\pi a n_0^2 \left[1 + 4\pi a \int \frac{d^3k}{(2\pi)^3} \left(\frac{1}{-k^2 + 2\mu + i0^+} + \frac{1}{k^2} \right) \right] \\ E_{(c2)} &\simeq 2 \frac{t^2(0,0)n_0^2}{2} \int \frac{d^3k}{(2\pi)^3} \left(\frac{1}{-k^2 + 2\mu + i0^+} \right)^2 2n_0 t(\mu - \epsilon_k, 0) \qquad \text{(B.2)} \\ &\simeq 2\pi a n_0^2 \left[(4\pi a)(16\pi n_0 a) \int \frac{d^3k}{(2\pi)^3} \left(\frac{1}{-k^2 + 2\mu + i0^+} \right)^2 \right]. \qquad \text{(B.3)} \end{aligned}$$

For the leading-order correction beyond the mean-field theory, it suffices to set $t(\mu - \epsilon_k, 0) \simeq 4\pi a$ in Eq. (B.3) and in higher-order diagrams. Similarly, we can get the contributions from the higher-order diagrams in this series,

and the sum is

$$\begin{aligned} E_{(c)} &\simeq 2\pi a n_0^2 \left[1 + 4\pi a \int \frac{d^3k}{(2\pi)^3} \left(\frac{1}{-k^2 + 2\mu + i0^+} + \frac{1}{k^2} \right) \right] \\ &+ 2\pi a n_0^2 (4\pi a) \sum_{m=1}^{\infty} (16\pi a n_0)^m \int \frac{d^3k}{(2\pi)^3} \left(\frac{1}{-k^2 + 2\mu + i0^+} \right)^{m+1} \quad \text{(B.4)} \\ &\simeq 2\pi a n_0^2 \left[1 + 4\pi a \int \frac{d^3k}{(2\pi)^3} \left(\frac{1}{-k^2 + 2\mu - 16\pi n_0 a} + \frac{1}{k^2} \right) \right]. \quad \text{(B.5)} \end{aligned}$$

We see that the energy given by the diagrams in Fig. 2.2(c) is *exactly* the same as the one used in our self-consistent equation, e.g., $g_2 n_0^2/2$, where g_2 should be expanded as Eq. (A.1) in the dilute limit.

Next, we can sum up the rest of the one-loop diagrams that are not included in the self-consistent equations; they represent the lowest-order contributions to four- and six-body forces and so on. In the dilute limit, these diagrams [as shown in Fig. 2.2(d)] can be summed as

$$E_{(d)} = -(4\pi a n_0) \int \frac{d^3k}{(2\pi)^3} \sum_{m=2}^{\infty} \frac{1}{2} \frac{(2m-2)!}{m!\,(m-1)!} \left(\frac{4\pi a n_0}{2\epsilon_k - 2\mu + 16 n_0 \pi a} \right)^{2m-1}. \quad \text{(B.6)}$$

Indeed, we can recover Beliaev's result by summing up one-loop diagrams in Figs. 2.2(c) and 2.2(d) as

$$\begin{aligned} &\frac{\partial}{\partial n_0} \left(E_{(c)} + E_{(d)} \right) = 4\pi n_0 a \\ &+ 4\pi a \int \frac{d^3k}{(2\pi)^3} \left[\frac{(\epsilon_k - \mu + 6\pi n_0 a)}{\sqrt{(\epsilon_k - \mu + 8\pi a n_0)^2 - (4\pi a n_0)^2}} - 1 + \frac{4\pi n_0 a}{k^2} \right] \\ &= 4\pi n_0 a \left[1 + \frac{40}{3} \sqrt{\frac{1}{\pi} n_0 a^3} \right] = \mu_{Beliaev} \quad \text{(B.7)} \end{aligned}$$

Appendix C

Including Three-Body Forces in the Self-Consistent Equations in Three Dimensions

We now calculate the amplitude of three-body scatterings corresponding to the processes described in Fig. 2.2(b). First, we consider a general case where the three incoming momenta are $\mathbf{k}_1 = \mathbf{p}/2 - \mathbf{q}$, $\mathbf{k}_2 = \mathbf{p}/2 + \mathbf{q}$, and $\mathbf{k}_3 = -\mathbf{p}$, and the outgoing ones are $\mathbf{k}'_1 = \mathbf{p}'/2 - \mathbf{q}'$, $\mathbf{k}'_2 = \mathbf{p}'/2 + \mathbf{q}'$, and $\mathbf{k}'_3 = -\mathbf{p}'$. The scattering amplitude between these states is then given by $A(E - 3\eta; \mathbf{p}, \mathbf{p}')$, which represents the sum of diagrams identical to Fig. 2.2(b) except that the external lines carry finite momenta.

For the estimate of three-body contributions of g_3, we first treat the sum of diagrams in Fig. 2.2(b) as the limit of $A(E-3\eta; \mathbf{p}, \mathbf{p}')$ when $\mathbf{p}$ and $\mathbf{p}'$ approach zero and the total frequency E is set to zero. It is therefore more convenient to work with the reduced amplitude $G_3(E-3\eta; \mathbf{p}) = A(E-3\eta; \mathbf{p}, 0)$, where $\mathbf{p}'$ is already taken to be zero. $G_3(E - 3\eta; \mathbf{p})$ itself obeys a simple integral equation, as can be seen by listing the terms in the summation explicitly. Indeed, when E is further set to zero, we find that the diagrams in Fig. 2.2(b) yield

$$G_3(-3\eta, p) = \frac{2}{\pi} \int dq \frac{K(-3\eta; p, q) q^2}{\sqrt{\frac{3}{4}q^2 + 3\eta} - \frac{1}{a}} \frac{-1}{q^2 + 3\eta} \tag{C.1}$$

$$+ \quad \left(\frac{2}{\pi}\right)^2 \int dq dq' \frac{K(-3\eta; p, q) q^2}{\sqrt{\frac{3}{4}q^2 + 3\eta} - \frac{1}{a}} \frac{K(-3\eta; q, q') q'^2}{\sqrt{\frac{3}{4}q'^2 + 3\eta} - \frac{1}{a}} \frac{-1}{q'^2 + 3\eta} + \cdots , \tag{C.2}$$

where $K(-3\eta; p, q)$ is the kernel defined in chapter 2. The sum of the above

infinite series leads to the following integral equation of G_3 :

$$\begin{aligned} G_3(-3\eta,p) &= \frac{2}{\pi}\int dq \frac{K(-3\eta;p,q)q^2}{\sqrt{\frac{3}{4}q^2+3\eta}-\frac{1}{a}}\frac{-1}{q^2+3\eta} \\ &+ \frac{2}{\pi}\int dq \frac{K(-3\eta;p,q)q^2}{\sqrt{\frac{3}{4}q^2+3\eta}-\frac{1}{a}}G_3(-3\eta,q). \end{aligned} \tag{C.3}$$

Note that $G_3(-3\eta,0)$ defined above includes a diagram [the leftmost one in Fig. 2.2(b)] that has already been included in g_2. To avoid overcounting, we subtract the first diagram in Fig. 2.2(b) from G_3 as

$$g_3 = 6g_2^2 \mathrm{Re}\left[G_3(-3\eta,0) - \frac{2}{\pi}\int dq \frac{K(-3\eta;0,q)q^2}{\sqrt{\frac{3}{4}q^2+3\eta}-\frac{1}{a}}\frac{-1}{q^2+3\eta}\right]. \tag{C.4}$$

Alternatively, one can also carry out a direct summation of the diagrams in Fig. 2.2(b). It leads to a result that numerically differs very little from the estimation obtained above via an asymptotic extrapolation. For instance, a direct evaluation of those diagrams yields

$$G_3(-3\eta,0) = \frac{2}{\pi}\int dq \frac{K(-2\eta;0,q)q^2}{\sqrt{\frac{3}{4}q^2+3\eta}-\frac{1}{a}}\frac{-1}{q^2+2\eta} \tag{C.5}$$

$$+ \left(\frac{2}{\pi}\right)^2 \int dq dq' \frac{K(-2\eta;0,q)q^2}{\sqrt{\frac{3}{4}q^2+3\eta}-\frac{1}{a}}\frac{K(-3\eta;q,q')q'^2}{\sqrt{\frac{3}{4}q'^2+3\eta}-\frac{1}{a}}\frac{-1}{q'^2+2\eta}+\cdots \tag{C.6}$$

The only difference between Eqs. (C.6) and (C.2) is that the frequencies appearing in the first kernel $K(E;0,q)$ in the integrands and in the last denominators are now -2η instead of -3η.

One can easily verify that the sum can be written in the following compact form:

$$G_3(-3\eta,0) = \frac{2}{\pi}\int dq \frac{K(-2\eta;0,q)q^2}{\sqrt{\frac{3}{4}q^2+3\eta}-\frac{1}{a}}[\frac{-1}{q^2+2\eta}+G_3'(-3\eta,q)], \tag{C.7}$$

where $G_3'(-3\eta,p)$ is a solution of the following integral equation:

$$G_3'(-3\eta,p) = \frac{2}{\pi}\int dq \frac{K(-3\eta;p,q)q^2}{\sqrt{\frac{3}{4}q^2+3\eta}-\frac{1}{a}}[\frac{-1}{q^2+2\eta}+G_3'(-3\eta,q)] \tag{C.8}$$

Note that $G_3^{'}(-3\eta, p)$ defined here describes an off-shell scattering between three incoming atoms with momenta $\mathbf{p}/2 - \mathbf{q}$, $\mathbf{p}/2 + \mathbf{q}$, and $-\mathbf{p}$ and three condensed atoms. As a consequence of the Hartree-Fock approximation we have employed here, $G_3(-3\eta, 0)$ is not equal to $G_3^{'}(-3\eta, 0)$. $G_3(-3\eta, 0)$ and $G_3^{'}(-3\eta, 0)$ can be obtained numerically.

Finally, after subtracting the leftmost one-loop diagram in Fig. 2.2(b) we again find the three-body contribution to be:

$$g_3 = 6g_2^2 \mathrm{Re}\left[G_3(-3\eta, 0) - \frac{2}{\pi}\int dq \frac{K(-2\eta; 0, q)q^2}{\sqrt{\frac{3}{4}q^2 + 3\eta} - \frac{1}{a}} \frac{-1}{q^2 + 2\eta}\right]. \quad \text{(C.9)}$$

Now we can include the three-body forces $\frac{g_3 n_0^3}{6}$ in a set of differential self-consistent equations similar to Eq. (2.5). We solve the equation numerically, and the results are shown in Fig. 2.3, where in the inset we show the momentum cutoff Λ dependence in the chemical potential. In our numerical program, we further use the approximation $\frac{\partial \Sigma}{\partial n_0} = 2g_2$, $\frac{\partial \Sigma}{\partial \mu} = 0$, and $\Sigma_{11} = \beta\mu$ ($\beta = 2$) to simplify the numerical calculations (see Appendix D). We have tested other types of approximation schemes for the self-energy, such as $\Sigma_{11} = 8\pi a n_0$ or $\Sigma_{11} = 2g_2 n_0$. We find that the chemical potential and the value of the critical point $n a_{cr}^3$ are insensitive to approximation schemes.

Appendix D

Single Parameter Limit

Here we explain the single parameter limit, where the physics of two- and three-dimensional Bose gases could be described by a single parameter, μ. We determine this limit by looking at the behavior of the two-body interaction potential. Three-dimensional g_2 is written as:

$$g_2^{-1} = U_0^{-1} - i \int \frac{d\omega}{2\pi} \frac{d^3\mathbf{k}}{(2\pi)^3} G(\omega, \mathbf{k}) G(-\omega, -\mathbf{k}), \tag{D.1}$$

where $G(\omega, \mathbf{k})^{-1} = \omega - \epsilon_{\mathbf{k}} - \Sigma + \mu + i\delta^+$ is the interacting Green's function. Here, Σ is the self-energy of non-condensed particles which in general is a function of momentum and frequency. The self-energy is almost flat for momenta smaller than $1/a$ while after this point it decays to zero. Furthermore, we can supplement the above equation with the following relation to regulate ultraviolet divergency in three dimensions:

$$\frac{1}{U_0} = \frac{1}{4\pi a} - \frac{1}{\Omega} \sum_k \frac{1}{2\epsilon_k}. \tag{D.2}$$

And after a little bit calculation, we can write:

$$g_2^{-1} = \frac{1}{4\pi a} - \frac{1}{\pi^2} \int dk \frac{\Sigma}{k^2 + 2\Sigma - 2\mu} + \frac{1}{\pi^2} \int dk \frac{\mu}{k^2 + 2\Sigma - 2\mu}. \tag{D.3}$$

One can look at the two integrals in the above equation separately. The first integral does not have ultra-violet divergency, since Σ decays to zero for large momenta. So, the main contribution comes from low energy limit of the integral and since Σ is equal to 2μ for small momenta, this integral could be considered as a single variable function of μ. Similarly, there is no ultraviolet divergency for second integral and again the physics is determined by low energy limit. Above calculation shows that two-body interaction is a function of only a and μ. In chapter 2, we found that the instability point happens for relatively small value of scattering length. This results the self-energy to be independent of momenta for a wider range which make above estimation of integrals more reasonable. In addition, we assume Σ to be

independent of momentum in our calculations in this thesis. In this regime, the above equation could be evaluated exactly and the result is:

$$g_2(2\mu) = \frac{4\pi}{\frac{1}{a} - \sqrt{2m\mu}}. \tag{D.4}$$

One can also look at three-body interactions in three dimensions and as it mentioned before in chapter 2, g_3 is a function of the ultra-violet cut off as well as a and μ. But since the contribution of the three-body forces to the energy of the system is approximated to be around few percent, our results remain robust.

Similar arguments could be used for a two-dimensional Bose gas. The single parameter approximation is still valid in this dimension. In addition, since three-body forces are universal in two-dimensions, our calculation is robust for such systems.

Appendix E

Two- and Three-Body Scattering Amplitudes in a Condensate in Three Dimensions

In the following, we show the explicit calculation of the three-atom scattering amplitude G_3, and $E(n_0, \mu)$ for a given $\Sigma(= \eta + \mu)$ by adding the diagrams with a minimum number of virtual particles involved. The model Hamiltonian could be written as:

$$\begin{aligned} H &= \sum_{\mathbf{k}} (\epsilon_{\mathbf{k}} - \mu) b^\dagger_{\mathbf{k}} b_{\mathbf{k}} + 2U_0 n_0 \sum_{\mathbf{k}} b^\dagger_{\mathbf{k}} b_{\mathbf{k}} \\ &+ \frac{1}{2} U_0 n_0 \sum_{\mathbf{k}} b^\dagger_{\mathbf{k}} b^\dagger_{-\mathbf{k}} + \frac{1}{2} U_0 n_0 \sum_{\mathbf{k}} b_{\mathbf{k}} b_{-\mathbf{k}} \\ &+ \frac{U_0}{\sqrt{\Omega}} \sqrt{n_0} \sum_{\mathbf{k}', \mathbf{q}} b^\dagger_{\mathbf{q}} b_{\mathbf{k}' + \frac{\mathbf{q}}{2}} b_{-\mathbf{k}' + \frac{\mathbf{q}}{2}} + h.c. \\ &+ \frac{U_0}{2\Omega} \sum_{\mathbf{k}, \mathbf{k}', \mathbf{q}} b^\dagger_{\mathbf{k} + \frac{\mathbf{q}}{2}} b^\dagger_{-\mathbf{k} + \frac{\mathbf{q}}{2}} b_{\mathbf{k}' + \frac{\mathbf{q}}{2}} b_{-\mathbf{k}' + \frac{\mathbf{q}}{2}} + h.c., \end{aligned} \tag{E.1}$$

where the sum is over non-zero momentum states. U_0 is the strength of the contact interaction which is related to scattering length a as:

$$\frac{1}{U_0} = \frac{m}{4\pi a} - \frac{1}{\Omega} \sum_k \frac{1}{2\epsilon_k}, \tag{E.2}$$

where Ω is the volume. Taking into account only two- and three-body interactions, the energy density could be written as:

$$E(n_0, \mu) = \frac{1}{2} n_0^2 g_2(2\eta) + \frac{1}{3!} n_0^3 g_3(3\eta), \tag{E.3}$$

where g_2 and g_3 are irreducible two- and three-body potentials respectively. g_2 could be found by writing the Bethe-Salpeter equation as:

$$g_2(2\eta)^{-1} = U_0^{-1} - i\int \frac{d\omega}{2\pi}\frac{d^3\mathbf{k}}{(2\pi)^3}G(\omega,\mathbf{k})G(-\omega,-\mathbf{k}), \tag{E.4}$$

where $G(\omega,\mathbf{k})^{-1} = \omega - \epsilon_{\mathbf{k}} - \eta + i\delta^+$ is the interacting Green's function. So, the two-body potential could be obtained as:

$$g_2(2\eta) = \frac{4\pi}{\frac{1}{a} - \sqrt{2m\eta}} \tag{E.5}$$

Similarly, g_3 could be estimated by summing up all N-loop diagrams with 3 incoming and outgoing lines which are depicted in Fig. 3.3(b). We consider a general case where three incoming momenta are $\mathbf{k}_1 = \mathbf{p}/2-\mathbf{q}$, $\mathbf{k}_2 = \mathbf{p}/2+\mathbf{q}$ and $\mathbf{k}_3 = -\mathbf{p}$, and outgoing ones are $\mathbf{k}_1' = \mathbf{p}'/2 - \mathbf{q}'$, $\mathbf{k}_2' = \mathbf{p}'/2 + \mathbf{q}'$ and $\mathbf{k}_3' = -\mathbf{p}'$. The scattering amplitude between these states is then given by $A_3(E;\mathbf{p},\mathbf{p}')$. At the tree-level, the effective three-particle interaction is:

$$\Gamma^{(0)} = \frac{f_0}{E - \omega_{in} - \omega_{out} - \epsilon_{\mathbf{p}+\mathbf{p}'} - \eta + i\delta^+}, \tag{E.6}$$

where ω_{in} and ω_{out} are frequencies of lines with momenta $\mathbf{k}_3$ and $\mathbf{k}_3'$ respectively. Furthermore, f_0 is the product of the perturbation factor f_p, vertex factor f_v and symmetry factor f_s which will be explained later.

To keep the notation simple, we set $m = 1$ from now on. We consider on-shell limit and substitute ω_{in} and ω_{out} by $p^2/2+\eta$ and $p'^2/2+\eta$ respectively. To project into the S-wave channel, we take the average over all directions,

$$\overline{\Gamma}^{(0)} = \frac{-f_0}{2pp'} ln\left(\frac{p^2+p'^2+pp'+3\eta-E}{p^2+p'^2-pp'+3\eta-E}\right) \equiv \frac{-f_0}{2}K(E-3\eta;p,p'), \tag{E.7}$$

where we have defined the kernel K as:

$$K(E-3\eta;p,p') = \frac{1}{pp'} ln\left(\frac{p^2+p'^2+pp'+3\eta-E}{p^2+p'^2-pp'+3\eta-E}\right) \tag{E.8}$$

The *perturbation factor*, f_p, comes from the expansion, in perturbation theory, of the evolution operator $exp(-iH_{int}t)$. The diagrams with l vertices could be written as:

$$\frac{1}{l!}(V_A + V_B)^l, \tag{E.9}$$

where V_A and V_B stand for interaction terms corresponding to different types of vertices namely A and B. For example, for a diagram with 2 vertices of type A and one vertex of type B, f_p is the factor in front of the $V_A^2 V_B$ term in the numerator of the above equation divided by $l!$. In the vacuum case, where all the vertices are the same and all the lines can have non-zero momenta, f_p is simply equal to $(1/l!)$.

The *vertex factor*, f_v, is defined as the product of the factors in front of g_2 for different vertices shown in the Hamiltonian. For the vacuum case, all the vertices have $1/2$ factor and f_v is equal to $(1/2)^l$.

The last factor is the *symmetry factor*, f_s which shows the number of identical diagrams generated for a given number of vertices. For the vacuum case, $f_s = l! \times 4^l$ where $l!$ shows the number of permutations of vertices and 4^l is the number of different ways of connecting vertices (2 for incoming lines and 2 for outgoing lines).

So, in general the prefactor appearing in $\Gamma^{(n)}$ where n is the number of loops ($n = l - 2$) would be

$$f_n = 2^{(n+2)}; \tag{E.10}$$

and $f_0 = 4$.

$\Gamma^{(1)}$ could be written in terms of the kernel defined above as:

$$\Gamma^{(1)} = 8 \int \frac{d^3k}{(2\pi)^3} (-\frac{1}{2} K(E - 3\eta; p, k)) g_2(E - 3\eta - \frac{k^2}{2}; k)(-\frac{1}{2} K(E - 3\eta; k, p')), \tag{E.11}$$

where the integral over internal frequency has been taken. $g_2(\omega; Q)$ has the following form in 3D:

$$g_2(\omega; Q) = \frac{4\pi}{\frac{1}{a} - \sqrt{\frac{Q^2}{4} - \omega}}, \tag{E.12}$$

where the above equation reduces to Eq. (E.5) in the limit of zero energy and momentum. The effective three-body interaction then could be obtained by summing over $\Gamma^{(n)}$s:

$$\begin{aligned}\Gamma_{eff} &= -2K(E-3\eta;p,p') \\ &+ \frac{4}{\pi}\int dkk^2 \frac{K(E-3\eta;p,k)}{\frac{1}{a}-\sqrt{\frac{3k^2}{4}-E+3\eta}} \times K(E-3\eta;k,p') \\ &- \frac{8}{\pi^2}\int dkk^2\int dk'k'^2 \frac{K(E-3\eta;p,k)}{\frac{1}{a}-\sqrt{\frac{3k^2}{4}-E+3\eta}} \times \frac{K(E-3\eta;k,k')}{\frac{1}{a}-\sqrt{\frac{3k'^2}{4}-E+3\eta}} \\ &\times K(E-3\eta;k',p')+\ldots \end{aligned} \tag{E.13}$$

The sum of the above infinite series leads to the following integral equation for scattering amplitude A_3:

$$A_3(E;p,p') = -2K(E-3\eta;p,p') - \frac{2}{\pi}\int dkk^2 \frac{K(E-3\eta;p,k)}{\frac{1}{a}-\sqrt{\frac{3k^2}{4}-E+3\eta}} A_3(E;k,p') \tag{E.14}$$

One then obtains the reduced scattering amplitude $G_3(E;\mathbf{p}) = A_3(E;\mathbf{p},0)$ in Eq. (3.22).

For the calculation of g_3 for condensates, one has to exclude the tree level diagram that no longer exists because of momentum conservation. The sum of the rest of the infinite series leads to the following integral equation for the scattering amplitude $A_3(E;p,p')$,

$$A_3(E;p,p') = \frac{2}{\pi}\int dk \frac{K(E-3\eta;p,k)k^2}{\frac{1}{a}-\sqrt{\frac{3k^2}{4}-E+3\eta}} \left(2K(E-3\eta;k,p') - A_3(E;k,p')\right) \tag{E.15}$$

The above scattering amplitude could then be applied to calculate the scatterings between condensed atoms when setting E, $\mathbf{p}$ and $\mathbf{p}'$ to be zero in the above equation but with two further modifications. The first change is the numerical factor in front of the effective interactions. This factor in the condensate case is 1/4 of the factor in the vacuum case, because there is a 2×2 factor for changing the external legs of the external vertices for non-zero incoming momenta. So we will get the same integral equation, but the first term in the bracket of the integrand of Eq. (E.15) would be substituted by $1/2K$.

The second change would be in the shift of the energy. If we set the momentum of external legs to zero from the beginning, in the on-shell limit

there is no shift of the energy for ω_{in} and ω_{out} in our diagrammatic calculations. So, the energy of the first and the last kernel in all the terms of the Eq. (E.13) other than the tree-level term would be $E-2\eta$ in the condensate case. Subtracting the one-loop contribution which has already been counted in the renormalized g_2 and taking into account the above two modifications, we obtain ${g_3}^{16}$.

[16] As mentioned before in chapter 3, there are two ways of estimating G_3 which slightly differ from each other; the difference is due to singular behavior of the Green's function at $k = 0$ in the Hartree-Fock approximation as commented on in Appendix C. Here we evaluate G_3 by first setting all external lines to be the condensed atoms.

Appendix F

Two- and Three-Body Scattering Amplitudes in a Condensate in Two Dimensions

Two-body effective interaction could be obtained by using Dyson's equation in the following closed form:

$$\begin{aligned} -ig_2(E;Q) &= -iU_0 \\ &+ \int \frac{d\omega}{2\pi}\frac{d^2\mathbf{k}}{(2\pi)^2} g_2(E;Q)U_0 G(\omega, \mathbf{Q/2}+\mathbf{k})G(E-\omega, \mathbf{Q/2}-\mathbf{k}). \end{aligned} \tag{F.1}$$

where $G(\omega,\mathbf{k})^{-1} = \omega - \epsilon_{\mathbf{k}} - \eta + i\delta^+$ is the interacting Green's function, U_0 is the attractive bare interaction strength and $\eta = \Sigma - \mu$.

So, two-body scattering amplitude could be written as:

$$\begin{aligned} g_2(E;Q)^{-1} &= U_0^{-1} \\ &- i\int \frac{d\omega}{2\pi}\frac{d^2\mathbf{k}}{(2\pi)^2} G(\omega, \mathbf{Q/2}+\mathbf{k})G(E-\omega, \mathbf{Q/2}-\mathbf{k}), \end{aligned} \tag{F.2}$$

After integration over frequency and momentum space one obtains:

$$\begin{aligned} g_2(E;Q)^{-1} &= U_0^{-1} + \frac{1}{4\pi} log(|\frac{\Lambda}{Q^2/4 - E - 2\eta}|) + \frac{i}{4} \\ &\equiv \frac{1}{4\pi} log(|\frac{B_2}{Q^2/4 - E - 2\eta}|) + \frac{i}{4}, \end{aligned} \tag{F.3}$$

where Λ is the ultra-violet energy cutoff. Here B_2, two-body bound state energy is defined to be:

$$B_2 = \Lambda e^{\frac{4\pi}{U_0}}. \tag{F.4}$$

$a_{2D} = \sqrt{\hbar^2/mB_2}$, the effective two-dimensional scattering length is introduced as the size of two-body bound state. Λ is set by the interaction range R^*, via $\Lambda = \frac{\hbar^2}{mR^{*2}}$.

For repulsive interactions ($U_0 > 0$), B_2 is larger than Λ. As a result, a_{2D} can not exceed form range of interaction, and for a short range interaction the system is always in the dilute regime. By increasing U_0, the range of a_{2D} becomes more restricted from below and at an extreme limit when U_0 goes to infinity, a_{2D} is exactly equal to the range of interaction R^*. This limit is known as the hard-core limit. For attractive interactions ($U_0 < 0$), which is the case we are interested in, B_2 is smaller than Λ. This condition sets the lower-bound of the 2D scattering length equal to the range of the interaction. So, a_{2D} could be arbitrary large and potentially the system can go beyond the dilute limit and approach resonance.

For two-dimensional Bose gases, the imaginary part of the two-body effective interaction is independent of the total energy of the incoming scattering particles. As a result, the imaginary part exists even for zero total energy. This unique property of the two-dimensional gases is due to the fact that two-dimensional density of states is independent of energy. The real part of the g_2 is:

$$Re(g_2(E;Q)) = \frac{4\pi}{log(|\frac{B_2}{Q^2/4-E-2\eta}|)}. \tag{F.5}$$

Three-body scattering amplitude, g_3, could be estimated by summing up all N-loop diagrams with three incoming and outgoing lines. We consider a general case where three incoming momenta are $\mathbf{k}_1 = \mathbf{p}/2 - \mathbf{q}$, $\mathbf{k}_2 = \mathbf{p}/2 + \mathbf{q}$ and $\mathbf{k}_3 = -\mathbf{p}$, and outgoing ones are $\mathbf{k}'_1 = \mathbf{p}'/2 - \mathbf{q}'$, $\mathbf{k}'_2 = \mathbf{p}'/2 + \mathbf{q}'$ and $\mathbf{k}'_3 = -\mathbf{p}'$. The scattering amplitude between theses states is then given by $A_3(E;\mathbf{p},\mathbf{p}')$. For tree level diagram with no loop, the effective three-particle interaction is:

$$\Gamma^{(0)} = \frac{f_0}{E - \omega_{in} - \omega_{out} - \epsilon_{\mathbf{p}+\mathbf{p}'} - \eta + i\delta^+}, \tag{F.6}$$

where ω_{in} and ω_{out} are frequencies of lines with momentum $\mathbf{k}_3$ and $\mathbf{k}'_3$ respectively. Furthermore, as in Appendix E f_0 is the product of perturbation factor f_p, vertex factor f_v and symmetry factor f_s which will be defined later.

Although this diagram does not exist when we set the momenta of external lines to zero (the reason is that in this case, the momentum of the internal line also has to be zero due to the conservation of the momentum at each vertex which makes this diagram trivial), it is the building block of the scattering processes with more number of loops. Since eventually we set the momenta of external lines equal to zero in order to find the effective interaction between condensed particles, the angle between these momenta is not well-defined. So, we project $\Gamma^{(0)}$ to s-wave channel by taking the average over all solid angles. In addition, for on-shell particles, ω_{in} and ω_{out} are substituted by $p^2/2+\eta$ and $p'^2/2+\eta$ respectively. η could be understood as the energy shift due to interaction of condensed and non-condensed particles.

$$\overline{\Gamma}^{(0)} = \frac{1}{2\pi}\int_0^\infty d\theta \frac{f_0}{E - p^2 - p'^2 - 3\eta - pp' cos\theta + i\delta^+} \tag{F.7}$$

after doing the integration over angle we have:

$$\overline{\Gamma}^{(0)} = \frac{-f_0}{\sqrt{(E-p^2-p'^2)^2-(pp')^2}} \equiv \frac{-f_0}{2} K(E-3\eta; p, p'), \tag{F.8}$$

where the kernel K is defined as:

$$K(E; p, p') = \frac{2}{\sqrt{(E-p^2-p'^2)^2-(pp')^2}}. \tag{F.9}$$

To obtain the numerical factor in front of each diagram, it is important to remark that each of the terms in the Hamiltonian (2.1) corresponds to different vertices in the scattering diagrams (See Fig. F.1). These vertices differ by the number of the condensed atoms (dashed lines) involved in the interaction. In addition, each diagram is the depiction of different terms produced by expanding the exponential of the interacting Hamiltonian in perturbation theory. For example, considering only two kinds of vertices, the $l-th$ order term could be written as:

$$\frac{1}{l!}(H_A + H_B)^l, \tag{F.10}$$

where H_A and H_B are interaction terms corresponding to different types of vertices A and B. The perturbation factor, f_p is the numerical factor in front of each term of the above equation. As an example, consider a diagram with s vertices of type A and $l-s$ vertices of type B. f_p is the factor in

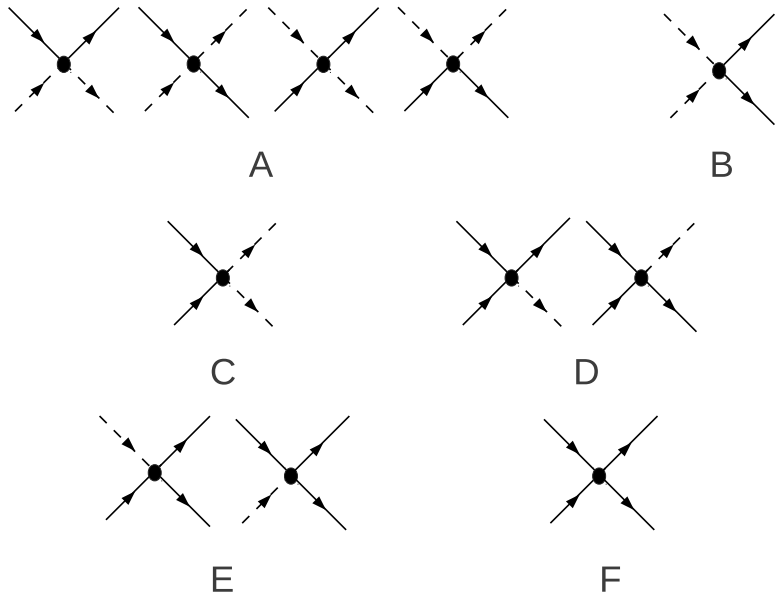

Figure F.1: Different types of the interaction vertices between condensed and non-condensed atoms which corresponds to different terms of the Hamiltonian (2.1).

front of $H_A^s H_B^{l-s}$ term. The perturbation factor for this example could be written in terms of combination factors as following:

$$f_p = \frac{1}{l!} C_s^l C_{l-s}^{l-s} = \frac{1}{s!(l-s)!}. \tag{F.11}$$

In general, if we have s_1 vertices of type A_1, s_2 vertices of type A_2 and so on until s_m vertices of type A_m, the perturbation factor would be:

$$\frac{1}{s_1! \times s_2! \times ... \times s_m!} \tag{F.12}$$

In the vacuum case, where all the momenta could be non-zero, all the vertices are the same and the perturbation factor is simply equal to $1/l!$.

As mentioned before in chapter 2, Hamiltonian (2.1) is generated by explicitly putting the momenta of some of the creation and annihilation operators equal to zero. For some of the terms, there are more than one way to set the momenta equal to zero. These choices cause different numerical prefactors in front of the terms in the Hamiltonian. For example, the second term in the Hamiltonian is produced by setting the momentum of one of the creation and one of the annihilation operators equal to zero. This term represents the interaction between one condensed atom and one non-condensed atom as incoming particles and one condensed atom and one non-condensed atom as outgoing particles. There are four different ways to produce this term and therefore the numerical prefactor in front of this term is 2 instead of 1/2. The vertex factor, f_v, is defined as the product of these prefactors for all the vertices involved in the scattering processes. Since for the vacuum case, all the vertices have the same prefactor of 1/2, f_v is equal to $(1/2)^l$.

The last factor is the symmetry factor, f_s which shows the number of different ways of connecting legs of these vertices. For the vacuum case, $f_s = l! \times 4^l$ where $l!$ is the number of permutations of vertices and 4^l is the different ways of choosing lines of each vertex (2 for incoming lines and 2 for outgoing lines). For the condensate case, finding the symmetry factor is a little tricky. Since only solid lines corresponding to non-condensed particles are connecting the vertices, the symmetry factor in this case depends on the number of the solid lines in each vertex. Again, suppose we have s_1 vertices of type A_1, s_2 vertices of type A_2 and so on until s_m vertices of type A_m. The number of permutation of the similar vertices would be $s_1! \times s_2! \times ... \times s_m!$ which cancels out f_p for the condensate case. In addition, different vertices have different ways of connecting their legs to other vertices. This numbers for vertex type A is *one* and for vertex types of B, C, D and E is *two* and for vertex type F is $four$ (see Fig. F.1). Note that if you multiply these

factors by the prefactors in front of each vertex, you would get 2 except for vertex types of B and C when you get 1. Since there is only one vertex of type B and one vertex of type C in any three-body diagram, f_n for the condensate case is equal to:

$$f_n = f_p \times \ f_v \times f_s = 2^{l-2} = 2^n \qquad \text{(condensate case)} \tag{F.13}$$

where l is the number of vertices and n is the number of the loops in each diagram. Similarly, for the vacuum case the numerical factor could be obtained as:

$$f_n = f_p \times \ f_v \times f_s = 2^l = 2^{n+2} \qquad \text{(vacuum case).} \tag{F.14}$$

Note that numerical factor found for the vacuum case is bigger than the numerical factor for the condensate case by the factor of 4. This difference is due to the exchange of the external legs of the diagrams. In the vacuum case, the external legs has non-zero momentum and could be interchanged. This produces the extra factor. Finally, $f_0 = 4$ in the vacuum case.

The contribution from the 1-loop diagram, $\Gamma^{(1)}$, to the effective interaction between condensed atoms in vacuum case could be written in terms of kernel defined above as:

$$\Gamma^{(1)} = 8 \int \frac{d^2k}{(2\pi)^2}(-\frac{1}{2}K(E-3\eta;p,k))g_2(E-3\eta-\frac{k^2}{2};k)(-\frac{1}{2}K(E-3\eta;k,p')), \tag{F.15}$$

where the integral over internal frequency has taken and $g_2(\omega;Q)$ is obtained before in Eq. (F.5) in two dimensions. Here, 8 is the numerical factor found in the vacuum case. Note that the shift of energy is 3η everywhere which corresponds to the case where we set the momenta p and p' to zero at the end, vacuum case. The effective three-body interaction in the vacuum case is obtained by summing over $\Gamma^{(n)}$s:

$$A_3(E;p,p') = \int \frac{d^2q}{(2\pi)^2}K(E;p,q)g_2(E-\epsilon_q;q)\Big(2K(E-\epsilon_q;q,p') - A_3(q,p')\Big) \tag{F.16}$$

The reduced amplitude is defined by setting the outgoing momentum to zero, $G_3(E;p) = A_3(E;p;p'=0)$. So, the integral equation for G_3 would be:

$$G_3(E;p) = \int dq \frac{4q}{log(|\frac{B_2}{3q^2/4-E}|)} \frac{1}{\sqrt{(E-p^2-q^2)^2-(pq)^2}} \Big(\frac{4}{|E-q^2|} - G_3(q)\Big) \tag{F.17}$$

The three-body irreducible potential could be found as:

$$g_3 = (6/4) g_2^2(0;0) Re(G_3^*(0;0)) \tag{F.18}$$

where $G_3^*(0;0)$ has obtained by subtracting the one-loop contribution from $G_3(0;0)$ defined above to prevent over-counting this diagram. The division by 4 in the last equation is due to the fact that the factors in the vacuum case are 4 times bigger than the factors in the condensate case because of exchange factor of 2 external legs in the vacuum case.

The alternative scheme is to set the external momenta p and p' to zero from the beginning. In this case, the shift of the energy for the first and the last kernel in any order of the loops would be 2η. In this scheme, the three-body irreducible potential is

$$g_3 = 6 g_2^2(0;0) Re(\int \frac{4qdq}{2\eta+q^2} \frac{1}{log(|\frac{B_2}{3q^2/4+3\eta}|)} G_3'(-3\eta;q)) \tag{F.19}$$

where $G_3'(-3\eta;p)$ is obtained from following integral equation:

$$\begin{aligned} G_3'(-3\eta;p) &= 4\int dq \frac{q}{log(|\frac{B_2}{3q^2/4+3\eta}|)} \frac{1}{\sqrt{(3\eta+p^2+q^2)^2-(pq)^2}} \\ &\times \Big(\frac{-1}{2\eta+q^2} - G_3'(-3\eta;q)\Big) \end{aligned} \tag{F.20}$$

Note that in the second scheme we don't need to subtract the one-loop contribution because it starts from two-loop diagram. Although the solutions for two schemes are very close to each other, we focus on the second scheme in our studies which is more accurate.

Appendix G

Numerical Method to Find The Three-Body Interaction Potential in Two Dimensions

Here we explain the numerical method we used to solve the integral equation of three-body scattering amplitude for a two-dimensional Bose gas showed in Eq. (F.20). First, we only keep the real part of g_2 and later we also take into account the imaginary part of the two-body interaction potentials.

The integral equation for G_3' derived in Eq. (F.20) could be rewritten as:

$$\begin{aligned} G_3'(y,z) &= a(y,z) + \int G_3'(y,x)K(x,y,z)dx \\ &= a(y,z) + \sum_i K_i(y,z)G_{3i}'(y)\Delta x \end{aligned} \tag{G.1}$$

where we have introduced following dimensionless variables:

$$\frac{3\eta}{B_2} \equiv y, \quad \frac{p}{\sqrt{B_2}} \equiv z, \quad \frac{q}{\sqrt{B_2}} \equiv x \tag{G.2}$$

and following functions:

$$\begin{aligned} a(y,z) &= \int dx \frac{4x}{log(3x^2/4+y)} \frac{1}{\sqrt{(y+x^2+z^2)^2-(xz)^2}} \frac{1}{2y/3+x^2} \\ K(x,y,z) &= \frac{4x}{log(3x^2/4+y)} \frac{1}{\sqrt{(y+x^2+z^2)^2-(xz)^2}} \end{aligned} \tag{G.3}$$

Furthermore, we discretized the x direction in the second line of the Eq. (G.1). By discretizing the space in z direction, the integral equation could be written in discrete space:

$$\begin{aligned} G'_{3j}(y) &= a_j(y) + \sum_i K_{ji}(y) G'_{3i}(y) \Delta x \\ \sum_i \delta_{ji} G'_{3i}(y) &= a_j(y) + \sum_i K_{ji}(y) G'_{3i}(y) \Delta x \end{aligned} \tag{G.4}$$

So, finally we can derive $a_j(y)$ in the following equation:

$$\begin{aligned} a_j(y) &= \sum_i (\delta_{ji} - K_{ji}(y)\Delta x) G'_{3i}(y) \\ a_j(y) &\equiv \sum_i M_{ji} G'_{3i}(y) \end{aligned} \tag{G.5}$$

This gives a matrix-form equation for G'_{3i} as:

$$\begin{aligned} \mathbf{a}(y) &= M \mathbf{G}'_3(y) \\ \mathbf{G}'_3(y) &= M^{-1} \mathbf{a}(y). \end{aligned} \tag{G.6}$$

Numerically, $\mathbf{G}'_3(y)$ is calculated by inverting the matrix $\mathbf{M}$ and multiplying that by vector $\mathbf{a}(y)$.

In general, we need to consider the imaginary part of the two-body potential as well. This part could be obtained using following simple expression:

$$\frac{1}{\ln(\frac{3}{4}q^2 + 3\eta - i\delta^+)} = \frac{1}{\ln(\frac{3}{4}q^2 + 3\eta)} + i\pi\delta(\frac{3}{4}q^2 + 3\eta - 1) \tag{G.7}$$

This imaginary term gives correction to the real part of the integral equation and results in g_3 being complex. The imaginary part of g_3 is related to the rate of three-body recombination process. Here, we first show the full expression for the two-loop contribution to g_3 and then determine the matrix-form equation for real and imaginary part of G'_3.

The full expression for the two-loop contribution to three-body interaction potential is:

$$
\begin{aligned}
B_2\ g_3^{\text{2-loop}} &= 96 g_2^2 \int \frac{z dz}{2/3y + z^2} \frac{-x dx}{2/3y + x^2} \frac{1}{\sqrt{(y + x^2 + z^2)^2 - (xz)^2}} \\
&\times \left(\frac{1}{\ln(3z^2/4 + y)} \frac{1}{\ln(3x^2/4 + y)} \right. \\
&- \left. \pi^2 \delta(\frac{3}{4}x^2 + y - 1)\delta(\frac{3}{4}z^2 + y - 1) + \frac{2i\pi\delta(\frac{3}{4}z^2 + y - 1)}{\ln(\frac{3}{4}x^2 + y)} \right)
\end{aligned}
\tag{G.8}
$$

where the correction to the real part of $g_3^{\text{2-loop}}$ due to imaginary term in g_2 is:

$$
B_2\ \Re\Delta g_3^{\text{2-loop}} = \left(\frac{2}{3}\right)^2 g_2^2 \left(\frac{1}{-2/3y + 4/3}\right)^2 \frac{3 \times 96\pi^2}{\sqrt{(-5y + 8)^2 - (4(1 - y))^2)}}
\tag{G.9}
$$

and the imaginary part of $g_3^{\text{2-loop}}$ has the following form:

$$
\begin{aligned}
B_2\ \Im\Delta g_3^{\text{2-loop}} &= -\frac{4}{3}\ 96\pi\ g_2^2\ \frac{1}{-2/3y + 4/3} \int \frac{x dx}{2/3y + x^2} \frac{1}{\ln(3x^2/4 + y)} \\
&\times \frac{1}{\sqrt{(y + 4/3(1 - y) + x^2)^2 - x^2\ 4/3(1 - y)}}
\end{aligned}
\tag{G.10}
$$

Similarly, one can add the imaginary part of g_2 in the integral equation and separate real and imaginary parts to get a system of equations for real and imaginary parts of G_3' as:

$$
\begin{aligned}
\Re[\mathbf{G}_3'] &= (M + BM^{-1}B)^{-1}(\mathbf{a} - BM^{-1}\mathbf{a}^*) \\
\Im[\mathbf{G}_3'] &= (M + BM^{-1}B)^{-1}(\mathbf{a}^* + BM^{-1}\mathbf{a})
\end{aligned}
\tag{G.11}
$$

where in addition to a and M functions which have been defined earlier, we introduce the following functions:

$$
\begin{aligned}
a^*(y, z) &= \frac{4}{3} \frac{2\pi}{\sqrt{(z^2 + 4/3 - 1/3y)^2 - (4/3 - 4/3y)z^2}} \frac{1}{-2/3y + 4/3} \\
B(x, y, z) &= 4\pi \frac{x}{\sqrt{(y + z^2 + x^2)^2 - (xz)^2}} \frac{\delta(x - \sqrt{4/3(1 - y)})}{\sqrt{3}(1 - y)} \Delta x.
\end{aligned}
\tag{G.12}
$$

The system of these equations can be solved numerically. By inserting the real and imaginary parts of G_3' and g_2 in Eq. (F.19), one can obtain the real and imaginary parts of three-body potentials as:

$$\begin{aligned}\Re[g_3(y)] &= -6\left(\frac{4\pi}{\ln(2/3y)}\right)^2\left(\int\frac{4x\ dx}{2/3y+x^2}\left(\frac{1}{\ln(3x^2/4+y)}\,\Re[G_3'(y,x)]\right.\right.\\ &+ \left.\left.\pi\delta(3x^2/4+y-1)\Im[G_3'(y,x)]\right)\right) \qquad \text{(G.13)}\end{aligned}$$

$$\begin{aligned}\Im[g_3(y)] &= -6\left(\frac{4\pi}{\ln(2/3y)}\right)^2\left(\int\frac{4x\ dx}{2/3y+x^2}\left(\frac{1}{\ln(3x^2/4+y)}\,\Im[G_3'(y,x)]\right.\right.\\ &- \left.\left.\pi\delta(3x^2/4+y-1)\Re[G_3'(y,x)]\right)\right) \qquad \text{(G.14)}\end{aligned}$$

Eq. (G.14) gives the imaginary part of three-body potential which is related to the three-body recombination process rate. We have estimated this imaginary contribution and we found that for the range of interest, $\Im[g_3(y)]$ is always much smaller than $\Re[g_3(y)]$ (see Fig. 4.3). As a result, we did not consider this effect in our self-consistent calculations to find the chemical potential of the Bose gas.